USING STATISTICAL METHODS TO OPTIMIZE POWDER FLOW MEASUREMENTS AND TO PREDICT POWDER PROCESSING PERFORMANCE

by

Sara Koynov

A dissertation submitted to the

Graduate School – New Brunswick

Rutgers, The State University of New Jersey

in partial fulfillment of the requirements

for the degree of

Doctor of Philosophy

Graduate Program in Chemical and Biochemical Engineering

written under the direction of

Fernando J. Muzzio and Benjamin J. Glasser

And approved by

_____

_____

_____

_____

New Brunswick, New Jersey

May 2015

ABSTRACT OF THE DISSERTATION

Using statistical methods to optimize powder flow measurements and to predict powder processing performance

By Sara Koynov

Dissertation Directors:

Fernando J. Muzzio and Benjamin J. Glasser

The flow behavior of powders - key raw materials, intermediates, and final products across many industries - is poorly understood, making the prediction of manufacturability and process performance difficult. Common manufacturing problems include non-uniform flow, jamming, segregation, and content uniformity issues. Due to the complex nature of granular materials, their flow behavior, typically, cannot be described using a single parameter. Many methods have been developed that utilize a range of sample sizes and characterize the material in a variety of consolidation states. The path for using these techniques for increasing process understanding remains unclear since the relationships between material properties and powder processing conditions remain partly unknown.

In this work, principal component analysis of large material property datasets was used to identify the most relevant material properties for a given application. This statistical approach was demonstrated using a database of raw material properties. The number of material properties needed to explain the observed variability was reduced to the minimum, while retaining the same predictive capability as the original dataset.

Additionally, the three characterization techniques that provided the most predictive capability were identified.

Fundamental understanding of the characterization techniques is critical for the successful application of material flow properties to solids processing operations. Two commonly used techniques are the shear cell and compressibility tests. These tests were also among those previously identified as relevant for distinguishing maximally between raw materials. It was found that different shear cells yield statistically different measurements even when testing the same powders under the same consolidation stress. Further, a novel compressibility method for reducing the amount of material required, to less than 50mg, for measuring flow properties was developed.

The use of material property characterization to increase process understanding was demonstrated through a case study of axial mixing in a rotating drum. The axial dispersion coefficient was found to be dependent on the material properties and increased with decreasing flowability. In this case, particle size, shear cell, and compressibility measurements explained 95% of the variation observed in the axial dispersion coefficient.

Acknowledgements

During the course of my studies I benefited greatly from the guidance and encouragement of many individuals. I would like to thank my thesis advisors, Fernando Muzzio and Benjamin Glasser, for their support and mentoring. I would especially like to thank Ben for his dedication to reviewing my manuscripts and Fernando for his dedication to improving my communication and presentation abilities. I would like to thank my committee members, Gerardo Callegari and Bill Borghard, for their suggestions and feedback.

I would also like to thank the National Science Foundation's Engineering Research Center for Structured Organic Particulate Systems (ERC-SOPS) and the Catalyst Manufacturing Science and Engineering Consortium at Rutgers University for the opportunities to interact with industrial partners, ensuring that my research remained focused and industrially relevant. The students and faculty that participated in these organizations have provided invaluable insight into my research.

Throughout my time at Rutgers, my fellow graduate students and colleagues have enriched my experience beyond measure providing insight, encouragement, and, most of all, friendship: Brenda Remy, Matthew Metzger, Eric Jayjock, Frank Romanski, Heather Emady, Kellie Anderson, James Scicolone, Bill Engisch, Sarang Oka, Pallavi Pawar, Yifan Wang , Fani Boukouvala, Amanda Rogers, Sebastian Escotet, and Kristin Steeley. I would also like to acknowledge the undergraduate students who have spent many hours aiding me in the lab: Matthew Rodis, Ramon Pena, Agnesa Redere, and Prashani Amin.

I would particularly like to thank my family and closest friends. I would like to thank my parents, James and Kathy Holt, and sister, Christina Black, for always believing I could do anything I put my mind to. I would also like to thank my grandmother, Patty Cross. It was because of her that I was able to take advantage of many opportunities that furthered my education. I would like to thank Leann Briggs for the support, encouragement, and laughter. Finally, a most heartfelt thank you to my husband, Athanas Koynov, for his endless love, patience, and support.

Table of Contents

List of Tables

List of Figures

Chapter 1. Introduction

1.1. Background

Powder and granular materials are ubiquitous, appearing in both nature and industrial processes [1, 2]. In fact, it has been reported that over 50% of all products manufactured are either in granular form or require the processing of granular materials during their production [3, 4]. For example, Ennis et al estimates that 40% of the value added in the chemical industry is the result of the use of particle technology [5].

The processing of granular materials, like many other processes, is done through a series of unit operations. Some examples of powder-based unit operations in industry are the use of fluidized catalytic reactors in the bulk chemical industry [6], freeze drying during the manufacture of food and pharmaceutical products [7], the compaction of granular materials into tablets in the pharmaceutical industry [8], and the blending of multiple powders to form cosmetic, personal care, and food products [9].

The flow of powders in process equipment is a complex and challenging area of study. Companies would like to predict how a given powder would flow in a given piece of process equipment or compare the flow of one powder to another powder. In the pharmaceutical industry, during the initial stages of development, one often has only a small amount available of Active Pharmaceutical Ingredient, so companies would like to measure powder properties using lab scale tests to predict behavior in production-scale processing steps such as agitated drying and blending [6, 9-12]. In the catalyst manufacturing industry, new formulations may dictate the use of new powders in existing process equipment for steps such as impregnation, drying, mulling, and calcination [13, 14]. Again, being able to predict the flow of a powder using lab scale tests is desirable. In

many cases an easy way to predict how a new powder may behave in a piece of equipment is to compare how that new powder flows relative to an existing powder that has already been used in that piece of equipment. Companies, therefore, often develop libraries of powder flow properties to compare new powders to existing powders [15].

Despite the prevalence of granular materials, their behavior is poorly understood [16]. A granular material is comprised of individual particles. A key element needed to describe powder flow behavior is to determine how force is transmitted through the bulk material, i.e. between particles. This has been studied via two main approaches.

The first is by considering the individual particles. In principle, the behavior of a bulk of granular material can be determined from the inter-particle interactions. Modeling of systems using the discrete element method (DEM) is based on the interactions between individual particles. However, this approach has two main problems. The first is that the number of particles in a typical system containing granular material is very large. For example, the number of 10 micron particles in a one cubic centimeter volume is on the order of 10^9. The second challenge is that is it very difficult to describe accurately the adhesive and cohesive forces. The large number of inter-particle interactions and the difficulty in describing them accurately combine into a complex problem such that the number of particles that can be considered in models using the discrete element method is limited by available processing power [17]

The second approach considers the bulk material as a continuum. The application of continuum mechanics has become the standard treatment for powder flow behavior. Two limiting regimes of granular flows are often considered (quasi-static slow flows and

collisional rapid flows) [18]; each based on a different branch of established science. Quasi-static models are based on the Mohr-Coulomb frictional yield condition from metal plasticity theory. Models used for the collisional rapid flow regime are derived based on the kinetic theory. Campbell [19-21] has been able to fill in the gap between the quasi-static and collisional regimes by introducing the elastic properties of the particles into the models. Flowmaps can be drawn that describe granular flow behavior across the regimes. However, the quasi-static and collisional models do not allow for the inclusion of all powder properties. Therefore, a unified set of governing equations for modeling powder flow behavior does not exist. This fact, coupled with the discrete nature of granular systems and the presence of inhomogeneities at the particle level, means that in practice the continuum approach is only able to yield an approximation of observed behavior [22].

In spite of the limitations of the continuum approach, several advances have been made in the field of powder flow characterization. Janssen [23] determined that the stress at the bottom of a powder bed, e.g. at the bottom of a silo, is not proportional to the height of the powder bed. In the 1960s, Jenike introduced the concept of the yield locus to the field of bulk solids technology [24, 25]

Due to the lack of a unified theory of granular flow behavior, processes that handle granular materials are not well understood. The flow properties of powders might change significantly throughout a process; these changes can be detrimental to product quality. The mechanisms of these changes might not be known and so many variables that may influence the manufacturing process are often unmonitored [26]. This situation can manifest itself by the presence of major processing problems that adversely affect product

quality. Such problems are experienced by more than 90% of solids process plants [27]. This is especially visible in the pharmaceutical industry where 80% of oral products are formulated as tablets, pills, or capsules [26].

1.2. Powder Flow Characterization

As mentioned, a unified framework capable of describing powder flow behavior does not exit [28]. Therefore, experiments and empirical approaches must be considered. The capacity of a powder or granular material to flow under a specified set of conditions is referred to as the flowability of the material. This is a complex characteristic, dependent on not only material properties but also the stress history the material has experienced. Because the flowability of a material is a function of both physical properties and environmental and processing factors, the flowability cannot be described by any single parameter [29]. As a result, there now exists a plethora of characterization techniques: shear cell methods, density testers, fluidized beds, avalanching devices, etc [30]. These techniques analyze powder flow behavior in a variety of states; ranging from a small amount of powder sample (on the order of grams) to a large sample (on the order of kilograms) and from a loosely packed state to a densely packed state. General knowledge of when to use which characterization technique remains to be developed.

The aforementioned techniques have been used by many researchers to study powder flow. The effect of material properties such as particle size and shape [31], environmental conditions such as moisture and storage conditions [32, 33], and formulation parameters such as lubricant concentration [34] on the flowability of granular materials, have been studied. In addition, several studies have been carried out comparing various characterization techniques. Guerin [35] found that a simplified shear

cell was more selective than measuring tapped density but required more time and material. Avalanche based methods have been compared to other techniques in several studies. Results of these studies have been inconclusive and somewhat contradictory. Lavoie [36] and Taylor [37] found that the results from avalanche methods did not agree with other techniques, Lindberg [38] found partial agreement, and Hancock [39] found full agreement. It is clear that the relationships between the results from the various characterization methods is not understood [40].

The prediction of the performance of solids processing operations relies on experimentally obtained powder flow characteristics [16, 30]. Many characterization techniques exist, each one examining the inter-particle surface forces differently [15]. But despite their differences, their results can be highly collinear [41]. In addition, each unit operation presents a unique processing environment exposing the material to various levels of stress, altering the flowability of the material [29]. Therefore, the selection of the most useful technique(s) for a given process is often unclear and complex [42].

1.3. Organization of the dissertation

The work presented in this dissertation focuses on using statistical methods to optimize powder flow measurements and to predict powder processing performance. A PCA-based method was introduced as a way to determine the most relevant characterization method(s) for a particular application (Specific Aim I). Following a detailed discussion of the available flow property characterization techniques, the PCA method is illustrated using a case study of a database of raw material properties. The successful application of powder flow characterization to improve process design and performance is also dependent on fundamentally understanding the characterization methods themselves.

Thus, the shear cell and the compressibility tester were studied in detail (Specific Aim II). These two techniques are among the most commonly used and were identified as the most useful in the first specific aim. Finally, the application of the PCA method and increased fundamental understanding of the characterization methods to a process is demonstrated through a case study, an axial mixing process. The axial dispersion coefficient is used as the process performance metric. The dependence of the axial dispersion coefficient on material properties is determined and the most useful characterization methods for describing the observed variation in axial dispersion coefficient between materials are identified. Given the preceding discussion, the three specific aims of this dissertation are as follows:

- Specific Aim I: Method development (Chapter 2)
- Specific Aim II: Fundamental investigation of flow property characterization methods (Chapters 3 and 4)
- Specific Aim III: Axial mixing and material properties - a case study (Chapter 5)

Chapter 2. Overview of powder flow characterization techniques and statistical methods for selection

2.1. Introduction

The current state of the art in characterizing raw material variability is to use a set of established techniques to measure a set of properties. The results are then used to inform formulation and processing decisions. This chapter discusses the properties typically characterized and the techniques used to measure them. The state of the art in applying this information to define a formulation or manufacturing process is also discussed.

It is a truism that the properties of raw materials can affect the properties and quality of the final product [26]. Therefore, understanding the properties of the raw materials is critical. Further, raw materials often have variability in their properties, and so it is prudent to monitor raw material properties and develop effective acceptance criteria in order to avoid easily preventable product/process failures.

The raw materials of interest here are powders and granular materials. Powders are complex and their behavior is poorly understood [16]. The flowability, or flow-related behavior, of a powder is a multi-dimensional characteristic. There are no general constitutive equations or unifying framework to describe powder dynamics. Instead, experimental characterization techniques and empirical correlations are used. There are several characterization techniques available, each measuring a slightly different aspect of flow behavior. These techniques also test powder in a variety of states: from fully aerated to varying degrees of consolidation, from confined to unconfined, from incipient flow to steady state flow. It is also frequently the case that a single characterization parameter is not sufficient to fully describe flow behavior; the information from multiple

tests is often required. Although there are several techniques, the tests can be classified as the measurement of one or more of the following properties: cohesion, bulk density, permeability, friability, hydrophobicity, electrostatics, and segregation tendency. Usually, rather than characterized directly, the effects of particle size and particle shape are incorporated into the cohesion and bulk density properties, respectively. As the particle size decreases, there is an accompanying increase in cohesion due to van der Waals forces. As a result, the effect of altering the particle size on the flowability of a powder can be ascertained by measuring the cohesion of the material, similarly to the way in which a change in the molecular weight of a polymer is often described in terms of the changes in viscosity of polymer solutions. The mechanism by which the particle shape affects the flowability of a material is through the mechanical interlocking between the particles. As compared to freely flowing spherical particles, particles with a large degree of interlocking can exhibit hindered flow.

It is important to understand raw material properties because of their great impact on the performance of the manufacturing process. Variation in raw material properties typically becomes variation in blend properties eventually becoming variation in final product quality. Raw material properties should not be characterized in a vacuum, but accompanying understanding of the manufacturing process. Identifying the relationship between raw material properties and process performance is critical to determining which raw material properties should be measured and the magnitude of variation in those properties will cause processing issues downstream.

Several studies have been performed in an effort to elucidate the relationship between raw material properties and process performance. These studies typically seek one of two

goals: improving powder flow or understanding individual unit operations. Powder flow is frequently improved by altering the surface properties of the particles. Flow additives such as magnesium stearate or colloidal silica will often dry-coat a fraction of the outer surface of poorly flowing particles. Magnesium stearate decreases the attraction force between particles either by rendering the surface hydrophobic, thus decreasing the formation of capillary bridges, or by physically separating particles, thus reducing the van der Waals forces [43-45]. Colloidal silica reduces the electrostatic properties of the particles [46-49]. In addition, unit operations have been individually investigated including hopper flow, spheronization, mixing, tabletting, and capsule filling [50-55].

This chapter will discuss commonly used powder flow properties and the methods by which to characterize them. A statistical method for determining the most relevant properties for a given application will be discussed.

2.2. Powder flow properties and characterization techniques

2.2.1. Cohesion

The cohesion of a material is indicative of how well a material flows or how "sticky" it is. Particles tend to stick together when the inter-particle forces exceeds the gravitational force pulling them apart. This ratio is described for dense flows using the granular bond number [56].

$$Bo_g = \frac{n^c}{mg}$$

Where n^c is the maximum attractive force and mg is the gravitational force exerted on a particle. Sources of the attractive inter-particles forces include van der Waals forces,

capillary forces from liquid bridges, and electrostatics originating from unlike charges or dipolar moments.

Cohesion can be measured, among other methods, by using avalanche testers (such as the Gravitational Displacement Rheometer [57, 58]) or shear cells [17]. During avalanche testing, cohesion is determined based on the size of the avalanches that are formed during tumbling flow; that is, the scale of the self-assembled chunks formed within the powder bed. The shear cell measures the degree by which arches formed within the powder bed strengthen (more, stronger arches tend to form in cohesive powders) in response to increase applied normal stress. The shear cell also measures cohesion as the shear stress required to move particles against one another under zero normal stress. The resulting flow index or flow function metrics, in addition to the cohesion parameter, can be used to rank the flowability of materials and to predict the behavior of a new material in a manufacturing process based on prior experience with other materials.

2.2.1.1. Avalanche testers

Commercially available avalanche testers, including the AeroFlow, Revolution Powder Analyzer, and the GDR, have been used for industrial applications in addition to academic studies [39, 59, 60]. The primary difference between the three technologies is the length of the cylinder used; the cylinder used in the GDR is much longer to reduce the effect of friction with the side walls. The GDR method is described in detail here. A comprehensive discussion comparing the GDR to other devices exists in the literature [42].

The GDR, a technology developed at Rutgers based on the method described by Davies *et al.* [61], is comprised of a rotating cylinder placed on a table supported by a hinge and

a load cell. The experimental setup is presented in Figure 2-1. To test the cohesive nature of a material, a characteristic known as the flow index is measured. An acrylic cylinder is given sufficient length to eliminate the wall effects on the powder flow. As the cylinder rotates, the powder flows in avalanches. As the avalanches fall, their force is measured by the load cell. Using these measurements, the sizes of the avalanches are determined. The sizes of the avalanches are correlated to the cohesiveness of the powder; a more cohesive powder will flow in large avalanches.

The load cell signal is recorded for rotation rates of 5, 10, 15, and 20 rpm. The load cell signal is filtered and normalized, in order to account for the material density. The standard deviation of the signals is then calculated for each rotation rate. The average of the standard deviations at 5, 10, 15, and 20 rpm is then reported as the flow index. Since the variation in the load cell signal increases with larger avalanches, lower flow index values indicate better flow.

2.2.1.2. Shear cell

The shear cell testing methodology was originally developed by A.W. Jenike for the specific application of sizing hoppers and silos based on the principles of solid state mechanics [24]. Shear cells are now commonly used to rank granular materials according to their flowability. From a series of shear tests, the angle of internal friction, the angle of wall friction, the slope of the hopper walls, and other design parameters can be extracted. This methodology has since been more generally applied in the field of powder characterization.

This characterization technique has become prevalent, and international standards detailing the procedure have been defined [62]. Because the shear cell is commonly

used, many studies and much research have been done involving it. Much of this work has been focused on determining if shear cell measurements are applicable to specific situations [60]. In addition, various aspects of the experimental procedure (ones not dictated by the standards) have been studied [63]. Lastly, some studies have been conducted that compare the measurements of a particular shear cell parameter between different types of shear testers [64].

While original shear cells used translational motion to measure "incipient failure", more modern versions of the technique use rotational motion to impart large strain and to achieve "steady state" mechanical behavior. The standard procedure involves three steps: pre-compaction of the powder bed, pre-shearing of the powder bed until steady state flow is achieved (powder stresses are equal in all directions and the bulk density is constant), and shearing until the powder yields. The pre-shearing/shearing process is repeated 4-5 times using normal stresses 20-80% of the consolidation stress. The result of the above process is a series of measurements of corresponding normal and shear stresses and is called the "yield locus". The yield locus is fit with a best-fit line that is extrapolated to the y-axis. This corresponds to the shear stress at zero normal stress, or cohesion.

In addition, Mohr circle analysis is performed on the yield locus. Mohr circle analysis is a geometric representation of a coordinate transformation to identify the principal stresses. Two circles are used. The first goes through the origin and is tangent to the best-fit line through the yield locus. This circle represents the conditions present at the free surface of an arch (as is present in hopper flow). The second circle is tangent to the yield locus and passes through the pre-shear (steady state flow) point. This circle represents the conditions for the critical state. The principal stresses extracted from this

analysis are called the unconfined yield stress and the compacting stress (major principal stress), i.e. the yield stress of the powder in the free surface of the arch (as in hopper flow) and the compacting stress in the powder bed, respectively as shown in Figure 2-2. The yield locus is measured at several consolidation stresses and the unconfined yield stress and compacting stress are extracted from each yield locus. The unconfined yield stress - compacting stress pairs are plotted from each yield locus to give the "flow function". The slope of the flow function indicates how well a powder flows; the steeper the slope, the more cohesive (i.e. poorly-flowing) the powder.

2.2.2.Bulk density

The bulk density of a material is indicative of a material's flowability and the degree to which the material may expand or consolidate under various conditions occurring during manufacturing [65, 66]. The bulk density, defined as the ratio of the mass of powder sample to the volume of that powder sample, takes into account both the particle density as well as the packing of the powder bed [67]. As this measurement is highly dependent on the consolidation, or packing, state of the material, the aerated bulk density measurement is traditionally paired with the tapped bulk density (the density of the bulk with a high degree of packing resulting from extensive settling). The tapped bulk density is measured according to Standard Test Method ASTM D6393-08 "Bulk Solids Characterization by Carr Indices" using instruments such as the Tap Density Volumeter (Quantachrome) and Hosokawa Micron Powder Tester (Hosokawa, Japan).

The compressibility of a granular material compares the aerated bulk density to the tapped bulk density. There are several acceptable ways of expressing the relationship

between the aerated and tapped bulk density including the Carr index, C [68], and Hausner ratio, HR [69].

$$C = \frac{V_0 - V_N}{V_o}$$

$$HR = \frac{\rho_N}{\rho_0} = \frac{V_0}{V_N}$$

where ρ_0, V_0, ρ_N, and V_N, are the aerated bulk density and powder volume, and the tapped bulk density and powder volume after N taps, respectively.

More recently, the bulk density has been measured over a range of packing states by varying the consolidation stress applied to the powder bed, such as with the Freeman Technology FT4 [70]. Alternatively, the difference in density between the tapped state and the dilated state can be measured using the dilation method from the Gravitational Displacement Rheometer [71]. While these measurements give slightly different numerical results, the observed trends are highly co-linear between all of these methods.

2.2.2.1. F4 – Compressibility

The compressibility test is part of the Freeman Technology FT4 Powder Rheometer suite. This test measures bulk density over a range of packing states comparing the results to an initial, conditioned bulk density. A schematic of the test and sample raw data that can be obtained are shown in Figure 2-3. The test begins by conditioning the powder by passing an up-pumping helical blade through the bed in order to erase the history of the powder and create a uniform, reproducible loose packing state. A normal force is then slowly applied using a vented piston (allowing air to escape from the power bed). The normal force ranges from 0.5 kPa to 15 kPa and is applied over 10 intervals, holding each load

for 60 seconds. The change in volume due to the compression is measured at each interval. The compressibility index (I_c), is calculated as a ratio of the initial and final densities, analogous to the Hausner ratio. The compressibility (Comp %) is calculated as the percent change in volume after compression, analogous to the Carr index.

$$Comp\ \% = 100 * \frac{V_C - V_P}{V_C}$$

$$I_C = \frac{\rho_P}{\rho_C}$$

where ρ_C, V_C, ρ_P, and V_P are the conditioned bulk density and powder volume, and bulk density and powder volume after compression with piston, respectively.

2.2.2.2. GDR – Dilation

Using the GDR experimental setup described in section 2.1.1 and illustrated in Figure 2-1, a characteristic known as the dilation can be measured. In this test, the powder is initially at or close to an asymptotic tapped density state, usually obtained by tapping the cylinder 500 times using a tap density tester. The dilation is a measure of the expansion of the powder bed upon rotation of the cylinder [57, 71].

First, the material is loaded into the cylinder and the cylinder is tapped to consolidate the powder. The material is loaded into the cylinder such that after tapping the powder bed volume is about 40% of the cylinder volume. The cylinder is then placed on top of the load cell in front of an IR camera. The camera begins recording images of the tapped powder bed and continues as the cylinder rotates at 15rpm. The change in volume of the powder bed upon rotation is determined by image analysis. The change in volume is

reported as the dilation, in percent. The dilation is analogous to the Carr index, comparing the tapped bulk density to the dilated bulk density [15].

$$Dilation\ \% = \frac{V_{new} - V_{initial}}{V_{initial}}$$

where V_{new} and $V_{initial}$ are the dilated and tapped bulk densities, respectively.

One advantage of measurements such as the Carr Index, the Hausner ratio, or the dilation, which normalize the measurement using a ratio of densities (or volumes), is that they yield a measurement that is independent of the absolute density, thus facilitating comparison between powders that are composed of intrinsically heavier or lighter materials.

2.2.3.FT4 – Permeability

Permeability is a measure of how well air passes through a powder bed. In order for powder to flow smoothly, air must be able to travel upstream; otherwise vacuum is created. This is particularly critical at points during a manufacturing process where the powder is transitioning from a static (or nearly static) to a dynamic state, e.g. flow from a hopper, compaction in a tablet die, the initial aeration in a fluidized bed, or when the powder must fill a small cavity, such as in tableting. The permeability of a granular material is influenced by particle properties such as size, shape, surface texture, and stiffness as well as bulk properties such as cohesion and bulk density.

Permeability is typically measured as the pressure drop across a powder bed over a range of consolidation states, as achieved by the FT4 from Freeman Technology [72]. A schematic of the test and sample raw data that can be obtained are shown below in Figure 2-4. The powder sample is loaded into the test vessel and then is conditioned using the

helical blade mentioned previously. The conditioning step creates a uniform, reproducible loose packing state. An upward air velocity of 2mm/s is added to the bottom of the powder bed. A normal force is then applied to the powder bed with a vented piston (to allow the removal of air from the system) over a range of 0.5 to 15kPa. At each normal force, the pressure drop across the bed is measured.

A low, flat pressure drop profile is indicative of a highly permeable material. A high, curved pressure drop profile is indicative of a material with low permeability.

2.2.4.Friability

Friability is an indication of a material's propensity for attrition and sensitivity to shear. The ability to identify powders that are potentially sensitive to processing strain can lead to improvements in process design. For materials that are prone to attrition or sensitive to high levels of shear, certain unit operations can be detrimental to the final product quality. Therefore, unit operations that create high shear environments, such as milling, are not recommended for these materials. Instead, it is recommended that friable materials be diverted around such unit operations so that non-friable materials can still be processed in high shear environments. In addition, variability in the raw material properties of friable materials could be magnified during processing.

The friability of a granular material can be measured directly be repeated measurements of the particle size distribution, or indirectly by measuring changes in powder properties after exposure to a simulated processing environment. These changes can be in the mass of a sample [73] or in the amount of energy required to pass a blade through the powder bed [38].

2.2.4.1. Friability – Lost mass

The attrition of granular materials with larger particle size, such as the product of a granulation process or a finished tablet, manifests as the breaking off of pieces of the particles [74]. The extent to which this occurs, known as the friability, is measured by tracking the change in mass of the particles as a result of exposure to stress. Instruments such as the Friabilator [75] and the Friabimat [76] simulate the stresses particles experience during processing and handling. Each of these instruments follow the same basic procedure. The sample of material to be tested is initially weighed, m_i. The sample is then loaded into the testing apparatus, the drum of the Friabilator or bottle of the Friabimat shown in Figure 2-5. The sample is then agitated by the rotation of the drum or the oscillation of the bottle through an arc. After agitation, the sample is de-dusted and weighed, obtaining the remaining mass of the unbroken particle cores, m_f. The friability is calculated as the percent mass lost during testing.

$$\%\, mass\ lost = 100 * (\frac{m_i - m_f}{m_i})$$

2.2.4.2. FT4 – Dynamic test

The friability of powders and granular materials, including those with smaller particle size, can be measured as a function of the energy required to move a helical blade through a powder bed, known as the flow energy, E, which can be considered to be the energy required to make powder flow around the blade. The Freeman Technology FT4 dynamic test procedure measures this energy as a function of time and shear rate (variable blade tip speed) [77]. The powder sample is loaded into the test vessel and then is conditioned using a helical blade. The conditioning step creates a uniform, reproducible packing state. The helical blade is then used during the testing cycle where

the flow energy, the energy consumed to induce the powder to flow, is measured on the downward and upward traverse. The conditioning step followed by a testing cycle is repeated seven times with identical conditions, and then four additional repetitions are executed with variable blade tip speed [41]. A friable material may exhibit a change in the flow energy over time and over a variable shear rate due to attrition, agglomeration, or segregation. In addition, some materials that are cohesive or highly compressible can become caked (i.e. consolidated) or agglomerated during flow. This behavior can also manifest as a change in the flow energy. Figure 2-6 shows a schematic of the helical blade pattern as well as sample data obtained from the dynamic test procedure.

The stability index, SI, indicates the change in flow energy over time.

$$SI = \frac{E_7}{E_1}$$

where E_1 is the flow energy required on the first downward traverse blade pass and E_7 is the flow energy required on the seventh downward traverse blade pass, also known as the Basic Flow Energy (BFE). The BFE does not account for the density of the material, therefore the Normalized Basic Flow Energy (NBFE) is commonly used,

$$NBFE = \frac{BFE}{mass}$$

Where the *mass* is the amount of powder in the sampling cup. A stable, non-friable material has an SI of about 1; the energy consumed over the first blade pass is the same as the seventh pass. An SI value of greater than 1 indicates a material that requires more energy to flow over time. This increase in energy can be due to de-aeration, agglomeration, segregation, moisture uptake, or electrostatic charges. A decrease in the

energy required over time, an SI less than 1, can be caused by attrition, de-agglomeration, over blending of an additive, or the coating of the blade and vessel by an additive.

In addition to the energy consumed on the downward traverse, the BFE, the energy consumed during the upwards traverse is also measured, the Specific Energy (SE). The Specific Energy is also normalized by the mass of the powder sample. Due to the geometry of the helical blade (Figure 2-5) during the upwards traverse, the powder is unconfined. This condition is representative of powder flow in a low stress environment. Therefore, SE is more dependent on cohesive forces and less on compressibility.

Powders that are cohesive and compressible may be sensitive to shear and processing. For example, when forced to flow or exposed to stress, the material can become caked or agglomerated. The FT4 dynamic test also measures the sensitivity of a material's flow energy to a range of flow rates (via variable blade tip speed). The final four repetitions of the conditioning/testing cycle are performed with a tip speed ranging from 10 to 100 mm/s. The Flow Rate Index (FRI) is the ratio between the required flow energy at 100 to 10 mm/s.

$$FRI = \frac{E_{11}}{E_8}$$

where E_{11} and E_8 are the BFEs at a blade tip speed of 10 mm/s and 100 mm/s, respectively. Most powders exhibit an FRI value between 1.5 and 3.0, a modest decrease in flow energy at higher flow rates. The displacement of the particles due to the blade movement occurs on a timescale dependent on the blade tip speed. At higher flow rates, this occurs much faster than the repacking of the particles resulting in the entrainment of

air in the powder bed. This entrained air acts as a lubricant reducing the interparticle contacts and the required flow energy. Conversely, at low flow rates, the blade movement is slower than the repacking of the particles. As a result, the particles become more tightly packed increasing the number of particle contacts and the required flow energy. High FRI values, e.g. larger 3.0, are typically exhibited by very cohesive powders. Cohesive powders tend to be more sensitive to changes in flow rate due to higher air content. Flow rate insensitive powders, e.g. those with an FRI value of about 1, usually have larger particle size or surface treatments. Powders that require less flow energy with increasing flow rate (i.e. an FRI less than 1) usually contain flow additives.

2.2.5.Hydrophobicity

Hydrophobicity is a quantification of a material's affinity for water. One of the primary quality characteristics in the pharmaceutical industry is the dissolution of the final dosage form (tablet, capsule, etc). The hydrophobicity of the blends comprising the dosage forms is therefore critical. Because blend properties are often a function of the raw material properties as well the processing conditions, the hydrophobicity of the raw materials and the effect of processing should be characterized [78, 79].

The wettability of a powder can be measured using a modified Washburn technique [80]. The uptake of water into a powder bed due to capillary action was described by Washburn in 1921 [81]. The volume of water that permeates the powder bed increases linearly with the square root of time. A hydrophobic powder will resist the capillary action resulting in a slower rate of water uptake. The relationship of water uptake to time can also be expressed as a linear relationship between mass of water in the powder bed squared and time [82].

$$t = \frac{\eta}{C\rho^2\gamma\cos\theta}m^2$$

where t is the time, η is the liquid viscosity, C is a geometric factor comprising the effect of powder packing density and particle size, ρ is the liquid density, γ is the liquid surface tension, θ is the contact angle between the liquid and particles, and m is the mass of the liquid in the powder bed column. The slope of this line is related to the hydrophobicity of the material.

The experimental setup used to measure hydrophobicity is shown in Figure 2-7. The powder sample is loaded into a chromatographic column with a sintered glass bottom. To ensure a constant geometric factor, C, the powder bed plus column assembly is tapped using a tapped density tester. The column is dipped into a large water source. To prevent the dissolution of the power by the large water source, the water is saturated with the powder material (or materials in the case of a blend). The column is held by a support beam on a load cell. The weight of the water taken into the column is measured as a function of time. To calculate the hydrophobicity, the data is represented as time as a function of mass squared as shown in Figure 2-8 [83].

2.2.6.Electrostatics

Pharmaceutical processes are ripe with problems caused by electrical phenomena, such as powder agglomeration, powder sticking to the walls of containers, feeder jamming, poor mixing, intermittent flow, etc [84]. Figure 2-9 shows an example: Avicel 101 sticking to a gravimetric feeder during flow. The root cause of this phenomenon is electrostatics (i.e. charge transfer and charge buildup). Particle charging and electrostatics are complex phenomena. Material properties such as composition, density, and microstructure can

affect the electrostatic properties of the material. While some of the fundamentals causing this phenomenon have been examined, a complete theory of powder electrostatics does not exist [85-87]. Various techniques have been proposed to characterize various aspects of electrostatic behavior [88, 89]. Here, the characterization of electrostatic properties by measuring the impedance, resistivity, and dielectric permittivity is detailed. The impedance is the modular ratio of applied voltage to the current flowing through the bed. Knowing the geometry of the testing vessel, the resistivity and dielectric permittivity can be calculated.

The experimental set up and sample data are shown below in Figure 2-10. The powder sample is loaded into a test vessel. The vessel is cylindrical and has a conductive bottom with Teflon walls such that it acts as a Faraday cup. A heavy, conductive lid is placed on the sample. The weight of the lid produces a reproducible packing state within the powder bed, necessary for the reliable measurement of impedance, resistivity, and dielectric permittivity [90]. The conductive lid and bottom act as two electrodes. Sinusoidal voltage is applied to the top electrode and the resulting current flowing through the powder bed is measured using an oscilloscope [91].

2.2.7.Segregation tendency

Segregation is a phenomenon that is predominantly affected by material properties, rather than processing conditions, although a poorly designed process definitely worsens segregation. Continuous processing involves the flow of materials through channels of various sizes (mixers, pipes, feeders, etc.). For such processes, testing the segregation tendency of the materials can inform the selection of equipment and formulation parameters minimizing potential segregation issues [92]. In practice, sifting can occur

during powder flow. The tendency of a material (of either a raw material or a blend) to segregate can be described using a sifting metric, such as with the Jenike Sifting Segregation Tester (originally developed at Rutgers University) that simulates the sifting that can potentially occur during processing [29, 93].

The experimental setup is shown below in Figure 2-11. Two hoppers are placed in a vertical stack. Powder is discharged from the upper hopper into the lower hopper; once or multiple times. Samples are then collected and analyzed. Segregation can be characterized in this manner as a function of formulation factors including particle size and chemical composition, or processing factors such as shear history and moisture content.

2.3. Statistical methods for selection of relevant material properties

Principal Component Analysis (PCA) is a statistical method where a model is used to represent a data set (Y) in a reduced dimension (latent variable space) such that the major axes of variability are identified [94]. Specifically, the raw data set Y can be decomposed, based on the equation below, onto a set of scores (T) and loadings (P), while the remaining variability is modeled as left-out noise (ε).

$$Y = TP^T + \varepsilon$$

The columns T represent scores in the projected space; loadings P represent the weights/ significance of each variable in each dimension. One of the most common uses of PCA is the identification of hidden structures in large data sets. When constructing a PCA model, it is up to the user to select how many principal components to keep in order to sufficiently describe the data. The number of components (or active dimensions) should be chosen based on the type of analysis required for each case study. In certain cases, the

first few principal components capture (“explain”) most of the variability, with the remaining ones capturing very little, and thus it is relatively easy to distinguish between the true variability and noise. In other cases, this decision is not so trivial. Applied here, PCA can be used to identify the material flow properties that contain the most information about the materials. Thus, the testing necessary to effectively characterize and distinguish between materials can be minimized.

As detailed above, there are several methods by which to characterize the flow properties of a material. However, they do not all vary independently, quite the opposite, they are often highly correlated. This fact means that the variables of interest vary in a much lower dimensional space than the number of measurements.

2.3.1. Databases that contain missing data

In many cases, large databases are incomplete due to measuring errors, sensor failures, or inconsistencies due to the combination of historical datasets. However, if the amount of missing information is neither significant nor based on a particular pattern, there is not a significant effect on the building of multivariate latent space models. This is due to the fact that latent space models aim to capture overall trends in the data set and are not much affected by individual gaps in the data. In fact, in certain cases, if an outlier is detected in the data set, it is preferred to discard this observation/ measurement and treat it as a missing point, rather than let it affect the entire PCA model. Once the PCA model is built and the major axes of variability are found, the model can be used to predict these missing values.

In the specific case study presented next, a total of 25 measurements are available for a set of 31 materials. The measurements were obtained from the following tests: particle

size distribution (d_{10}, d_{50}, and d_{90} measured at two pressures), relative humidity at the time of testing, loss on ignition (LOI at 130 C and LOI at 1000 C), bulk density (tapped density and Carr index), FT4 compressibility (conditioned bulk density, compressibility, compressibility index), FT4 permeability (permeability and the air velocity during testing), FT4 shear cell (unconfined yield stress, major principal stress, hopper flow factor, cohesion, and angle of internal friction), FT4 variable flow rate and stability (basic flowability energy, stability index, and specific energy), and the Gravitation Displacement Rheometer (Flow Index). In this database, there is a small amount of missing information, about 12%. This amount should not affect the final results significantly. There are many approaches that can be employed to handle the missing data. One simplistic approach is to delete any rows and columns that contain missing information. However, this approach may lead to significant loss of valuable data. Alternatively, there are more sophisticated approaches where missing points are imputed and approximated. These have been shown to lead to more accurate PCA models [95-98]. In this work, the NIPALS (non-linear iterative partial least squares) method is used. NIPALS has been very well documented and tested in the literature for this amount of missing information [99].

2.3.2. Identification of the significant principal components

The first step in PCA is the identification of the most significant principal components as well as the number of principal components that contain maximum and useful variance of the data. Here, each principal component is a weighted, linear combination of the material properties and the weights of each property signifies its influence. The maximum number of principal components is the original number of variables (material properties, in this case). Success in choosing the right number of principal components

lies in identifying those that capture actual variance (R2), rather than noise, in the data. To identify this critical number of principal components, the cross-validation error (Q2) is also calculated each time a principal component is added to assess the model's predictive capability. Groups of observations are removed and a model is built based on the remaining data. Predictions are made based on the removed observations. The predictions are compared to the actual data. Thus, if the explained variance and cross-validation error do not increase significantly upon the addition of a principal component, it is concluded that the predictive capability of the model did not increase significantly since it is capturing more noise than trends.

The number of retained principal components is also highly connected to the type of analysis that is required. If the model will be used to predict the properties of new materials accurately, more principal components may be required. However, if the model will be used for classification purposes or for the identification of significant input variables (or qualitative analysis) then the number of principal components can be further minimized.

Based on the analysis of the current data set, Figure 2-12 shows the explained variance and cross-validation error values for up to 12 principal components. These have been identified as significant based on the following two criteria: the overall model cross-validation error increases by 1% and the cross-validation error for any specific variable (material property in this case) increases by 5%. This model would be useful for predicting the properties of any new material since its predictive ability is close to 100% and the cross- validation error is also satisfactory (Table 2-1). However, based on the results in Table 2-1, it is observed that the principal components that explain less than 5%

of the variability are not significant and thus the true dimensionality of the problem is approximately 4-5. In addition, only the first two principal components explain more than 10% of the variance. Thus, they are the most significant and can be used to make qualitative conclusions about the data (i.e., which are the most significant variables, or materials properties), even though this model's predictive capability is 57%. This discussion aims to demonstrate the number of principal components required could be different based on the final use of the model.

2.3.3. Identification of the most critical material properties

As discussed above, the first two components capture almost 60% of the variance within the data and are thus sufficient for qualitative analysis. The two-component model was used to identify the most critical properties, that is, the minimum set of properties that retains the same predictive capability as the whole set. The score plot shows the coordinates of each material in the new latent space (Figure 2-13). From this plot, groups of materials that have similar properties, and therefore behavior, can be identified. Several possible groups are observed in the score plot. These groups include two large groups of materials: group 1 consisting of materials 3, 4, 5, 6, 7, 8, 11, 17, 20, 27, and 28 and group 2 consisting of materials 13, 14, 23, and 24. Other possible, smaller groups include materials 1 and 2 located in the lower left corner and materials 20 and 28 in the center-left are of the plot. The score plot is significant for classification of new materials. More specifically, if a new material is characterized and its material properties are measured, its location on the score plot can convey whether the material has similar characteristics with other known materials.

In order to identify the significant material properties in this PCA model, the loadings plot of each principal component is used. The loadings plot for the two-component PCA is shown in Figure 2-14. Properties that are located near the origin do not contribute significantly to either the first or second principal component. Properties that lie on a 45 degree line passing through the origin have loadings that are inversely proportional and the property values are inversely correlated. That is, if one material property value increases for a specific material, then the other property for that material can be expected to decrease. Properties that are closely grouped together on the loadings plot have values that are highly correlated. This implies that if one increases, the other will have the same response. Therefore, it might be sufficient to consider only one of the properties in the model.

From Figure 2-14, it is observed that the stability index, LOI at 1000 C, the flow rate index, and the permeability all fall close to the origin and are therefore not as significant as the other measurements. The properties that lie furthest from the origin are the most influential, such as compressibility index, cohesion, unconfined yield strength, air velocity for permeability, D90 at pressure 1, and conditioned bulk density. The compressibility index and compressibility at 15kPa lie closely together and therefore can be considered highly correlated. The same is observed for bulk density, conditioned density, and tapped density. Only one measurement from each of these pairs is sufficient.

The weighted loadings plot for the retained principal components is also useful, Figure 2-15. This is a bar plot of the loadings (weights) of each variable in each principal component multiplied by the variance explained in each variable by the PCA model. From this plot it is observed that in the first principal component the most significant

material properties are conditioned bulk density and tapped density (which are highly correlated), particle size measurements (correlated except for d90 at pressure 1), compressibility at 15kPa and compressibility index (highly correlated), and basic flowability energy. In the second principal component, the significant material properties are major principal stress, angle of internal friction, unconfined yield stress, air velocity for permeability, and perhaps the relative humidity at the time of testing.

A trial-and-error approach was employed to verify the removal of the previously discussed material properties would not significantly alter the model, using the predictive capability as a metric. For each of the material properties identified as insignificant or highly correlated to another, it was removed from the database and the PCA model was reconstructed. The predictive capability and score plot of the reduced model was then compared to those of the prior model. By performing this procedure, one can identify the minimum set of material properties that is required to characterize the materials and lead the experimenter to the same conclusions as in the original model. Results show that by removing 11 of the 25 material properties completely from the model, the number of significant principal components as well as the score plot remain unchanged (Figure 2-14). Initially, both LOI measurements, Carr index, stability index, flow rate index and permeability were removed as these were observed to have the lowest loadings (Figure 2-14). After verifying that this action did not affect the model the following properties were removed: tapped density (due to its correlation with conditioned bulk density), particle size measurements at pressure 1 (due to their correlation with the remaining particle size measurements), and the compressibility index (due to its correlation with compressibility at 15kPa). The score plot of the new PCA, taking into account all of the

above modifications, is shown in Figure 2-16. It is observed that the same groupings are formed and the same set of materials belong in the same quadrants. Thus, a similar classification of materials can be made using 14 out of the 25 material properties. It is also observed that the confidence intervals of the model are different, however this should not be significant if the goal of the model is to classify materials based on their material properties. Based on the reduced model, the new loadings plot is shown in Figure 2-17. As in Figure 2-14, the measurements that are close to each other are expected to have similar trends for a given material. For example, if cohesion increases, it would be expected that the specific energy and unconfined yield strength would also increase. Using this reduced model, a new material can be characterized and classified with less experimental testing.

2.3.4. Identification of a subset of materials of a given size that retains maximum predictive capabilities

Based on previous analysis, it has been shown that the number of measured powder flow properties can be reduced to 14 of the original 25 measurements without significantly affecting the PCA model. Specifically, this has been shown by removing 11 measurements from the database, reconstructing the PCA model, and then using the model to classify a material that was not included in the database. Results showed that using the reduced model leads to the same classification as when using the full set of measurements. However, in many cases, the amount of testing that can be performed is restricted due to resource shortages (time, money, or materials). Therefore, it is also of interest to determine which material properties maximize the predictive capability and knowledge provided. Here, the case where a maximum of three tests can be performed is considered.

The first step, similar to the prior analysis, was to eliminate the variables that did not contribute significantly or ones that were highly correlated with others. It was identified that, based on the loadings plot in Figure 2-18, the LOI at 1000 C, LOI at 130 C, Carr index, stability index, and permeability, and flow rate index were the closest to the origin implying that their weights are low in both the first and second principal components. Thus, their contribution to the total variability of the model was expected to be negligible. Since most of the variability in the model is explained by the first principal component, properties that only contribute to the second component can also be considered less significant. Here, the relative humidity at the time of testing, the air velocity for permeability, and hopper flow factor all have low contributions to the first principal component. Additionally, some material properties that appear in groups can be removed. There are three main groupings that were observed: 1) compressibility index and compressibility at 15kPa, 2) conditioned bulk density and tapped density, and 3) particle size measurements at pressure 1. Choosing which of these variables to remove is dependent on the methods used to obtain the measurements. Certain test methods may be more expensive, difficult, time consuming, material consuming, or unreliable. In addition, some test methods may yield multiple parameters such that more than one property can be measured using the same test method. For group 1, the compressibility index and compressibility at 15kPa are measured using the same test so either one could be removed from the analysis; here, the compressibility index was selected for removal. For group 2, however, the conditioned bulk density and tapped density are obtained using different methods. Therefore, by removing one of these measurements, the total number of tests required could be reduced. The conditioned bulk density is obtained from the

same test as the compressibility measurements so by removing the tapped density measurement, one fewer test is needed. For group 3, the particle size measurements are all obtained using the same method. Here, the D10 at pressure 1 was kept in the model. The reduced model consists of the 12 remaining material properties, as listed in Table 2-2. Since the purpose of the PCA model is the classification of new materials, the efficiency of the reduced model can be validated using the score plot. Figure 2-19(b) shows the score plot for the reduced model. When compared to the original score plot (Figure 2-19(a)), it is observed that despite small differences, the materials cluster in the similar patterns and appear in the same quadrants of the plot. The reduced model contains 12 properties measured by 5 tests, as opposed to the original model containing 25 properties measured by 10 tests.

In order to further reduce the number of tests to three, the loadings plot (of the reduced model using 12 properties) shown in Figure 2-20 was considered. As previously discussed, loadings that are closely grouped imply that their corresponding variables are highly correlated. Three groupings are observed, shown in Figure 2-20 as groups A, B, and C. The upper-left group (A) contains the major principal stress, angle of internal friction, unconfined yield stress, specific energy, and cohesion. The upper-right group (B) contains basic flowability energy, the particle size measurements, and conditioned bulk density. The lower-left group (C) contains a single property, the compressibility at 15kPa. The compressibility is not correlated with any of the other two groups of measurements and so it should be included in the model. To form the optimal combination of three tests, the other two tests should be chosen out of each of the two remaining groups. From group A, it is observed that four of the five properties are

obtained from a single test. The major principal stress, angle of internal friction, unconfined yield strength, and cohesion are all measured using the shear cell test. Therefore, choosing the shear cell test would maximize the information obtained. From group B, the conditioned bulk density is obtained using the compressibility test, which is already been selected as one of the three final tests. Additionally, three of the particle size measurements at a single pressure can be obtained using a single test. Therefore the three tests that would maximize the information about material flow properties would be the compressibility test, the shear cell test, and the particle size (D10, D50, and D90).

2.4. Conclusions

Material properties can have a significant impact on process performance and, ultimately, final product quality. As such, it is critical to understand how variation in raw materials, and therefore blends, propagate throughout a manufacturing process. Raw material properties should be studied in concert with the process such that the measurements of the most suitable material characteristics are made. The material properties and the methods by which to characterize them have been discussed here. A statistical method (principal component analysis) has been introduced as a method to identify the most relevant material properties for a given purpose. In the case studied here, it was determined that the number of measurements can be reduced to 14 from 25 while retaining the same amount of predictive capability. In the case where only three characterization tests may be performed, it was determined that the compressibility test, shear cell test, and particle size measurements would optimize the information obtained.

2.5. Figures for Chapter 2

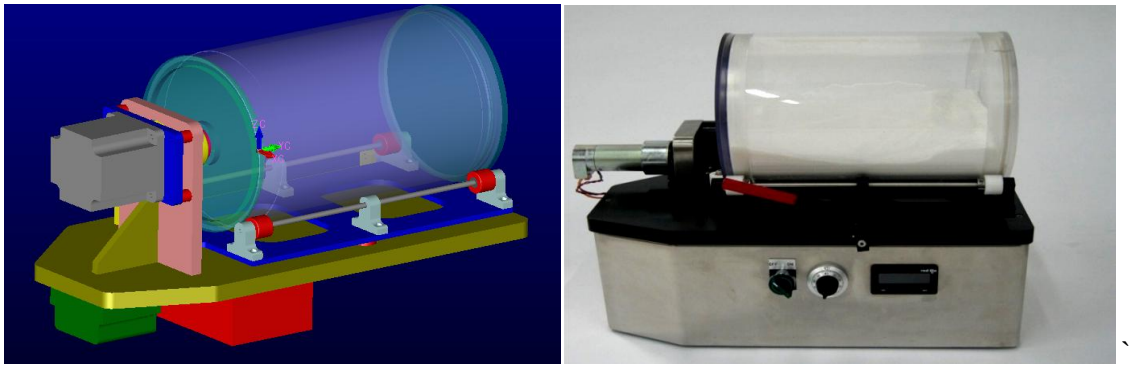

Figure 2-1: Schematic (left) and image (right) of the GDR experimental setup

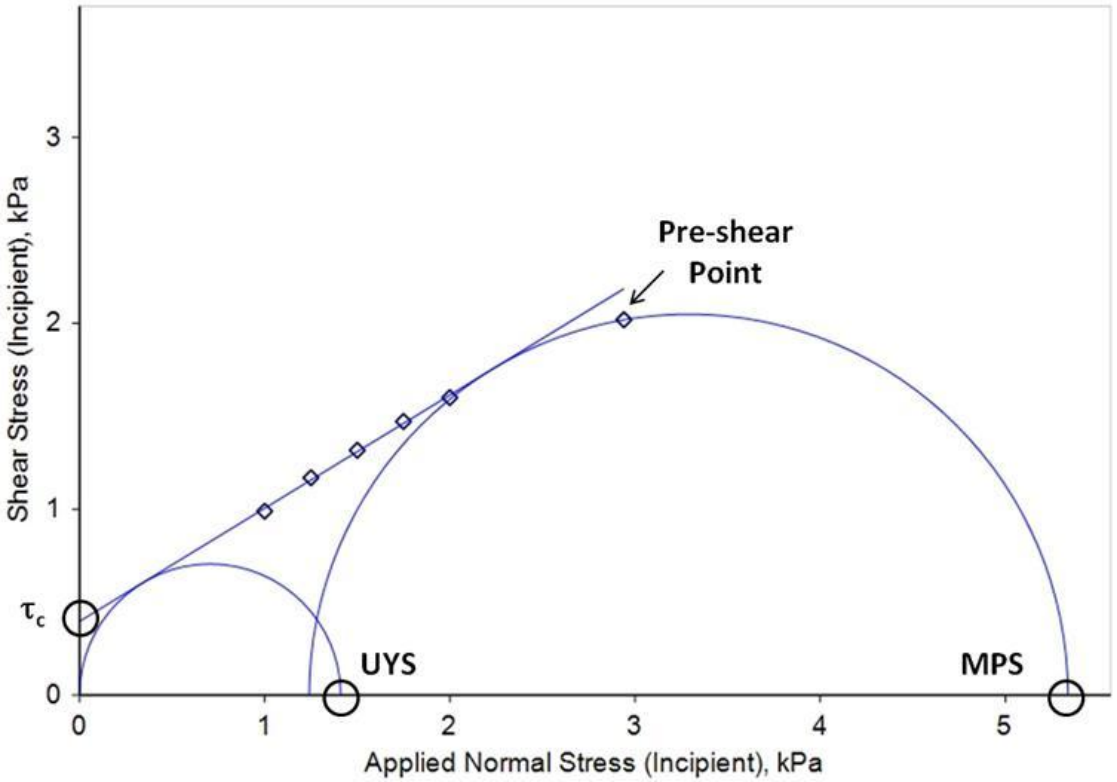

Figure 2-2: Yield locus with best-fit line and Mohr circles is shown. τ_c is the cohesion, UYS is the unconfined yield stress, and MPS is the compacting stress

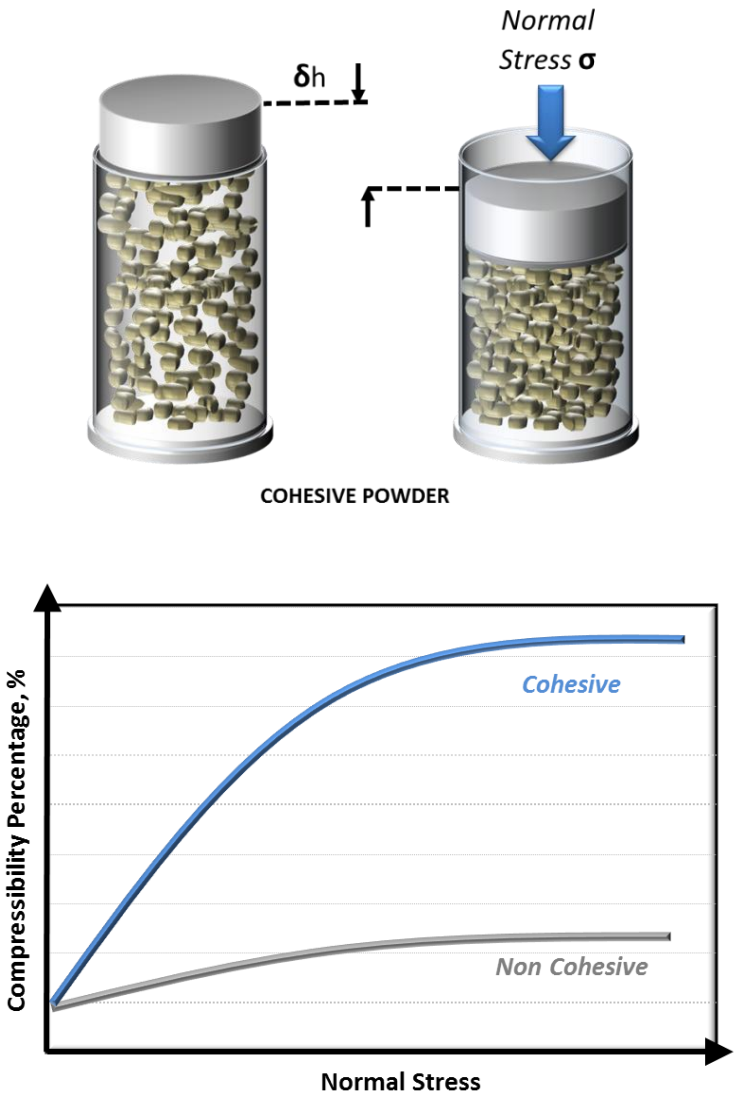

Figure 2-3: Courtesy of Freeman Technology, Inc (reprinted with permission). Schematic of compressibility test (left) and qualitative sample raw data obtained from compressibility test (right).

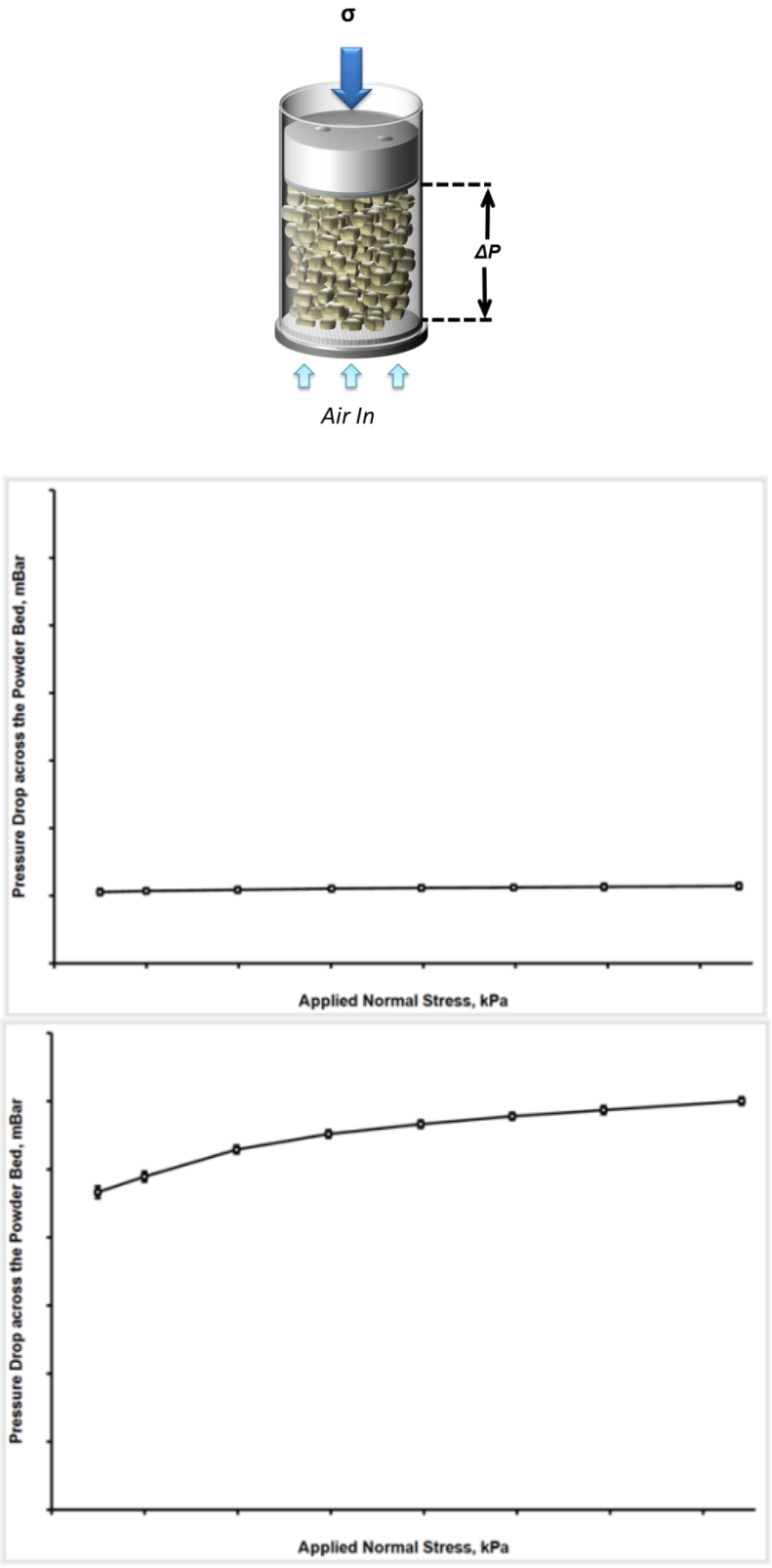

Figure 2-4: Courtesy of Freeman Technology, Inc (reprinted with permission). Schematic of permeability test (top) and qualitative sample raw data obtained (center and bottom).

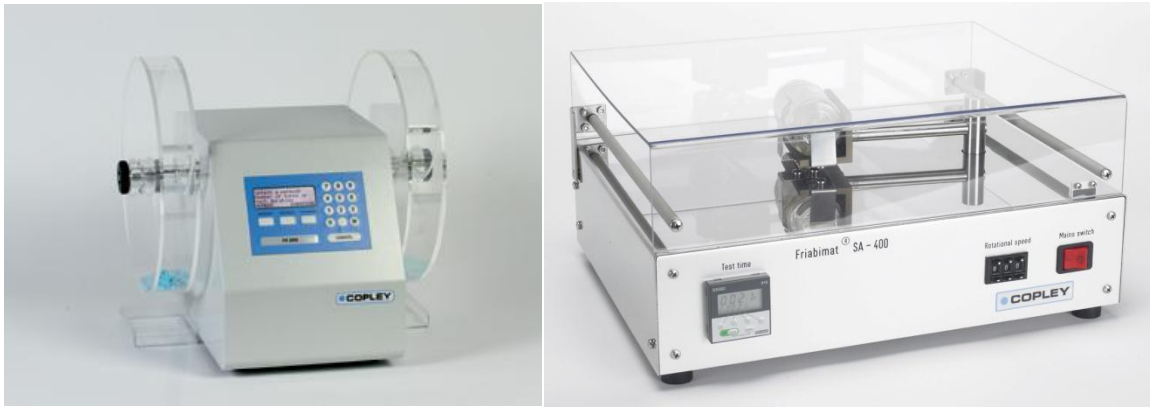

Figure 2-5: Courtesy of Copley Scientific (reprinted with permission). A Friabilator and Friabimat SA-400 used for friability testing.

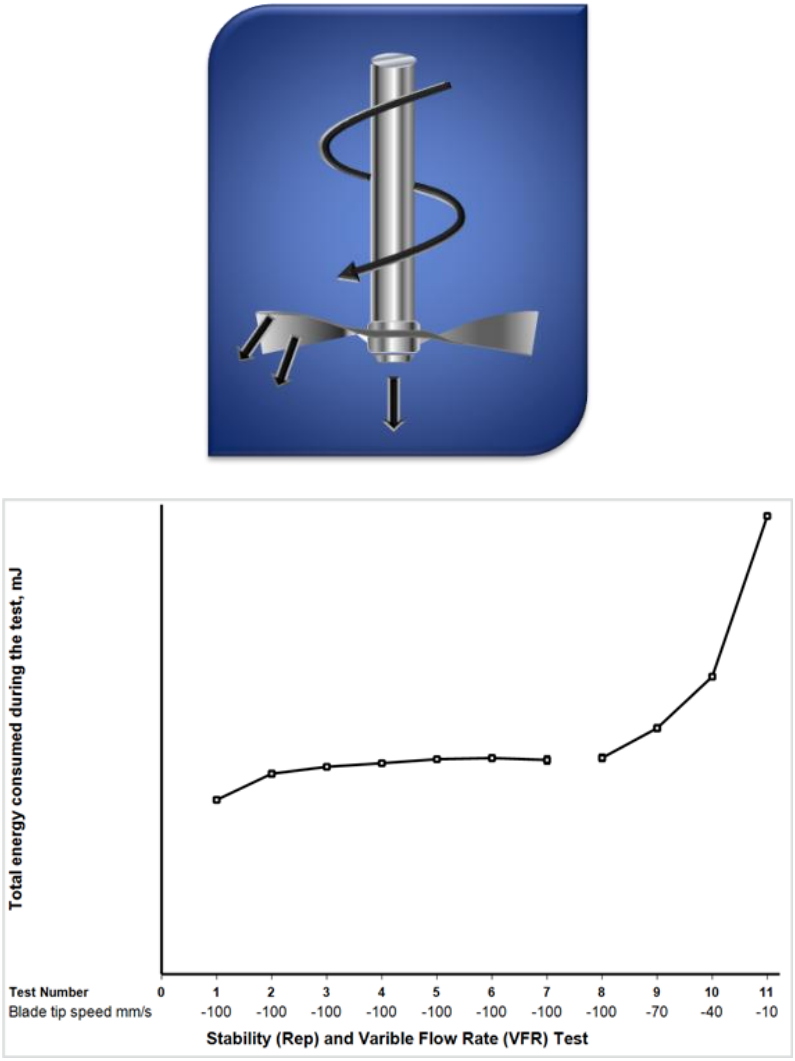

Figure 2-6: Courtesy of Freeman Technology, Inc (reprinted with permission). Schematic of helical blade pattern (top) and sample data obtained from the FT4 dynamic test (bottom).

Figure 2-7: Experimental setup of the hydrophobicity procedure

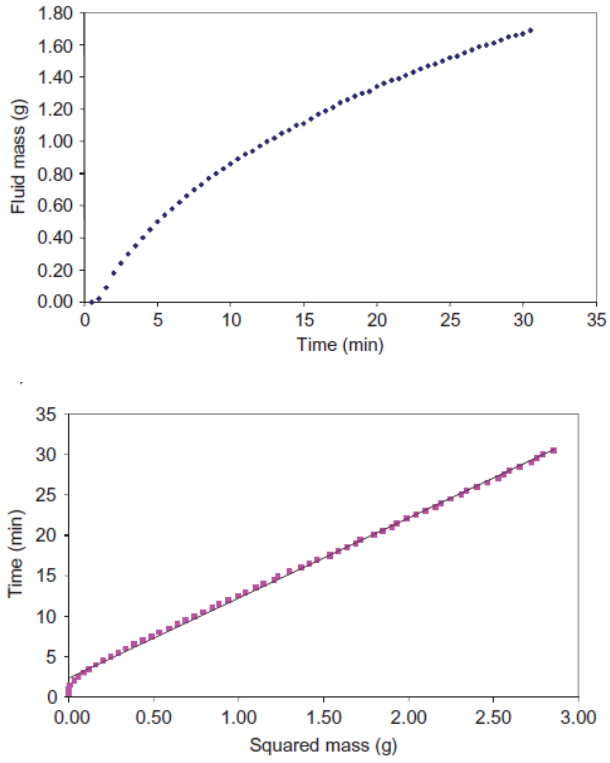

Figure 2-8: Data gathered from scale (top) and the representation of the data used to calculate the hydrophobicity (bottom)

Figure 2-9: Avicel 101 sticking to a gravimetric feeder during flow.

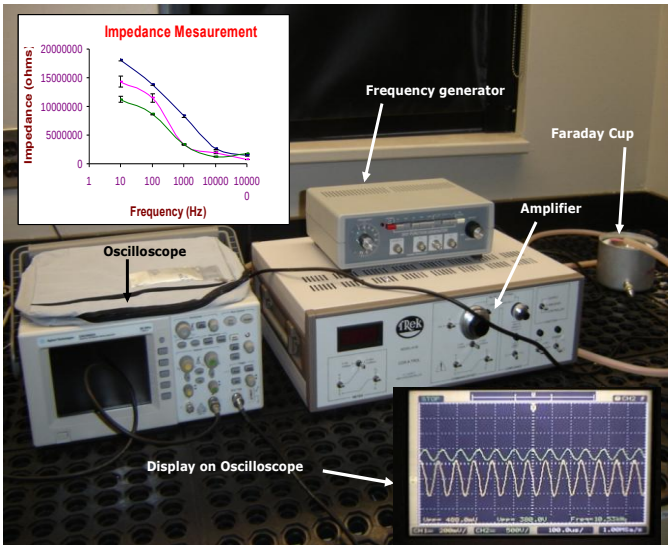

Figure 2-10: Experimental setup of the impedance measurement including sample oscilloscope data.

Figure 2-11: Experimental setup of the Jenike Sifting Segregation Tester

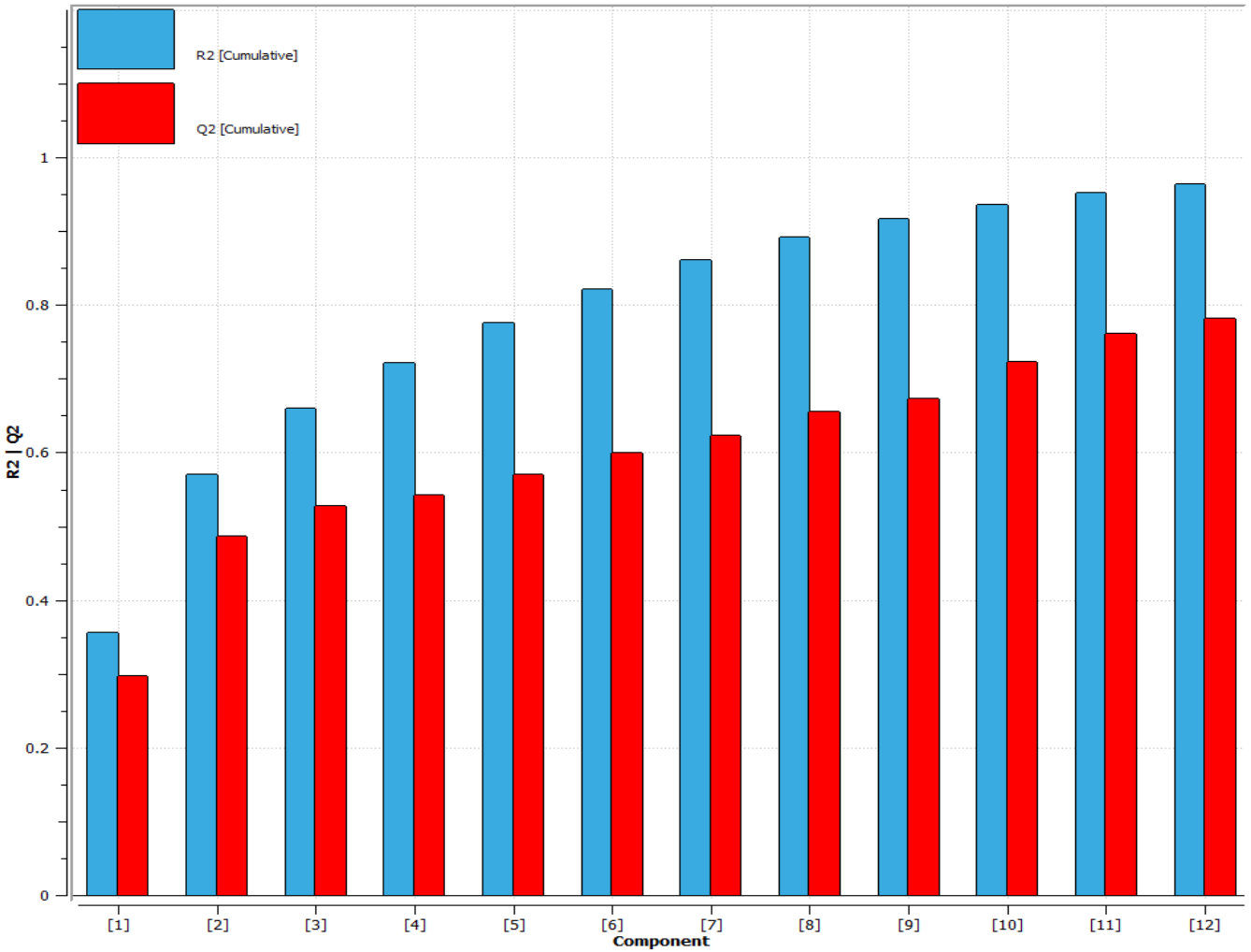

Figure 2-12: Model summary based on 12 principal components

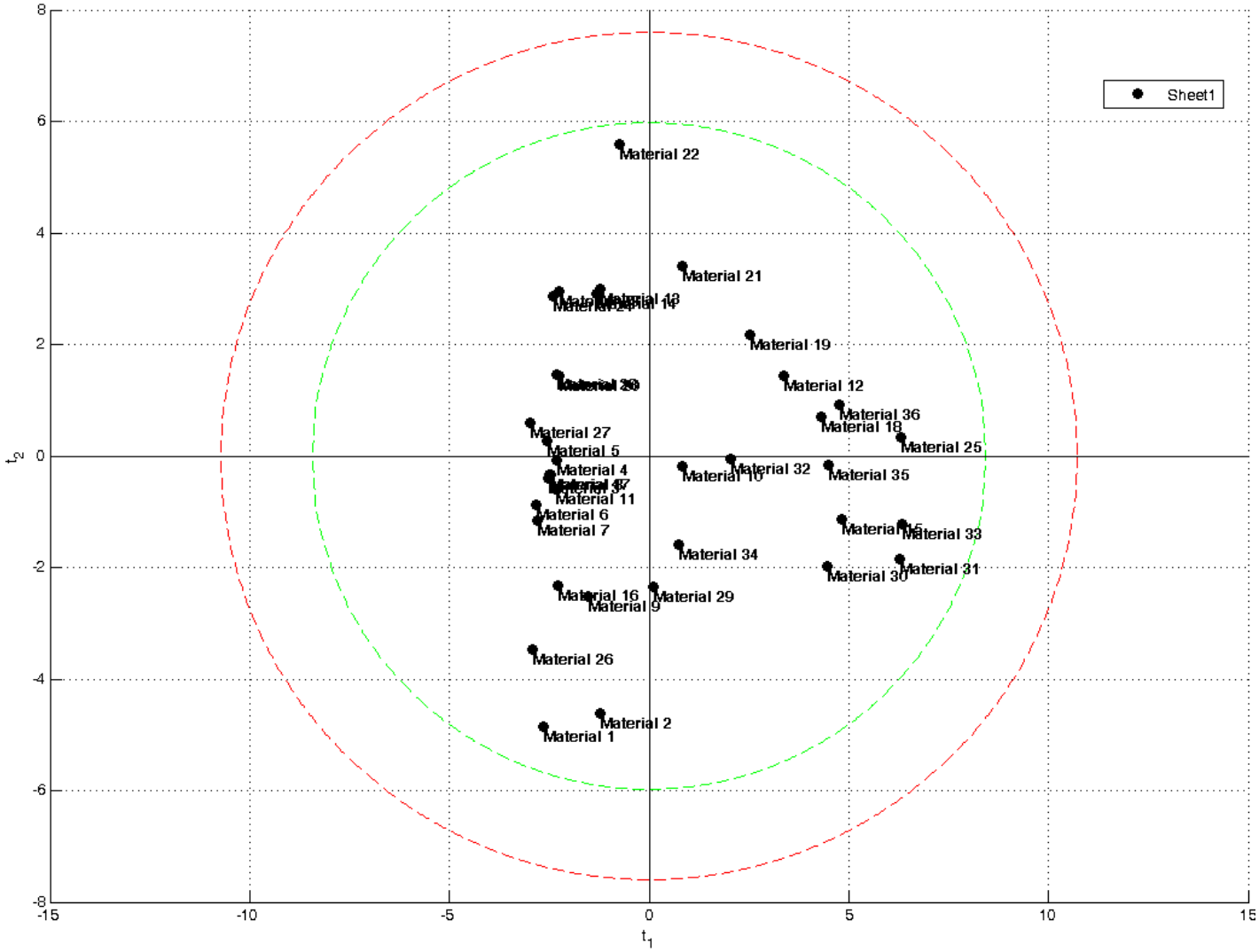

Figure 2-13: Score scatter plot of database with 36 materials

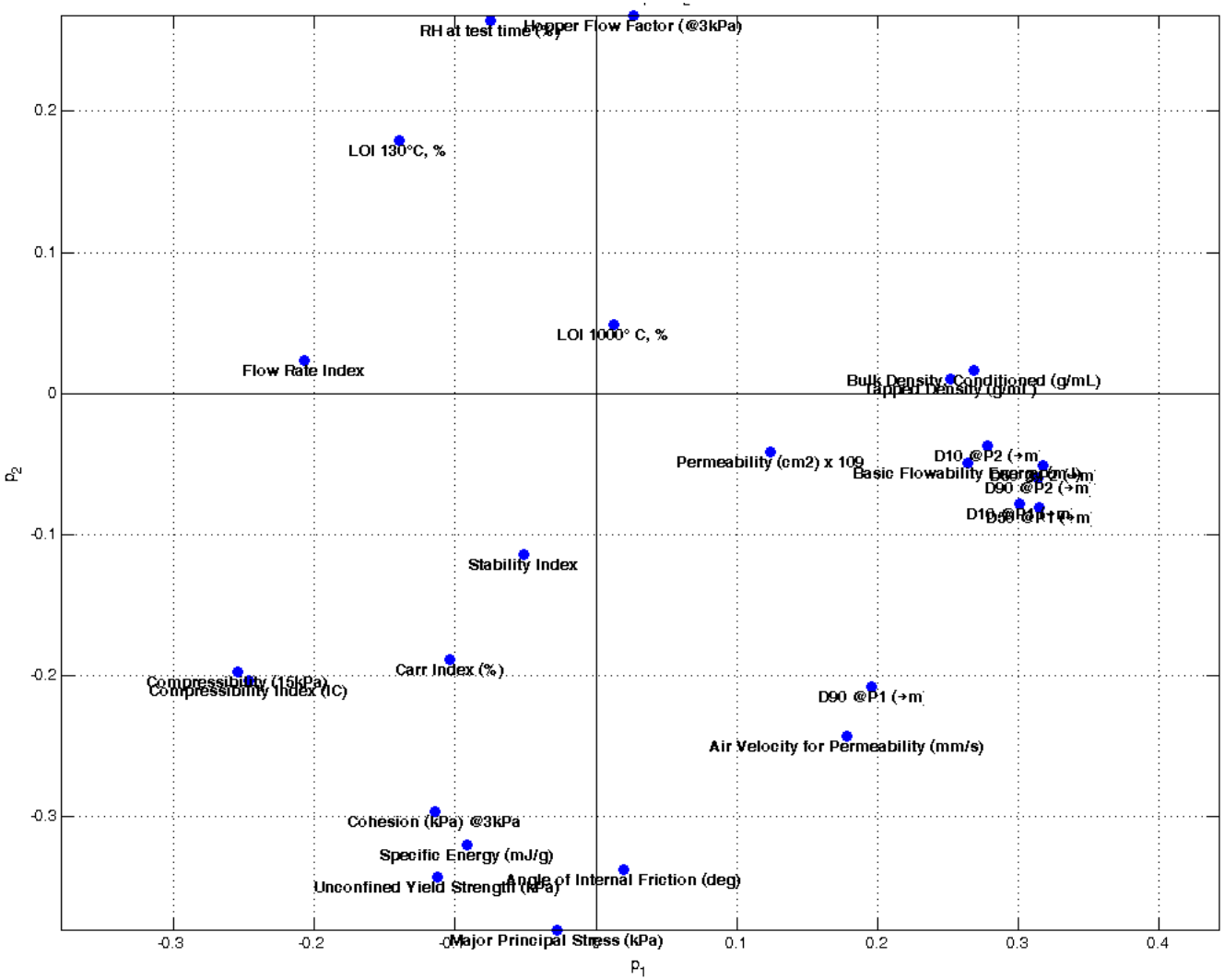

Figure 2-14: Loadings scatter plot

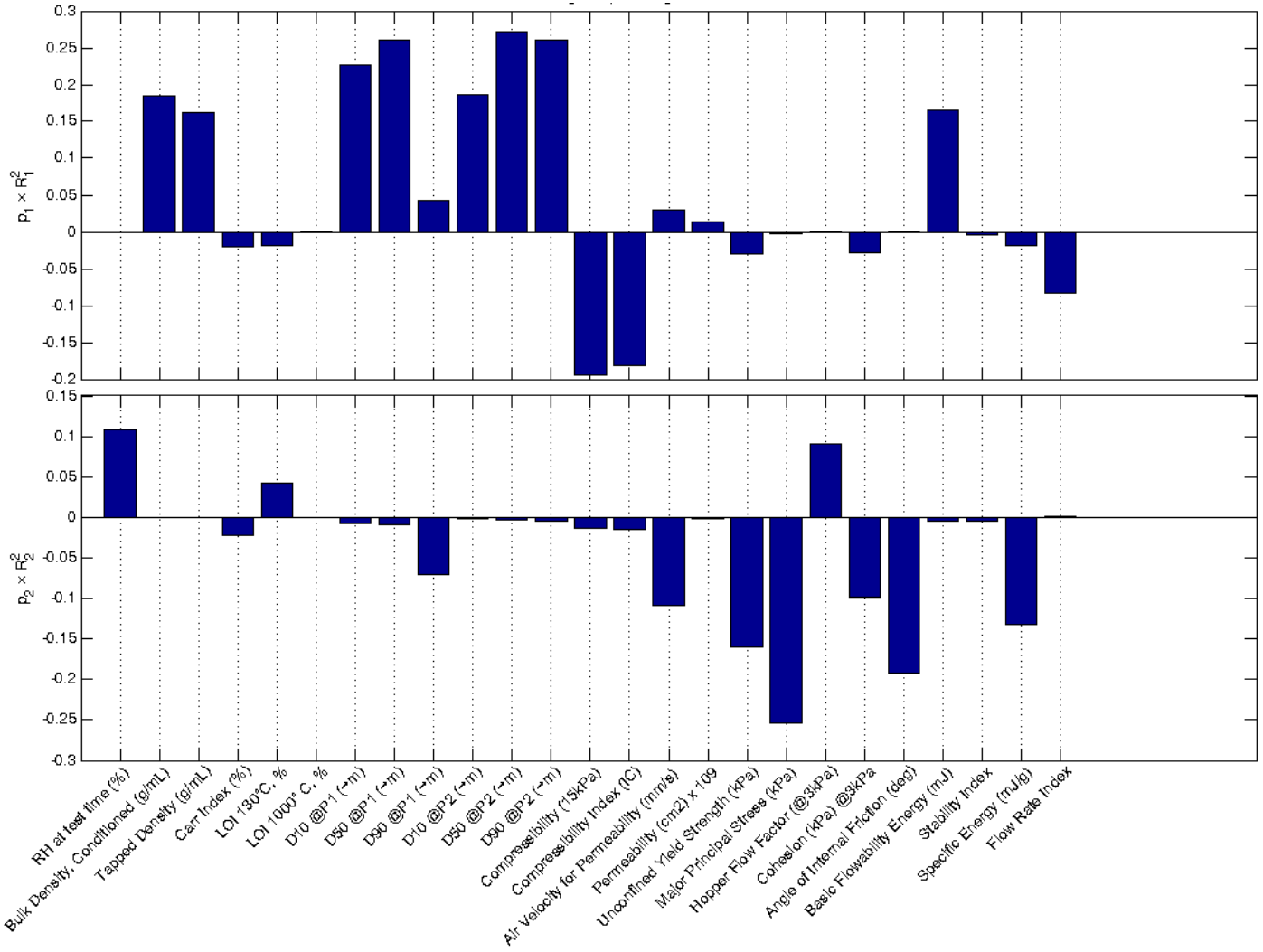

Figure 2-15: Weighted loadings for principal components 1 and 2

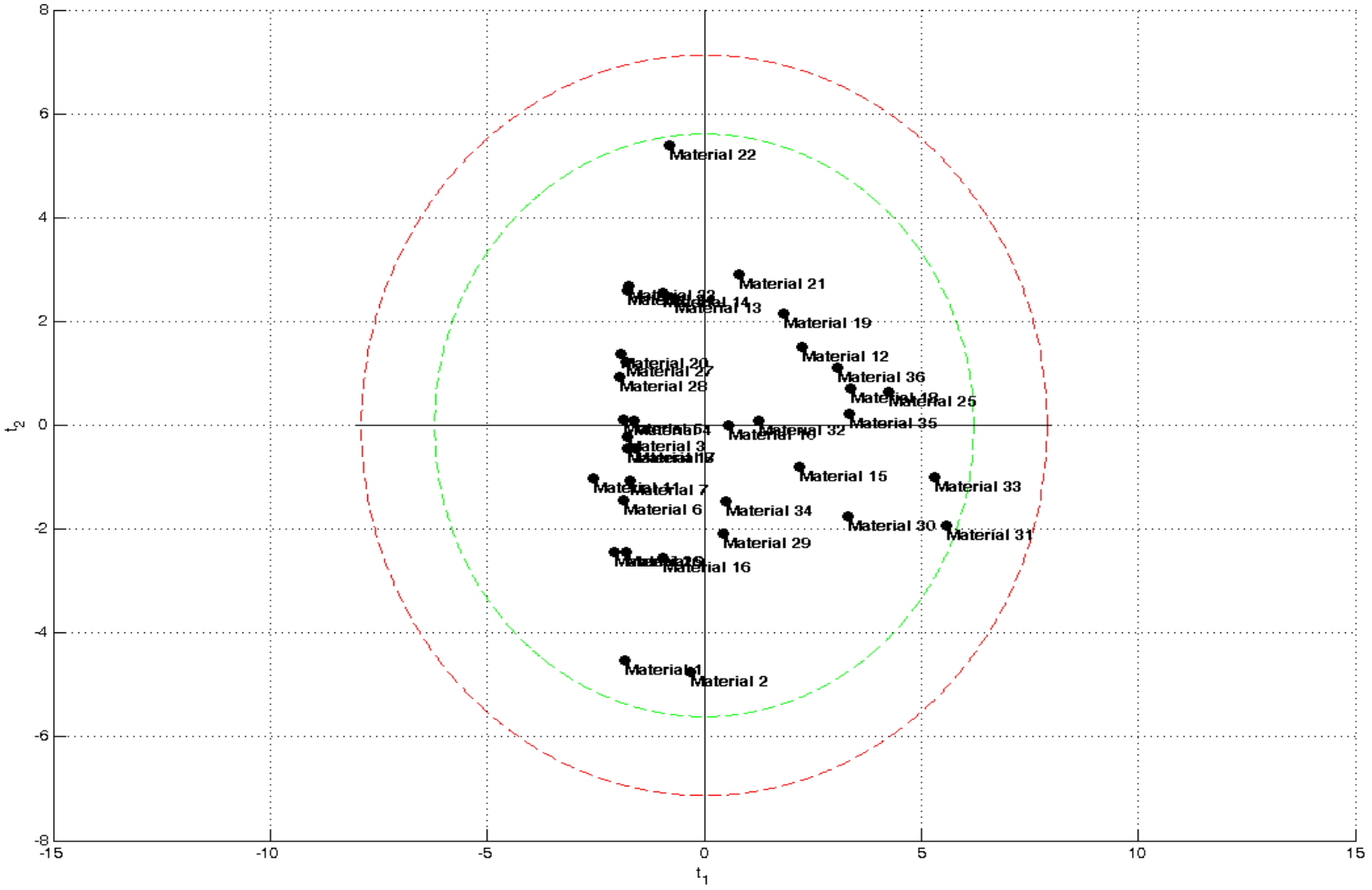

Figure 2-16: Score plot for reduced model (14 properties)

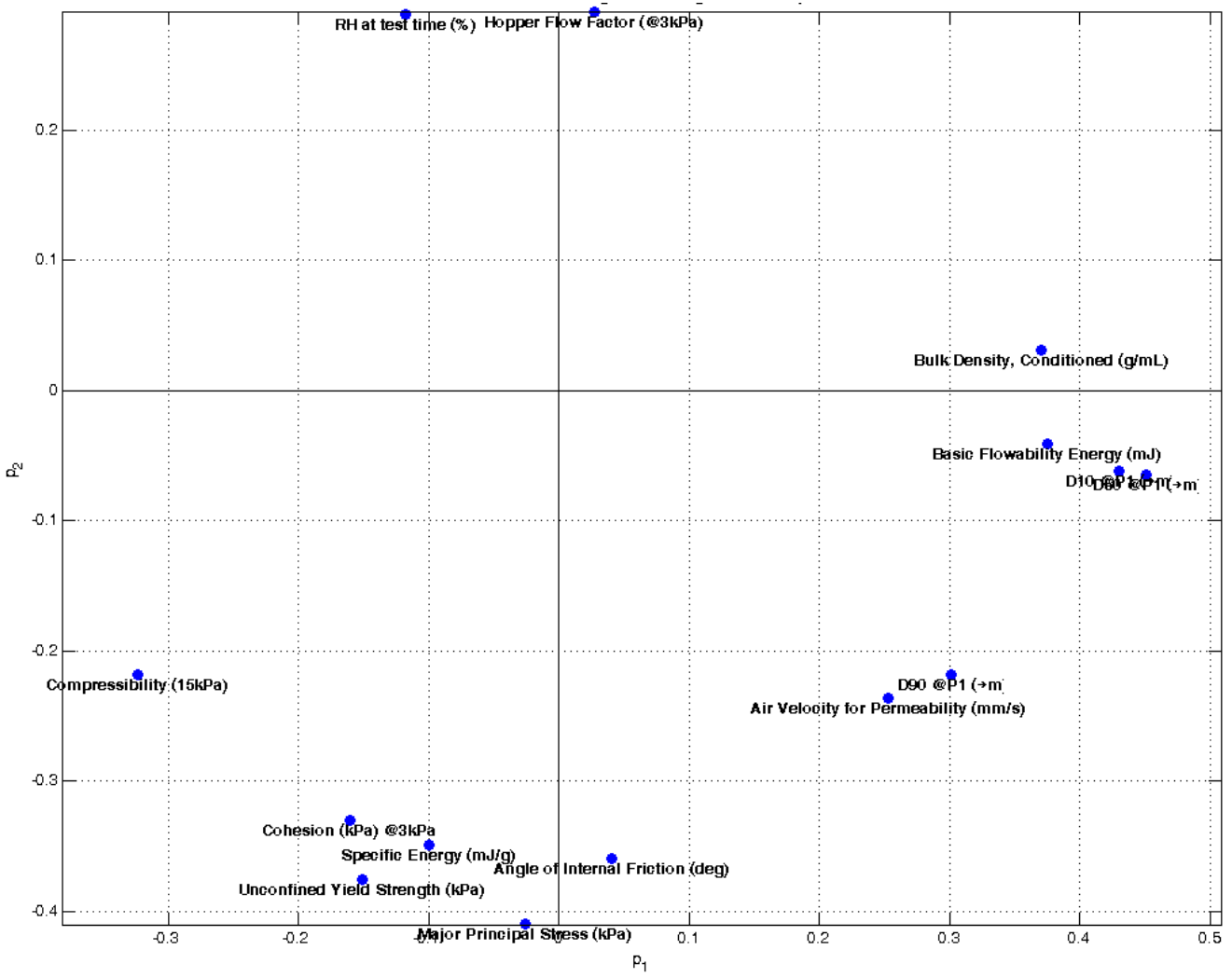

Figure 2-17: Loading scatter plot for reduced model (14 properties)

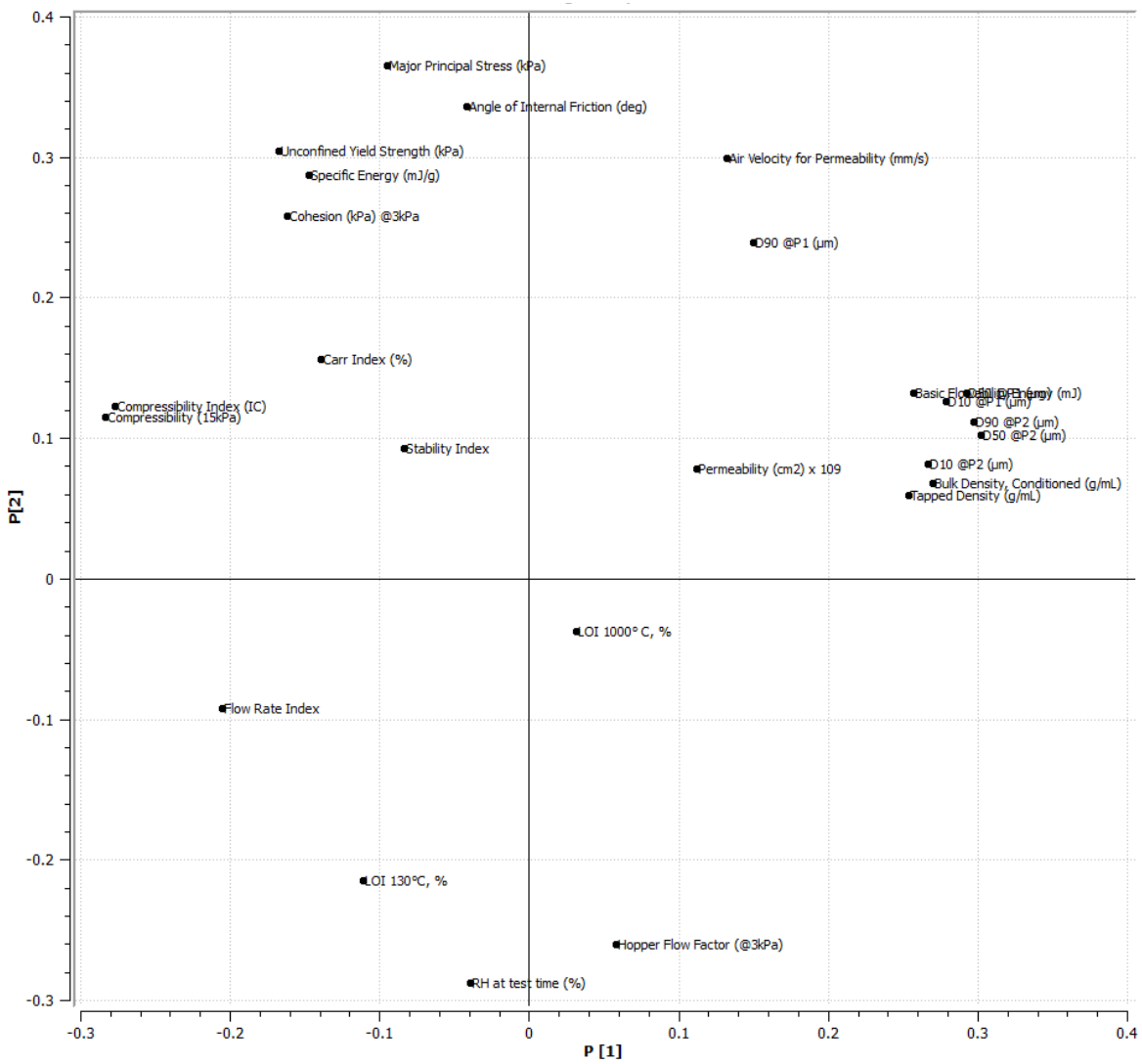

Figure 2-18: Loadings plot (25 properties)

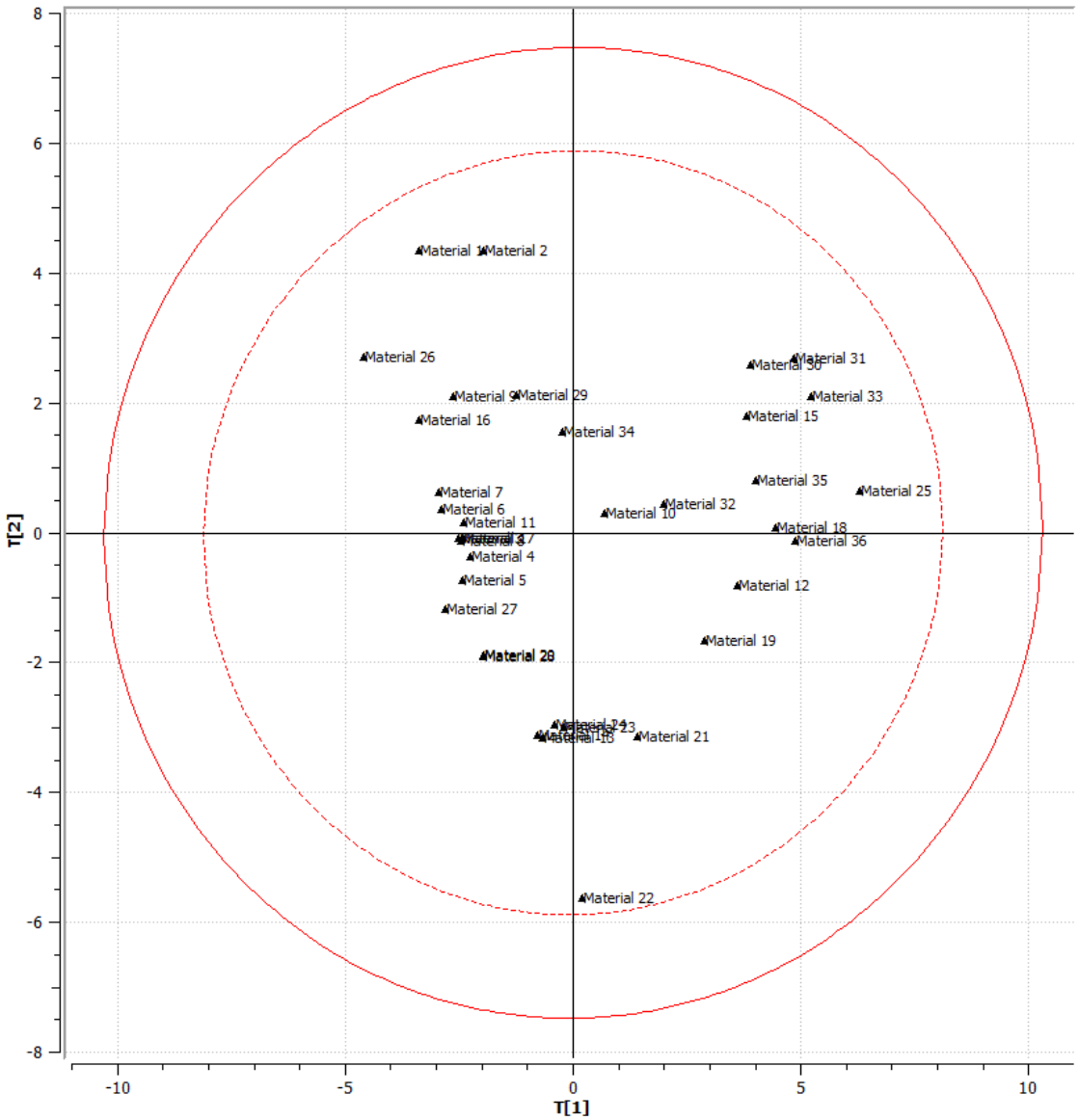
8
6
4
2
0
-2
-4
-6
-8
T[2]
-10
-5
0
5
10
T[1]
Material 1
Material 2
Material 26
Material 31
Material 30
Material 9
Material 29
Material 33
Material 16
Material 15
Material 34
Material 35
Material 7
Material 25
Material 32
Material 6
Material 10
Material 11
Material 18
Material 36
Material 4
Material 5
Material 12
Material 27
Material 19
Material 28
Material 21
Material 22

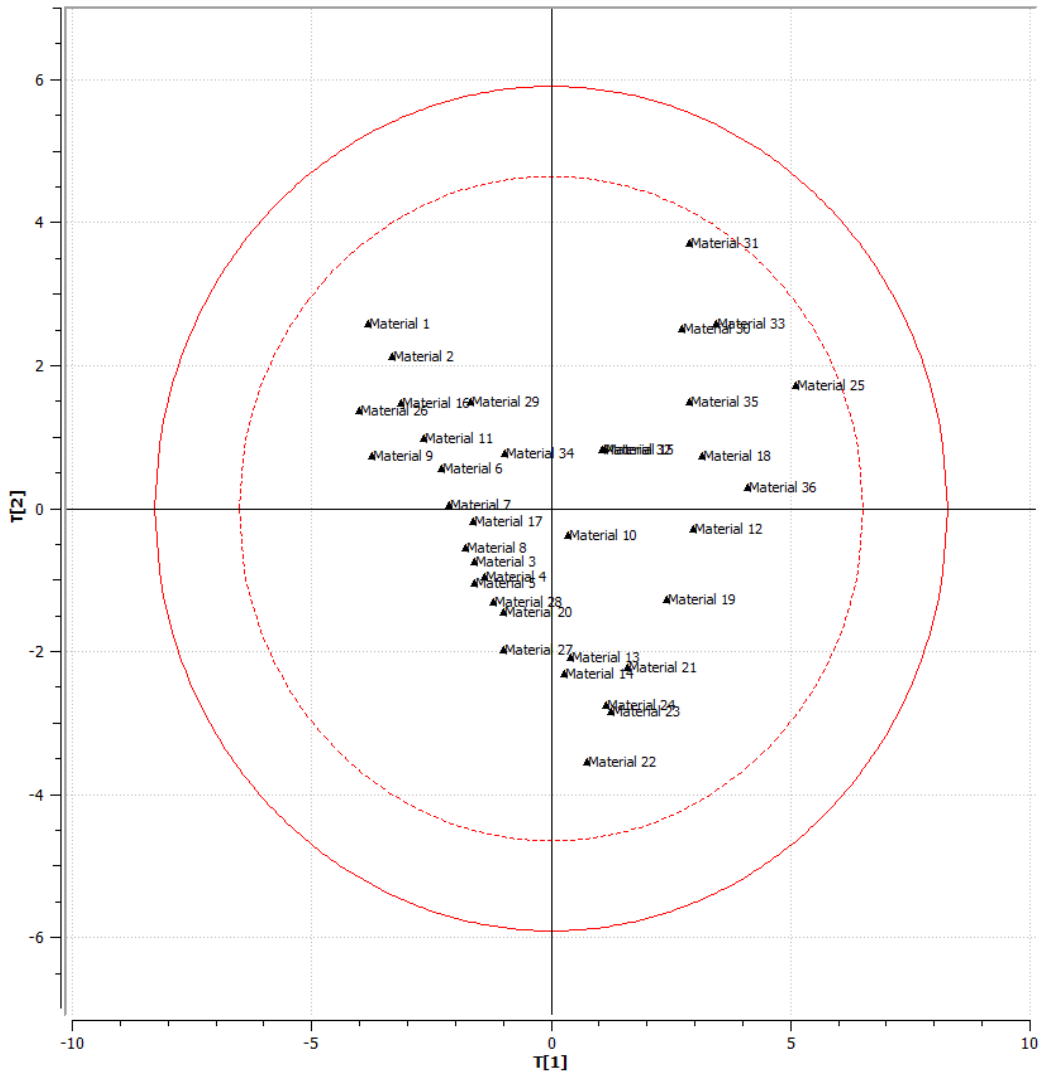

Figure 2-19: Score plot for a) full model (top) and b) reduced model based on 12 properties (bottom)

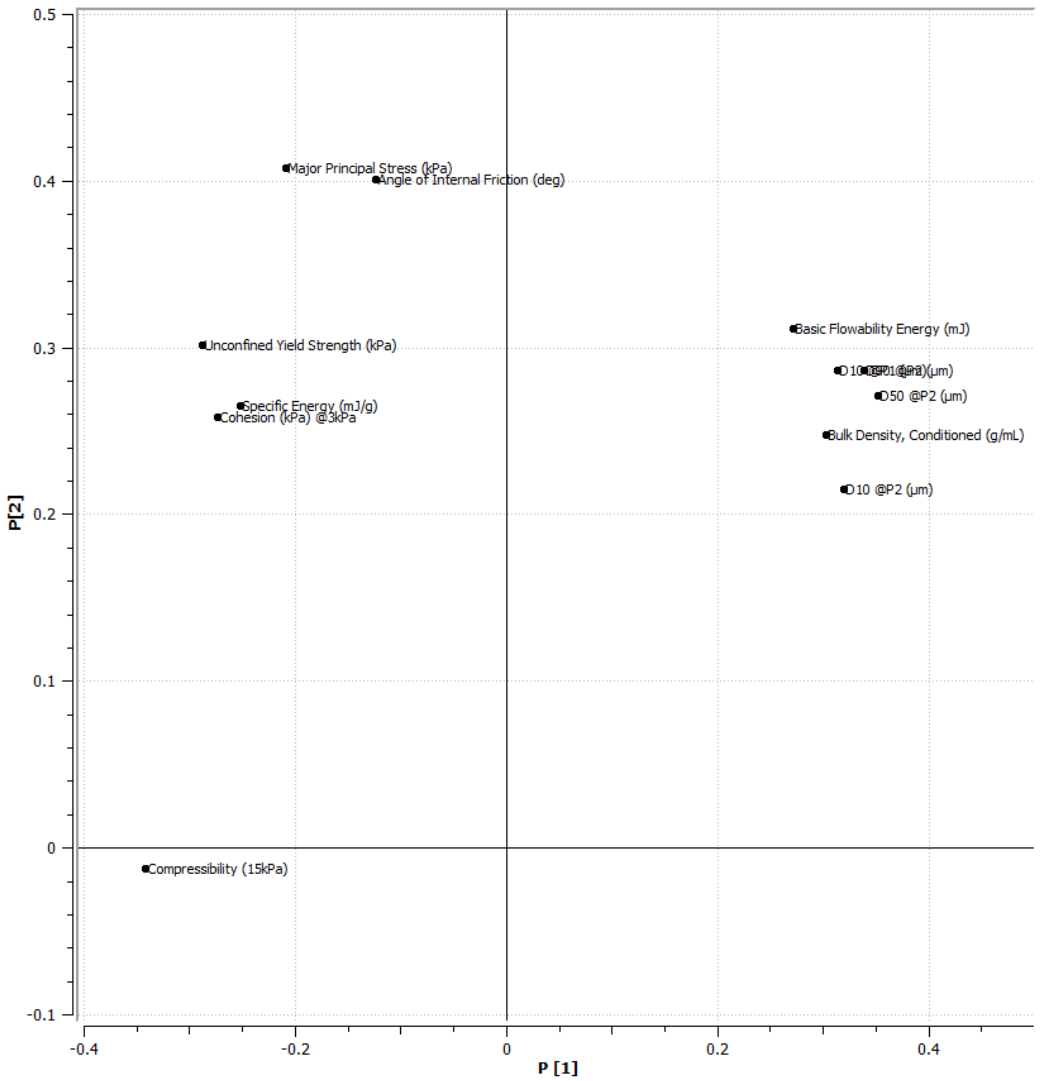

Figure 2-20: Loadings for reduced model (12 properties)

2.6. Tables for Chapter 2

Table 2-1: Variance explained and cross-validation error for the 12 principal component model

#PC	R2 (cum)	Q2	R2% (individual)
1	0.355021	0.296624	35.50
2	0.570569	0.486772	21.55
3	0.659524	0.527078	8.90
4	0.720901	0.542427	6.14
5	0.775121	0.569328	5.42
6	0.820993	0.599051	4.59
7	0.860902	0.622776	3.99
8	0.892112	0.654577	3.12
9	0.916657	0.67285	2.45
10	0.936077	0.722045	1.94
11	0.952463	0.760252	1.64
12	0.963491	0.781248	1.10

Table 2-2: Input variables for reduced model (12 material properties)

Variables contained in reduced model
Bulk Density, Conditioned (g/mL)
D_{10} @P1 (µm)
D_{10} @P2 (µm)
D_{50} @P2 (µm)
D_{90} @P2 (µm)
Compressibility (15kPa)
Unconfined Yield Strength (kPa)
Major Principal Stress (kPa)
Cohesion (kPa) @3kPa
Angle of Internal Friction (deg)
Basic Flowability Energy (mJ)
Specific Energy (mJ/g)

Chapter 3. Comparison of three rotational shear cell testers: powder flowability and bulk density

3.1. Introduction

The shear cell testing methodology was originally developed by A.W. Jenike for the specific application of designing hoppers and silos from the principles of solid state mechanics [24]. Shear cells are now commonly used to rank granular materials according to their flowability [17]. The shear cell can also be used to measure the bulk density of a material as a function of applied normal stress. The bulk density of a material is indicative of a material's flowability and the degree to which the material may expand or consolidate under various conditions occurring during manufacturing [65, 66]. The bulk density, defined as the ratio of the mass of powder sample to the volume of that powder sample, takes into account both the particle density as well as the packing of the powder bed [67]. From a series of shear tests, the angle of internal friction, the angle of wall friction, the slope of the hopper walls, and other design parameters can be extracted.

This methodology has since been more generally applied in the field of powder characterization. Powder flowability characterization has become so prevalent that international standards detailing the procedure have been defined [62, 100]. Many studies have been conducted involving the shear cell [77, 101]. Much of this work has been focused on determining whether shear cell measurements are applicable to specific situations [41, 60]. In addition, changes in various aspects of the procedure (ones not dictated by the standards) have been studied [63].

However, while a number of different shear cells are available commercially, there is only a limited amount of published work that compares the measurements of a particular

shear cell parameter between different types of shear testers. One such study by Pillai *et al.* compared an on-line wall friction tester and the Jenike wall friction tester. It was found that while some quantitative differences between the yield loci measured by the two testers were observed, each tester gave the same general trends [64]. Schulze has performed a round robin study of RST-XS and RST-01.pc shear cells using limestone CRM-116. Similar results were observed for the two shear cells, 30 and 900 mL in volume [102]. In comparison, our understanding of fluid rheological measurement has progressed to the point that we can readily expect that rheological measurements using a particular rheometric device will agree with those from another rheometric device. However, many unanswered questions remain as to whether powder flowability measurements performed in one shear cell would agree with measurements of the same powder in a different shear cell. Considering how common it is to measure powder flow properties in shear cells, we believe that it is important to answer these questions.

This chapter examines the effect of consolidation stress and tester type on eight responses measured using the shear cell: cohesion, unconfined yield stress, major principal stress, pre-shear stress, flow function coefficient, bulk density, effective angle of internal friction, and angle of internal friction. Three different shear cells were used. The effect of shear cell tester (differing in cell size and geometry) and initial consolidation stress on the results obtained from each shear cell were studied to determine if results from various shear cells measured under a range of experimental conditions are equivalent or, on the alternative, whether they are significantly different. The rest of the chapter is organized as follows. The materials characterized and the three shear cell testers studied are described. The results of the eight responses are discussed in the Results section. The

results include statistical analysis used in determining the statistical significance of the material, consolidation stress, and tester factors. It was found that each of these factors was generally statistically significant. Therefore, the results from shear cell tests executed under varying initial consolidation stresses using various shear cells should be compared only with caution.

3.2. Materials and Methods

3.2.1. Materials

Two materials, a cohesive and a free-flowing powder, were used in this study. These materials were two grades of γ-alumina supplied by Albemarle (Amsterdam, The Netherlands). The particle size distributions of the powders were measured using a Beckman-Coulter LS 13 320 series laser diffraction particle size analyzer (Pasadena, CA, USA) and are shown in Figure 3-1. The coarse grade had a d_{10} of 11 microns, a d_{50} of 59 microns, and a d_{90} of 122 microns. The fine grade had a d_{10} of 1 micron, a d_{50} of 4 microns, and a d_{90} of 11 microns.

3.2.2. Methods

3.2.2.1. Procedure

The standard shear cell procedure involves three steps: pre-compaction of the powder bed, pre-shearing of the powder bed until steady state flow is achieved (where the bulk density is constant), and shearing until the powder yields. The pre-shearing/shearing process is repeated 4-5 times using normal stresses that are from 20% to 80% of the consolidation stress. The result of the above process is a yield locus (see Figure 3-2). The yield locus is fit with a best-fit line that is extrapolated to the y-axis. This corresponds to the shear stress at zero normal stress, or cohesion, τ_c. The angle that the best-fit line creates with the x-axis is the angle of internal friction.

In addition, Mohr circle analysis is performed on the yield locus. Mohr circle analysis is a geometric representation of a coordinate transformation to identify the principal stresses. Two circles are used. The first goes through the origin and is tangent to the best-fit line through the yield locus. This circle represents the conditions present at the free surface of an arch (as is present in hopper flow) and represents the conditions for critical failure. The second circle is tangent to the yield locus and passes through the pre-shear (steady state flow) point. This circle represents the conditions for the critical state. The principal stresses extracted from this analysis are called the unconfined yield stress, UYS, and the compacting stress (major principal stress, MPS), as shown in Figure 3-2. The effective yield locus passes through the origin and is tangent to the greater Mohr circle. The angle that the effective yield locus creates with the x-axis is the effective angle of internal friction.

The yield locus is measured at several initial consolidation stresses and the unconfined yield stress and compacting stress are extracted from each yield locus. The unconfined yield stress - compacting stress pairs are plotted from each yield locus to give the flow function. The slope of the flow function indicates how well a powder flows.

The bulk density of the powder bed is also measured at each initial consolidation stress. The bulk density of a material is indicative of a material's flowability and the degree to which the material may expand or consolidate under various conditions occurring during manufacturing [65, 66]. As discussed previously, the bulk density, defined as the ratio of the mass of powder sample to the volume of that powder sample, takes into account both the particle density as well as the packing of the powder bed [67].

3.2.2.2. Commercially available shear cells used in this study

The RST-XS (Dietmar Schulze, Wolffenbuttel, Germany), FT4 (Freeman Technology, Tewkesbury, Gloucestershire, UK), and PFT (Brookfield Engineering Laboratories, Inc., Middleboro, MA, USA) shear cells were studied. The software related to each shear cell was used to derive the yield locus and flow properties. The Brookfield software included shearing data at the initial consolidation stress, while the FT4 and Schulze did not. Each of these shear cells are rotational, as opposed to translational, in nature. However, there are differences in procedure and cell attributes such as cell geometry and sample size. The measurement procedure of the three shear cells is different with respect to the initial steps of consolidation and pre-shearing repetitions. The similarities and differences of the shear cell attributes are highlighted in Figure 3-3 and Table 3-1. The Schulze and Brookfield shear cells use an annular, or ring, cell geometry (see Fig 3-3 center and right). The FT4 shear cell utilizes the entire circular area (see Fig 3-3 left). The FT4 and the Brookfield both measure torque directly while the Schulze measures force on attached tie rods. The Schulze and Brookfield both measure the applied normal force at the top of the powder bed while the FT4 measures this at the bottom of the powder bed. Each shear cell has the capability to test a range of sample sizes. For the purposes of this study the following sample sizes were used: 30mL vessel in the Schulze, 43mL vessel in the Brookfield, and 85mL vessel in the FT4. The heights of the powder bed once loaded into the vessels are 14mm, 43mm, and 23mm for the Schulze, FT4, and Brookfield shear cells, respectively.

The distribution of the applied normal force through the powder sample, and therefore at the shear plane, should greatly impact the shear cell results. Unlike fluids, when normal force is applied to a confined granular material, some of the force is converted to shear

stress and is transmitted to the walls as such. The dependence with depth of stress within a powder bed is different from that of a fluid. Shear stress at the walls is directly proportional to the normal stress within the powder bed. The three shear cells have a more than three-fold range in powder bed heights. This could result in differences in the applied normal forces acting on the particles at the shear plane. During testing, normal force is incremented until the desired value is obtained. The FT4 measures the applied normal force on the powder bed via a load cell located underneath the sample vessel. This is potentially different than the measurements taken at the top of the powder bed when using the Schulze and Brookfield shear cells. The applied normal forces measured by the FT4 have been subjected to losses due to transmission of shear stress to the vessel walls while those measured using the Schulze and Brookfield shear cells have not. Methods have been proposed for calculating the actual normal stress at the shear plane, e.g. the approach inspired by Janssen and illustrated by Bruni *et al*. [103]and Tomasetta *et al.* Therefore, the normal forces applied to the powder bed by the FT4 may not be directly comparable to those applied by the Schulze and Brookfield shear cells. Moreover, the magnitude of this difference could depend on the type of powder.

3.2.2.3. Experimental approach

The purpose of this study was to determine if the Schulze, FT4, and Brookfield shear cells give statistically similar or different results, and, if not, the magnitude of the differences. Each of the three shear cells was used to characterize each of the two materials at three initial consolidation stresses common to all shear cells (3, 6, and 9kPa).

3.3. Results and Discussion

3.3.1. Yield Loci, flow functions, and bulk density profiles

Typical data obtained using shear cells are yield loci, flow functions, and bulk density profiles. The yield locus for the coarse alumina for an initial consolidation stress of 3kPa is shown in Figure 3-4 for the Schulze, FT4 and Brookfield shear cells. Corresponding results for the fine alumina are shown in Figure 3-5. For a given initial consolidation stress, the applied normal stresses at which the yield points are measured are similar for each of the shear cells. The error bars represent the standard deviation of three repeated measurements. The error bars are generally smaller than the size of the symbols in Figures 3-4 and 3-5. The yield loci corresponding to the fine grade of alumina (Fig. 3-5) lie above those for the coarse grade of alumina (Fig. 3-4) especially at smaller normal stresses. This was expected, as the fine grade of alumina is known to have poor flowability, which is indicative of higher cohesion. As described in Section 2, the cohesion parameter is the y-intercept of the best fit line through the yield locus. There are more observable differences between the results of the different shear cells for the fine alumina (Fig. 3-5) as compared to the coarse alumina (Fig. 3-4). In particular, for the fine alumina (Fig. 3-5) the Schulze values lie systematically above those of the FT4 and Brookfield shear cells. Figures 3-6 and 3-7 show results for the coarse and fine alumina respectively, for an initial consolidation stress of 6 kPa. As before, the results for coarse alumina for the different shear cells are visually very similar (Fig. 3-6). For the fine alumina (Fig. 3-7), the Schulze values again lie systematically above those of the FT4 and Brookfield shear cells. Results for an initial consolidation stress of 9 kPa are then shown in Figure 3-8 and 3-9. At a consolidation stress of 9 kPa, the coarse alumina exhibits differences between the results for the different shear cells (Fig. 3-8) with the Schulze values lying systematically above those of the FT4 and the Brookfield shear

cells. Similar behavior is observed for the fine alumina at 9kPa (see Fig 3-9). We will return to these comparisons through use of statistical tools to quantify the differences between the different shear cells.

Best-fit lines through the yield loci were computed in order to determine the cohesion parameter, the y-intercept of the yield locus. The cohesion parameter calculated for the coarse and fine grade of alumina is shown in Figures 3-10 and 3-11, respectively. The cohesion values for the coarse grade of alumina range from near zero to about 0.2 kPa and appear to be relatively independent of initial consolidation stress, indicative of a freely-flowing material. The cohesion values for the fine grade of alumina range from about 0.4 to 1.0 kPa. In addition, there is a strong dependence on the initial consolidation stress: the material's cohesion increases with increasing initial consolidation stress. These higher values of cohesion and dependence on initial consolidation stress typically correspond to cohesive, poorly flowing materials.

As detailed in Section 2, flow functions were constructed using the unconfined yield stress and major consolidating stress. These parameters were obtained under initial consolidation loads of 3, 6, and 9 kPa. The resulting flow functions are depicted in Figure 3-12. There are six flow functions, one for each material and shear cell combination. The flow functions appear in two groups, one corresponding to each material. Direct inspection of the results shows that the variability between materials is larger than the variability between the different shear cells. The flow functions for the fine alumina have a higher slope than those for the coarse grade of alumina. This was expected, since it is known that the fine grade of alumina is more cohesive and flows more poorly. While all three shear cells give similar flow functions for the fine alumina,

the flow functions of the coarse grade of alumina appear to have some differences according to shear cell type. However, it is important to note that shear cells perform poorly in general for free-flowing powders. Shear cells can be used to identify a material as free-flowing, but shear cells should not be used to rank materials within the free-flowing regime [17]. Therefore, it can be concluded that the three shear cell types perform similarly since each one identifies the coarse grade of alumina as a free-flowing powder.

The bulk density profiles were also measured, as detailed in Section 2 Materials and Methods. These profiles are depicted in Figure 3-13. There are six bulk density profiles, one for each material and shear cell combination. The profiles, similar to the flow functions, appear in two groups corresponding to each material. The variability between materials is visually larger than the variability between testers. Again, this is expected as the test was intended to distinguish between materials. It is also observed that the tester type appears to introduce more variability to the bulk density response than the unconfined yield stress and major principal stress responses. It should be noted that the bulk density profiles of the two materials measured using the FT4 shear cell appear to decrease between 3 and 6 kPa. This is contrary to the expectation that the bulk density should increase with increasing applied normal stress. There are alternative methods for measuring the bulk density that may give results that are more accurate, such as ASTM D6683 and measuring the bulk density directly in the shear zone [104].

3.3.2. The variance in the responses

In order to appropriately assess the variability in responses between testers, the individual variability within each tester must be understood. This was achieved by analyzing the

repeatability of the measurements at each condition. Eight responses were considered for each of the 18 combinations of shear cell (3), initial consolidation stress (3), and material (2): cohesion, unconfined yield stress (UYS), major principal stress (MPS), flow function coefficient (FFC), steady-state/pre-shear point, bulk density, effective angle of internal friction, and angle of internal friction. The yield locus, pre-shear point, and bulk density were measured for each of the 18 conditions in either duplicate or triplicate. The cohesion, UYS, MPS, FFC (the ratio of MPS to UYS), effective angle of internal friction, and angle of internal friction were calculated from each measurement.

The average response was calculated for each condition. This average served as a predicted value. Each individual measurement was compared to the corresponding average. This comparison, after normalizing such that the maximum value for each response is 1, is shown in Figure 3-14. A tight distribution centered on the y=x axis is indicative of a repeatable measurement. This was quantified using a coefficient of determination, R^2. The R^2 of the best-fit line through the predicted versus measured values for each of the six responses were calculated, Table 3-2. The R^2 values for each of the responses indicated a good fit with all but one, FFC, having a value greater than 0.95. There are five outliers: one of the flow function coefficient (FFC) responses of the coarse material measured at an initial consolidation stress of 3 kPa using the Brookfield shear cell, two of the pre-shear stress responses of the coarse material measured at an initial consolidation stress of 6 kPa using the Schulze shear cell, and two of the major principal stress responses for the coarse material measured at an initial consolidation stress of 6 kPa using the Schulze shear cell. Each of the outliers corresponds to coarse material measurements. As discussed, the shear cell method is less suited for free-flowing

materials, such as the coarse grade of alumina used here. As a result, measurements of free-flowing materials are more likely to have a higher degree of variability and propensity to include outliers. As detailed in Section 2, the major principal stress is based, in part, on the pre-shear point. Therefore, any variability or noise in the pre-shear point measurement is propagated to the major principal stress.

3.3.3. Statistical analysis

Statistical analysis, using ANOVA methods, was used to verify that the material had a statistically significant effect on the shear cell responses. In addition, ANOVA was used to determine if the initial consolidation stress and shear cell type significantly affected the shear cell responses. However, a portion of the cohesion responses for the coarse material using the Brookfield shear cell tester had negative values. This is an artifact of the extrapolation of the best-fit line through the yield loci to the y-axis and has no physical meaning. Further, a negative cohesion value results in an undefined unconfined yield stress value. As can be observed from Figure 3-15, it is not possible to form a circle that passes through the origin and is tangent to the best-fit line. Further still, this results in an undefined flow function coefficient. Typically, when this occurs, the cohesion is reported as zero. This results in an unconfined yield stress value of zero, but the flow function coefficient remains undefined as the value approaches infinity. However, using this approach in conjunction with statistical analysis introduces artificially “good” data. Multiple values of zero have no variability. Since the ANOVA compares the variance to the means of the data, this adversely affects the results of the statistical analysis. To address this artifact, for this study, these results were not included in the statistical analysis. The block of coarse material measurements using the Brookfield shear cell were removed from the analysis. Without this block of data, the overall experimental

design was unbalanced. To simplify the analysis, the remaining data were analyzed in three experimental design configurations. The first DOE consisted of two materials, two testers (Schulze and FT4), and three initial consolidation stresses. The second DOE consisted of one material (the cohesive, fine grade of alumina), three testers, and three initial consolidation stresses. The third DOE consisted of one material (the free-flowing, coarse grade of alumina), two testers (Schulze and FT4), and three initial consolidation stresses.

3.3.3.1. Design of experiments

The first DOE retained both materials in the design so that the effect of the material can be compared to the effect of the other factors (the initial consolidation stress and shear cell type). The design was balanced by removing the Brookfield shear cell data block. The design consisted of three factors with two or three levels each: material (cohesive or free-flowing), shear cell type (Schulze and FT4), and initial consolidation stress (3, 6, and 9kPa).

Considering the removal of the coarse material measured by the Brookfield shear cell from the analysis, in order to compare all three of the shear cells, the coarse material was removed from the second DOE altogether. The design had two factors with three levels each: shear cell type (Schulze, FT4, and Brookfield) and initial consolidation stress (3, 6, and 9kPa).

The first DOE considered both materials and the second DOE solely considered the cohesive material. The third DOE considered solely the free-flowing material. To balance the DOE the Brookfield shear cell data block was removed. The design

consisted of two factors with two or three levels: shear cell type (Schulze and FT4) and initial consolidation stress (3, 6, and 9kPa).

3.3.3.2. ANOVA results

The measurements of the eight responses (cohesion, unconfined yield stress, major principal stress, pre-shear point, flow function coefficient, bulk density, effective angle of internal friction, and angle of internal friction) are analyzed using each of the three designs of experiment detailed above. The p-value for each factor and interaction was calculated using ANOVA. A factor with a p-value of less than 0.05 was considered statistically significant. The relative magnitude of the effects was determined by omega-squared. The omega-squared of each effect was calculated by:

$$\omega^2 = \frac{SS_{effect} - (DF_{effect} * MS_{error})}{SS_{total} + MS_{error}}$$

where SS_{effect} was the sum of squares of the effect, DF_{effect} was the degrees of freedom of the effect, MS_{error} was the mean square of the error, and SS_{total} was the total sum of squares. An orthogonal contrast was performed using Scheffe's method.

3.3.3.2.1. Cohesion

The ANOVA and omega squared results for the cohesion parameter are tabulated in Table 3-3 and the orthogonal contrast results in Table 3-4. These tables illustrate the structure of the results. The ANOVA and Scheffe contrast tables for each response are similarly structured. All three main factors, as well as the shear cell type/initial consolidation stress, were statistically significant in each of the three experimental designs. The initial consolidation stress/ material interaction was statistically significant in the analysis of the first DOE. In the first and second DOEs, where the effect of the

initial consolidation stresses was statistically significant, results for each stress were statistically different from one another. In the third DOE, the initial consolidation stress of 9 kPa was statistically different from the 3 and 6 kPa results. The results at 3 and 6 kPa were not statistically different. From the analysis of the first DOE (retaining two materials), the material had the largest effect on the cohesion parameter. From the second DOE (retaining only the cohesive material), the initial consolidation stress had the largest effect on the cohesion parameter. From the third DOE (retaining only the free-flowing material), the shear cell type and initial consolidation stress had comparable effect magnitudes.

3.3.3.2.2. Unconfined yield stress

The ANOVA and omega squared results for the unconfined yield stress parameter are tabulated in Table 3-5 and the orthogonal contrast results in Table 3-6. Each main factor was statistically significant in each of the three designs of experiment with one exception. The shear cell type was found to be not statistically significant in the analysis of the first DOE. The shear cell type/ material and initial consolidation stress/ material interactions were statistically significant in the analysis of the first DOE. The shear cell type/ initial consolidation stress interaction was statistically significant in the analysis of the third DOE. In each of the DOEs, each of the three initial consolidation stresses was statistically different from one another. From the analysis of the first DOE, the one retaining both materials, the material had the largest effect on the unconfined yield stress. From the second DOE, the one retaining the cohesive material, the initial consolidation stress had the largest effect on the unconfined yield stress. From the third DOE, the one retaining the free-flowing material, the shear cell type, initial consolidation stress, and the interaction factor had similar effect magnitudes.

3.3.3.2.3. Major principal stress

The ANOVA and omega squared results for the major principal stress parameter are tabulated in Table 3-5 and the orthogonal contrast results in Table 3-6. Each main factor was statistically significant in each of the three designs of experiment. The shear cell type/ material and initial consolidation stress/ material interactions were statistically significant in the analysis of the first DOE. The shear cell type/ initial consolidation stress interaction was statistically significant in the analysis of the first and third DOEs. In each of the three DOEs, each of the three initial consolidation stresses was statistically different from one another. In the second DOE, the Schulze shear cell was statistically different from the FT4 and Brookfield shear cells. The results obtained using the FT4 and Brookfield shear cells were not statistically different from each other. From the analysis of each of the DOEs, the effect with the largest magnitude was the initial consolidation stress.

3.3.3.2.4. Pre-shear point

The ANOVA and omega squared results for the pre-shear point are tabulated in Table 3-5 and the orthogonal contrast results in Table 3-6. Each factor, including the shear cell type/ initial consolidation stress interaction, was statistically significant in each of the three designs of experiment. The shear cell type/ material and initial consolidation stress/ material interactions were statistically significant in the analysis of the first DOE. In each of the three DOEs, each of the three initial consolidation stresses was statistically different from one another. In the second DOE, the Schulze shear cell was statistically different from the FT4 and Brookfield shear cells. The results obtained using the FT4 and Brookfield shear cells were not statistically different from each other. From the

analysis of each of the DOEs, the effect with the largest magnitude was the initial consolidation stress.

3.3.3.2.5. Flow function coefficient

The ANOVA and omega squared results for the flow function coefficient are tabulated in Table 3-5 and the orthogonal contrast results in Table 3-6. Each factor, including the shear cell type/ initial consolidation stress interaction, was statistically significant in each of the three designs of experiment with one exception. The shear cell type was found to be not statistically significant in the analysis of the second DOE. The shear cell type/ material and initial consolidation stress/ material interactions were statistically significant in the analysis of the first DOE. In the second DOE, each of the three initial consolidation stresses was statistically different from one another. In the first and third DOE, the initial consolidation stress of 3kPa was statistically different from the 6 and 9 kPa results. The results at 6 and 9kPa were not statistically different. From the analysis of the first DOE, the one retaining two materials, the material had the largest effect on the flow function coefficient. From the second DOE, the one retaining the cohesive material, the initial consolidation stress had the largest effect on the flow function coefficient. From the third DOE, the one retaining the free-flowing material, the initial consolidation stress had the largest effect, but the shear cell type and interaction factor also had moderate effect magnitudes.

3.3.3.2.6. Bulk density

The ANOVA and omega squared results for the bulk density are tabulated in Table 3-5 and the orthogonal contrast results in Table 3-6. Each factor, including the shear cell type/ initial consolidation stress interaction, was statistically significant in each of the three designs of experiment with one exception. The shear cell type was found to be not

statistically significant in the analysis of the third DOE. The shear cell type/ material and initial consolidation stress/ material interactions were statistically significant in the analysis of the first DOE. In the first and third DOE, the initial consolidation stress of 3kPa was statistically different from the 6 and 9 kPa results. The results at 6 and 9kPa were not statistically different. In the second DOE, the initial consolidation stress of 9kPa was statistically different from the 3 and 6kPa results. The results at 3 and 6kPa were not statistically different. In the second DOE, the FT4 shear cell type was statistically different from the Schulze and Brookfield results. The Schulze and Brookfield results were not statistically different. From the analysis of the first DOE, the one retaining two materials, the material had the largest effect on the bulk density. From the second DOE, the one retaining the cohesive material, the shear cell type had the largest effect on the bulk density. From the third DOE, the one retaining the free-flowing material, the initial consolidation stress had the largest effect, but the interaction factor also had a moderate effect magnitude.

3.3.3.2.7. Effective Angle of Internal Friction

The ANOVA and omega squared results for the effective angle of internal friction are tabulated in Table 5 and the orthogonal contrast results in Table 6. Each main factor was statistically significant in each of the three designs of experiment. The shear cell type/ initial consolidation stress was statistically significant in the analysis of the first and third DOEs. The initial consolidation stress/ material interaction was statistically significant in the analysis of the first DOE. In the first and second DOE, each of the initial consolidation stresses was statistically significant from each other. In the third DOE, the initial consolidation stress of 9kPa was statistically different from the 3 and 6kPa results. The results at 3 and 6kPa were not statistically different. In the second DOE, the Schulze

shear cell was statistically different from the FT4 and Brookfield shear cells. The results obtained using the FT4 and Brookfield shear cells were not statistically different from each other. From the analysis of the first DOE, the one retaining two materials, the material had the largest effect on the effective angle of internal friction, but the shear cell type and initial consolidation stress also had moderate effect magnitudes. From the analysis of the second DOE, the one retaining the cohesive material, the shear cell type and initial consolidation stress had the largest effects with similar effect magnitudes. From the analysis of the third DOE, the one retaining the free-flowing material, the shear cell type had the largest effect on the effective angle of internal friction, but the initial consolidation stress and the shear cell type/ initial consolidation stress interaction also had moderate effect magnitudes.

3.3.3.2.8. Angle of Internal Friction

The ANOVA and omega squared results for the effective angle of internal friction are tabulated in Table 5 and the orthogonal contrast results in Table 6. Each factor, including the shear cell type/ initial consolidation stress interaction, was statistically significant in each of the three designs of experiment. The shear cell type/ material and initial consolidation stress/ material interactions were statistically significant in the analysis of the first DOE. In the first DOE, the initial consolidation stress of 9kPa was statistically different from the 3 and 6kPa results. The results at 3 and 6kPa were not statistically different. In the second DOE, the initial consolidation stress of 3kPa was statistically different from the 6 and 9kPa results. The results at 6 and 9kPa were not statistically different. In the third DOE, each of the three initial consolidation stress was statistically different from one another. In the second DOE, each of the three shear cell types was statistically different from one another. From the analysis of each of the DOEs, the shear

cell type had the largest effect on the angle of internal friction. From the analysis of the first DOE, the one retaining two materials, the material also had a moderate effect magnitude. From the analysis of the second DOE, the one retaining the cohesive material, the initial consolidation stress also had a moderate effect magnitude. From the analysis of the third DOE, the one retaining the free-flowing material, the initial consolidation stress and shear cell type/ initial consolidation stress interaction also had moderate effect magnitudes.

3.3.3.3. Overall observations

The objective of the above statistical analysis was to determine if the material, initial consolidation stress, and shear cell type significantly affects shear cell measurements. As previously discussed, it was expected that the material would have a significant effect. In fact, this was indeed the case. For each of the eight responses considered, the ANOVA of the first DOE showed that the material effect was statistically significant. For the materials studied here, this indicates that each of the shear cells used can differentiate between a cohesive and free-flowing material. Each shear cell provides the same flowability ranking of the materials.

For each of the eight responses considered, in each of the DOEs, the initial consolidation stress applied to the powder bed was found to be statistically significant. The flowability of the powder bed is dependent upon the consolidation state of the material. This result is consistent with previous findings regarding the sensitivity of bulk properties to the density and consolidation state of the powder [15]. The flow function is often assumed to be linear. One common exception is at low stresses, where the yield loci curves downward. However, the results of this study indicate that the slope of the flow function

is not constant. It is dependent upon the test conditions, i.e. the initial consolidation stress. This should serve as a reminder that shear cell responses should be measured at multiple initial consolidation stress conditions, and if possible, at many conditions in order to obtain a reliable estimate.

With three exceptions, the shear cell type was found to be statistically significant for all eight responses analyzed with each DOE. For the data set available, we were unable to show a statistically significant effect of the shear cell type on the unconfined yield stress when analyzed using DOE 1, on the flow function coefficient when analyzed using DOE 2, and on the bulk density when analyzed using DOE 3. However, generally speaking, the Schulze, FT4, and Brookfield shear cells give statistically different results for all six responses under all three experimental designs. Therefore, quantitative comparisons of results obtained by different shear cells should be made with care. However, since the material type has the largest effect, the rankings of the flowability of materials may be independent of the shear cell type.

The relative size of the material effect was determined by analyzing the first DOE. The material effect had the largest magnitude for the cohesion, unconfined yield stress, flow function coefficient, bulk density, and effective angle of internal friction responses. Therefore, these parameters can be considered mainly material property dependent. The shear cell type effect had the largest magnitude for the angle of internal friction. This may indicate that the angle of internal friction response is more sensitive to the shear cell type than the other response. The consolidation stress effect had the largest magnitude for the major principal stress and pre-shear point responses. This means that the stress required to move the shear cell head blades though the material (the pre-shear point

measurement) is more dependent on the applied normal stress than the material properties. Therefore, these parameters can be considered mainly consolidation state dependent. For the cases studied here, the flow function, i.e. the ratio of major principal stress to unconfined yield stress, can then be interpreted as the ratio of the consolidation state of the powder bed to the material properties.

Finally, the magnitude of the shear cell type effect is moderate to large for more cases of the free-flowing material than the cohesive material. This was observed for three cases of the free-flowing material and one case for the cohesive material. The differences between the results of different shear cells were larger for the free-flowing material. That is, the reproducibility of the measurements of the free-flowing material is lower than that of the cohesive material. This is most likely a "signal to noise ratio" issue, since the magnitude of all measurements for free flowing materials is smaller, while the sources of error remain largely unchanged. This result supports the claim that shear cells are less suitable for free-flowing materials.

3.4. Conclusions

In this study, the measurements of three commercially available shear cells were compared. A model cohesive material, a fine grade of alumina powder, and a model free-flowing material, a coarse grade of alumina powder, were examined. Eight responses were studied: cohesion, unconfined yield stress, major principal stress, flow function coefficient, pre-shear/ steady-state point, bulk density, effective angle of internal friction, and angle of internal friction. A number of observations regarding the results were made:

a) The results of this study support the claim that the shear cell is less suitable for free-flowing materials. The intra- and inter- shear cell variability is larger for the

free-flowing material than the cohesive material. Shear cells can be used to identify a material as free-flowing, but care should be taken in ranking materials within the free-flowing regime.

b) For the cases studied here, the material tested is always statistically significant. This indicates that each of the three shear cells tested can distinguish between cohesive and free-flowing materials. The material had the largest effect on the cohesion, unconfined yield stress, bulk density, flow function coefficient, and effective angle of internal friction responses. Therefore, the ranking, as opposed to the numerical values, of the flowability of powders established under the same initial consolidation stress should be independent of shear cell type.

c) For the cases studied here, the initial consolidation stress is always statistically significant. As has been discussed by previous researchers, when one reports shear cell results, the initial consolidation stress used should be included. The flowability of a material is not a constant but is dependent upon several factors including the state of compaction of the powder bed. Further, the flow function may not always be linear.

d) For the cases studied here, the shear cell type is generally statistically significant. The distribution of the applied normal force throughout the powder bed is dependent on the shear cell geometry and/or the height of the powder bed. Therefore, when reporting shear cell results, the shear cell used should be included. In addition, care should be taken when comparing the numerical values of responses measured by different shear cells. However, since the size of the shear cell type effect is much smaller than the material effect, the results from

different shear cells can potentially be used to rank the flowability of materials. The one exception was for the angle of internal friction response where the shear cell type had the largest effect magnitude.

e) The flow function is constructed from the unconfined yield stress and major principal stress. For the cases studied here, the material has the largest effect on the unconfined yield stress. The initial consolidation stress has the largest effect on the major principal stress. The ratio of these two parameters is used to rank the flowability of the material tested. The flow function, and therefore the flowability, can be interpreted as the ratio of the consolidation state of the material to the material properties.

These results are based on only two materials, coarse and fine alumina, and three common shear cells. Thus, further work is needed on different materials to test the robustness of our results and to generalize across available instruments. Considering the large volume of work carried out on shear testing of powders, it is important to continue to compare results from different shear cells for the same material and consolidations in order to develop a better understanding of powder flowability testing. This chapter represents an initial effort to determine standard methods to perform such comparisons in an objective and reproducible manner. The data set reported here can be easily expanded to increase the significance and generality of our results.

3.5. Figures for Chapter 3

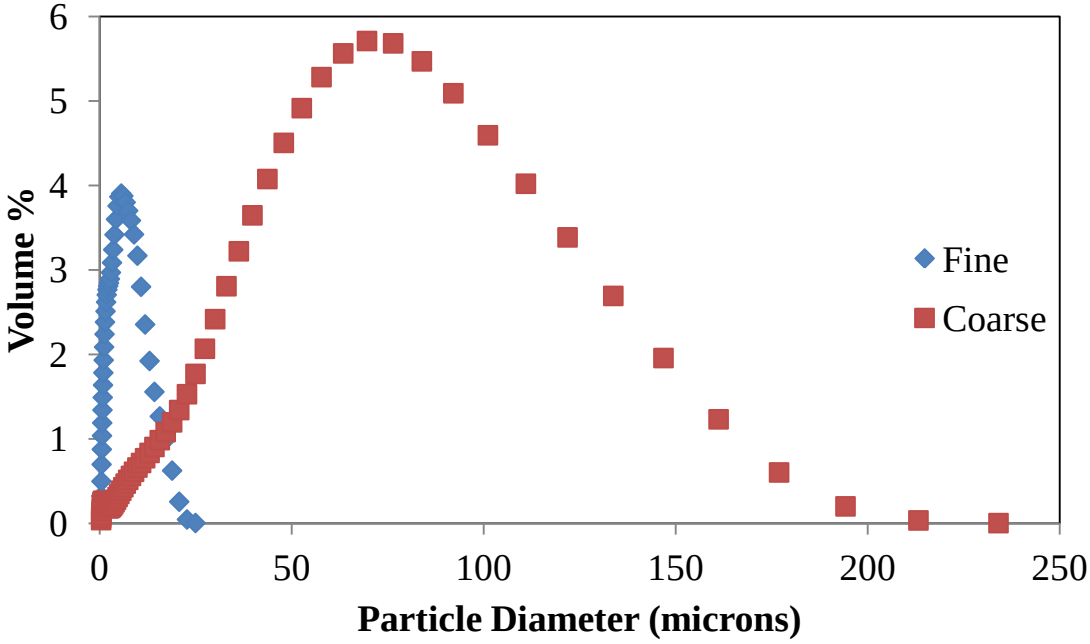

Figure 3-1: Particle size distributions of the fine and coarse grade of γ-alumina powder.

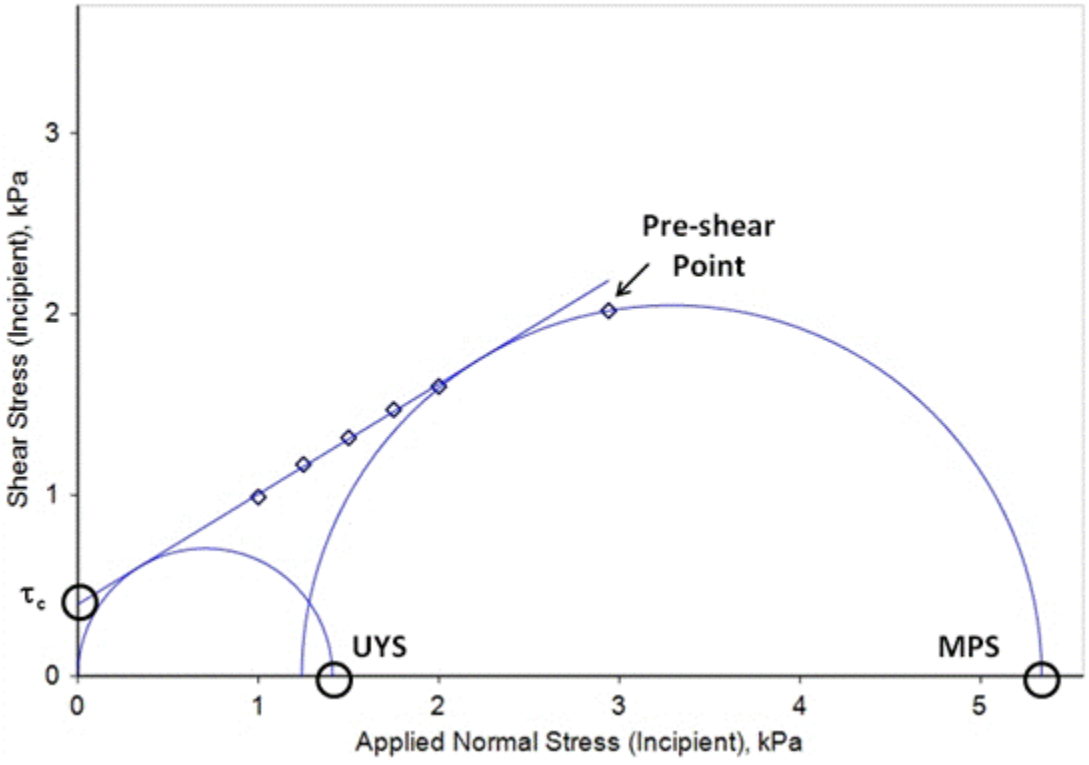

Figure 3-2: An example of a yield locus measured using a shear cell tester and the best-fit line and Mohr circle analysis

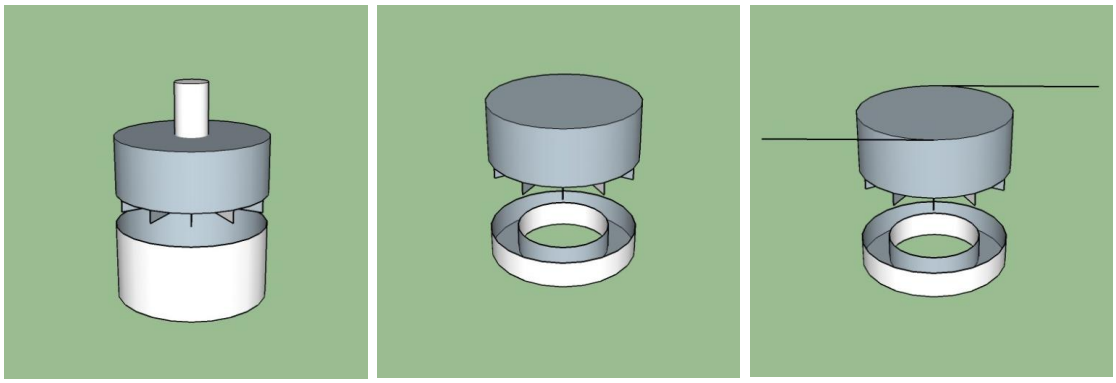

Figure 3-3: The FT4 shear cell (left), Brookfield Powder Flow Tester (center), and Schulze RST-XS (right).

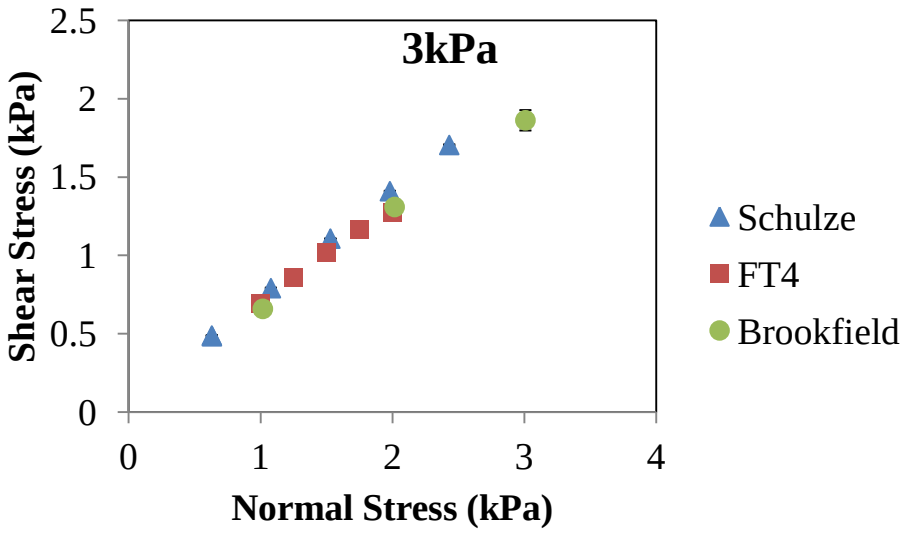

Figure 3-4: Yield loci of coarse alumina measured at an initial consolidation stress of 3kPa.

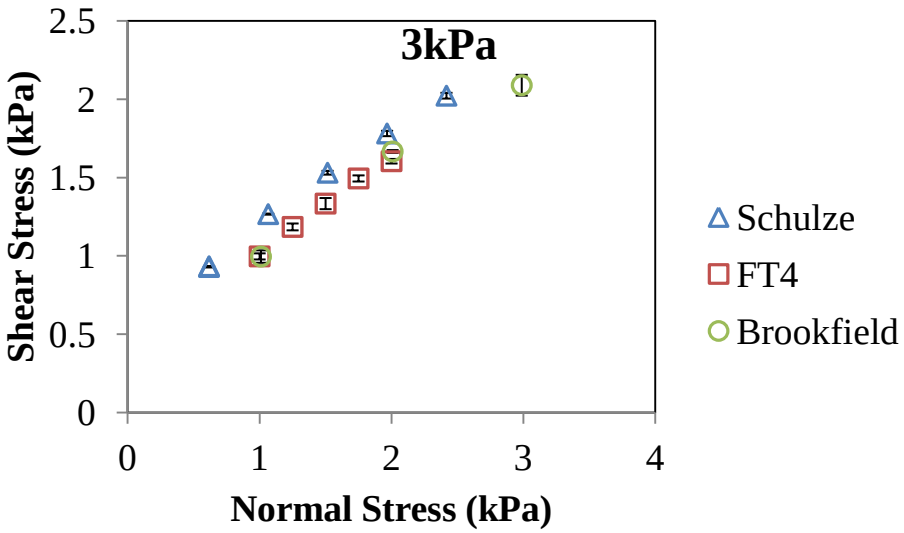

Figure 3-5: Yield loci of fine alumina measured at an initial consolidation stress of 3kPa.

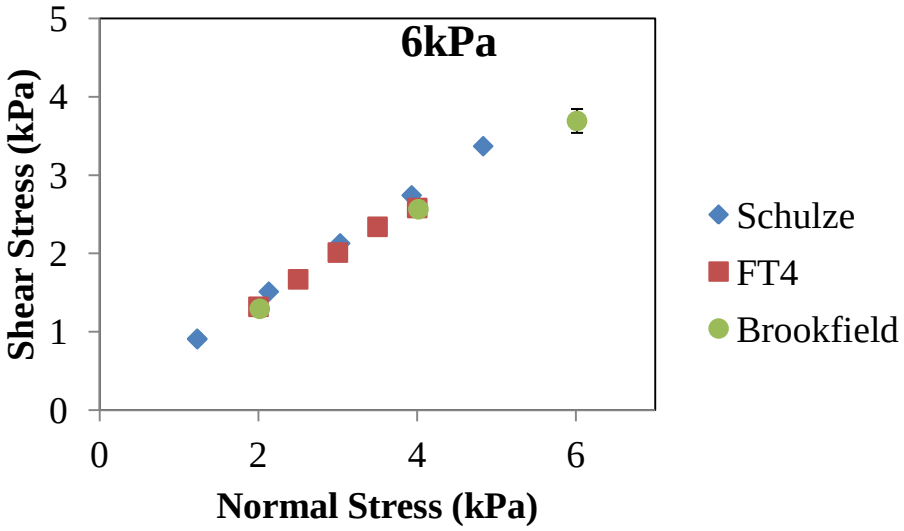

Figure 3-6: Yield loci of coarse alumina measured at an initial consolidation stress of 6kPa.

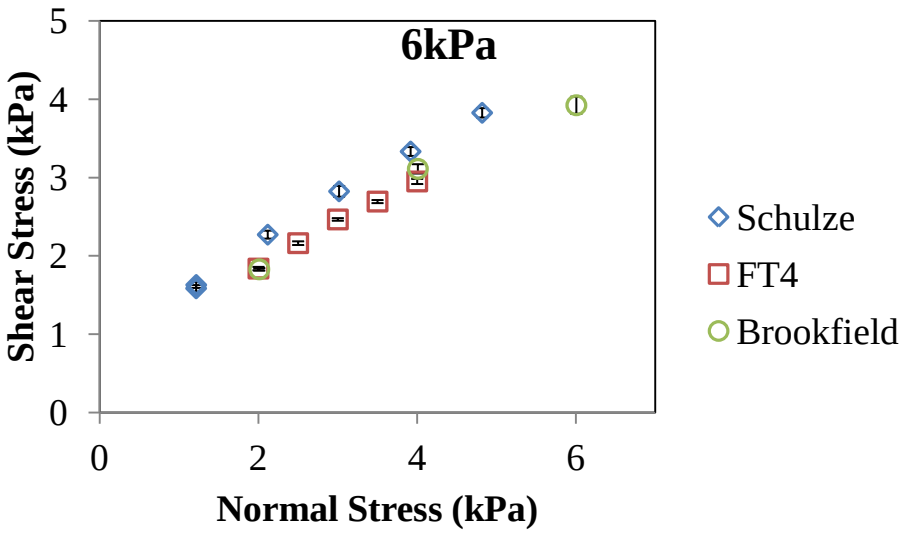

Figure 3-7: Yield loci of fine alumina measured at an initial consolidation stress of 6kPa.

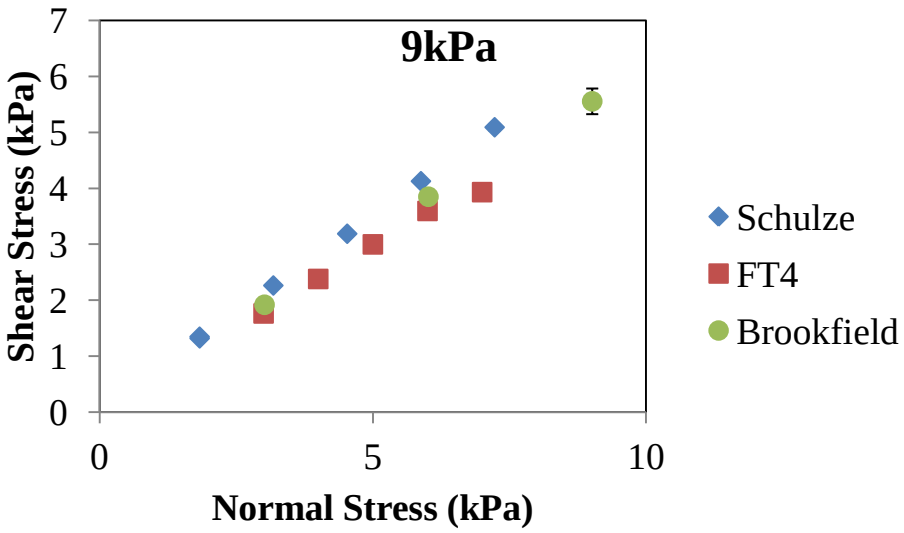

Figure 3-8: Yield loci of coarse alumina measured at an initial consolidation stress of 9kPa.

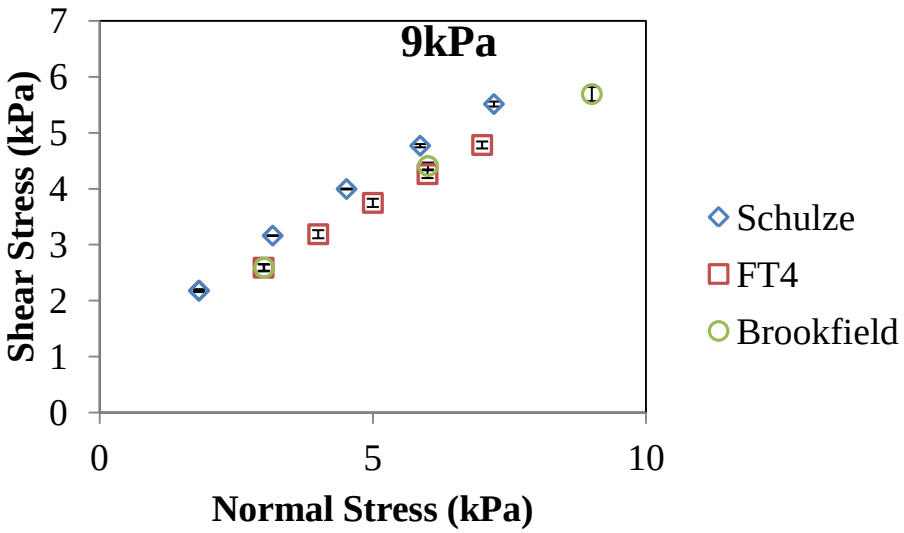

Figure 3-9: Yield loci of fine alumina measured at an initial consolidation stress of 9kPa.

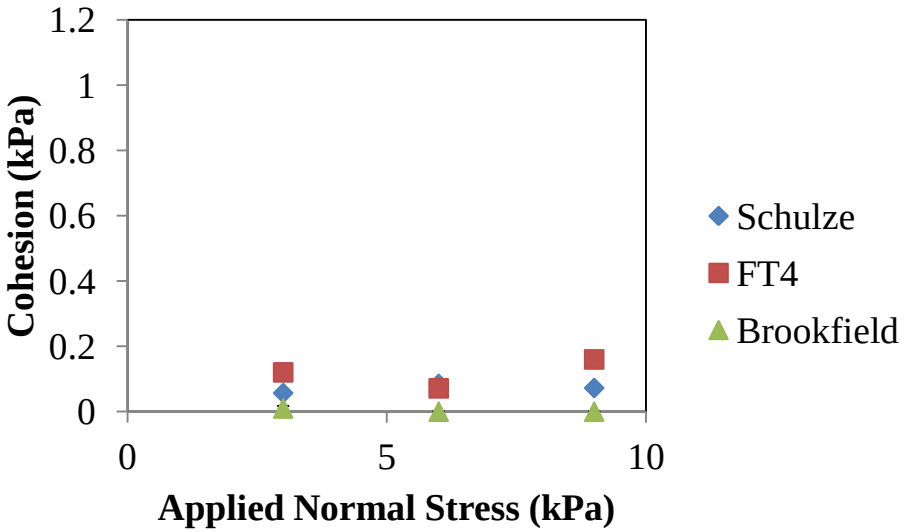

Figure 3-10: Cohesion as a function of applied normal stress for coarse alumina.

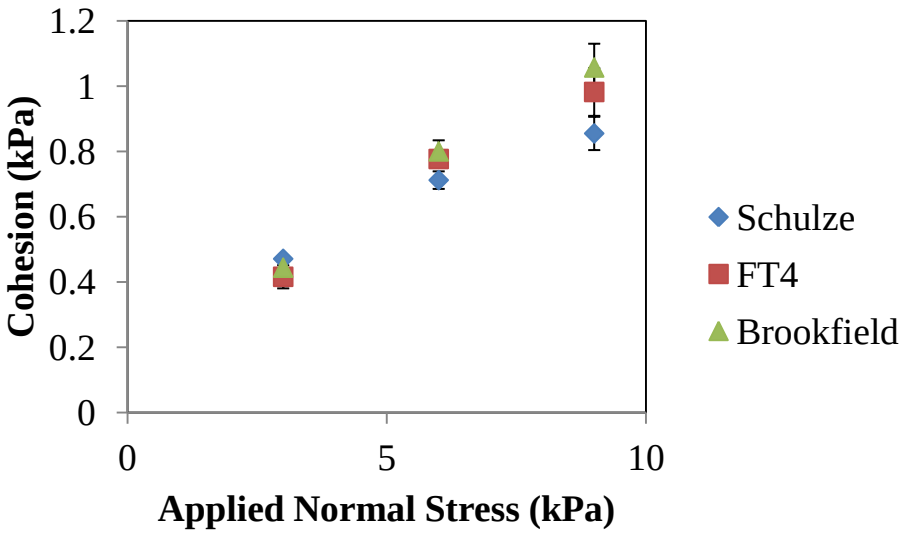

Figure 3-11: Cohesion as a function of applied normal stress for fine alumina.

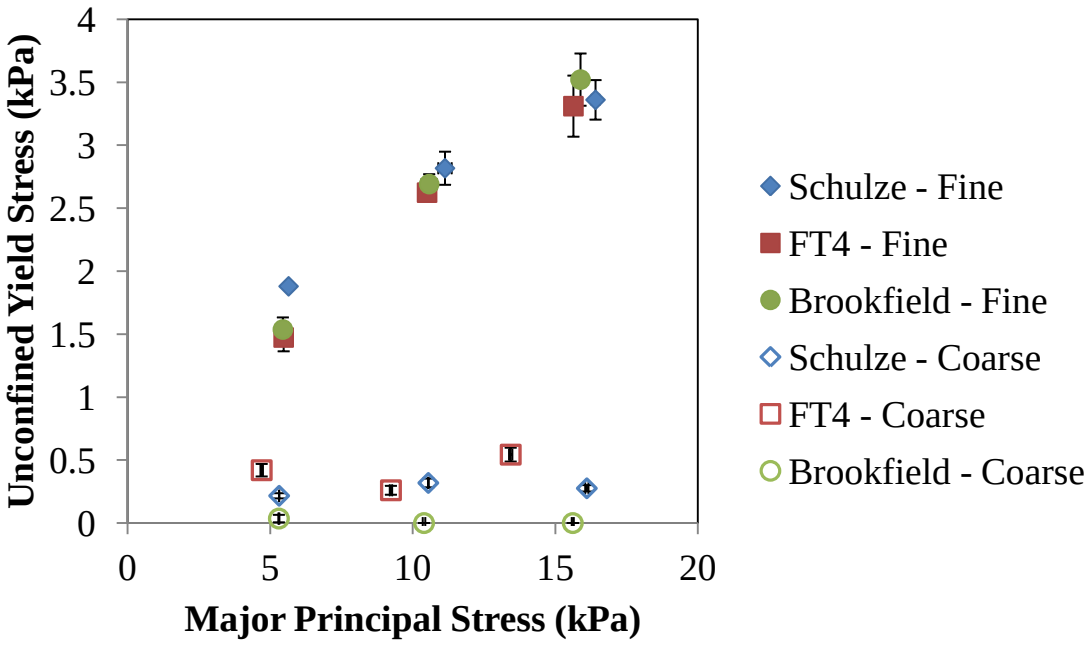

Figure 3-12: Flow function for fine and coarse alumina as measured using the Schulze, FT4, and Brookfield shear cell testers.

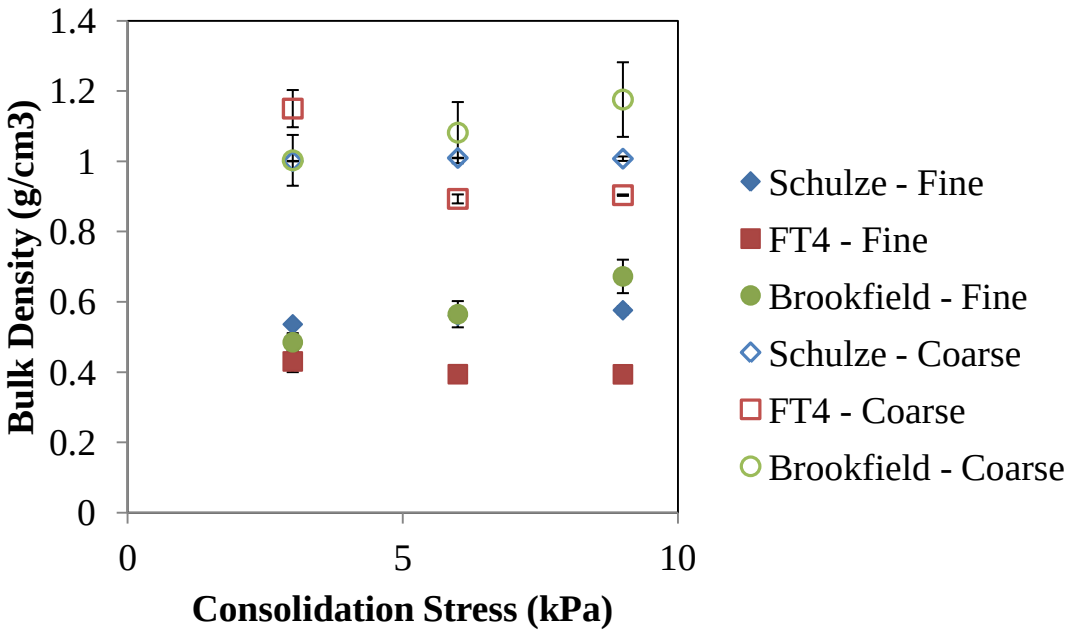

Figure 3-13: Bulk density profiles for fine and coarse alumina at consolidation stresses of 3, 6, and 9 kPa.

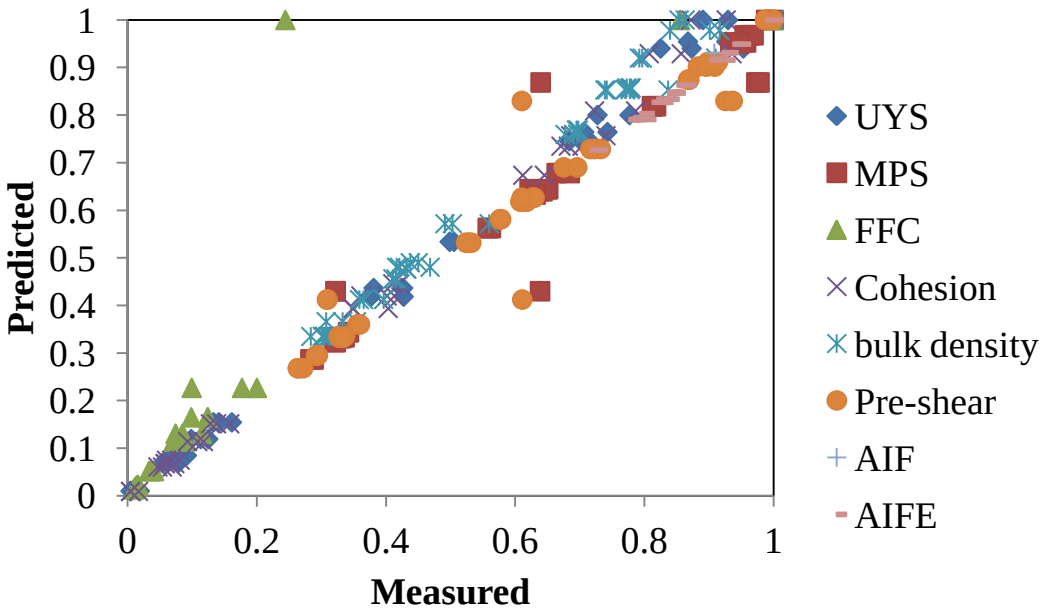

Figure 3-14: Normalized data points plotted against measurement averages.

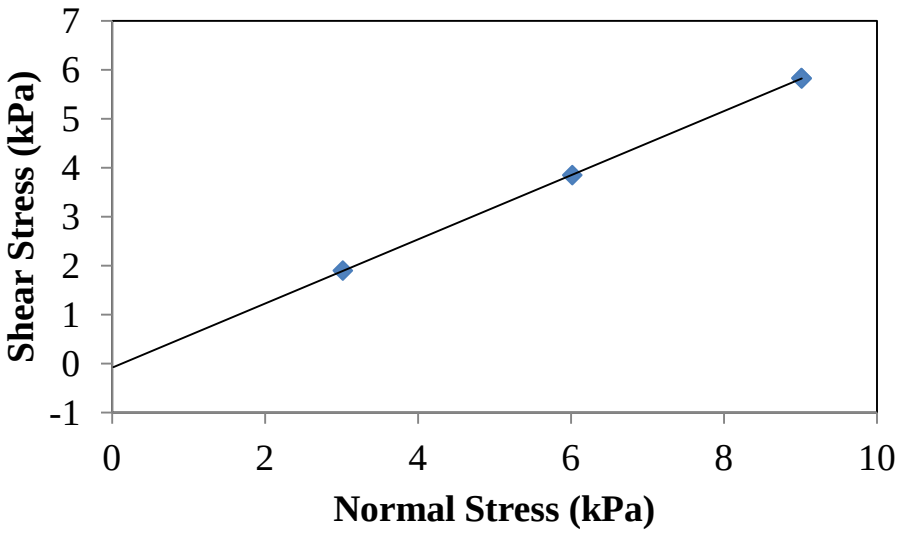

Figure 3-15: The yield locus measured for the coarse alumina using the Brookfield shear cell has a negative cohesion value. It is not possible to construct the unconfined yield stress Mohr circle in such a circumstance.

3.1 Tables for Chapter 3

Table 3.5-1: The sample geometry, measurement mechanism, and vessel volume of the Schulze, FT4, and Brookfield shear cells.

	FT4	Schulze	Brookfield
Sample area	Entire circle	Ring (Annulus)	Ring (Annulus)
Measurement	Torque	Force	Torque
Volume of Vessel	85mL	30mL	43mL

Table 3.5-2: R^2-values for the relationship between the predicted responses versus the measured responses.

Response	UYS	MPS	FFC	Cohesion	Bulk Density	Pre-shear	AIF	AIFE
R^2	0.995	0.954	0.796	0.994	0.982	0.952	0.980	0.991

Table 3.5-3: ANOVA and omega squared results for cohesion.

DOE 1						
Source of Variation	*SS*	*DF*	*MS*	*F*	*p-level*	*Omega Sqr.*
Factor #1 (Tester)	0.015	1	0.015	9.478	**0.006**	0.004
Factor #2 (Stress)	0.344	2	0.172	108.591	**0.000**	0.098
Factor #3 (Material)	2.770	1	2.770	1748.718	**0.000**	0.800
Factor #1 + #2	0.014	2	0.007	4.484	**0.025**	0.003
Factor #1 + #3	0.000	1	0.000	0.000	0.994	0.000
Factor #2 + #3	0.285	2	0.142	89.852	**0.000**	0.081
Within Groups	0.032	20	0.002			
Total	3.459	29	0.119			
DOE 2						
Source of Variation	*SS*	*DF*	*MS*	*F*	*p-level*	*Omega Sqr.*
Factor #1 (Tester)	0.028	2	0.014	6.525	**0.009**	0.019
Factor #2 (Stress)	1.177	2	0.589	274.934	**0.000**	0.921
Factor #1 + #2	0.034	4	0.009	4.009	**0.021**	0.020
Within Groups	0.032	15	0.002			
Total	1.272	23	0.055			
DOE 3						
Source of Variation	*SS*	*DF*	*MS*	*F*	*p-level*	*Omega Sqr.*
Factor #1 (Tester)	0.008	1	0.008	49.733	**0.000**	0.341
Factor #2 (Stress)	0.006	2	0.003	19.478	**0.001**	0.259
Factor #1 + #2	0.007	2	0.003	22.029	**0.000**	0.295
Within Groups	0.001	9	0.000			
Total	0.021	14	0.002			

Table 3.5-4: Scheffe orthogonal contrast results for cohesion.

DOE 1

Comparisons among groups (Factor 2 - Consolidation Stress)

Scheffe contrasts among pairs of means

Group vs Group (Contrast)	*Difference*	*98% Confidence Interval*		*Test Statistics*	*p-level*
1 vs 2	-0.147	-0.191	-0.104	52.322	**0.000**
1 vs 3	-0.262	-0.305	-0.218	164.936	**0.000**
2 vs 3	-0.114	-0.158	-0.071	31.465	**0.000**

DOE 2

Comparisons among groups (Factor 1 - tester)

Scheffe contrasts among pairs of means

Group vs Group (Contrast)	*Difference*	*98% Confidence Interval*		*Test Statistics*	*p-level*
1 vs 2	-0.046	-0.121	0.030	1.744	0.199
1 vs 3	-0.088	-0.163	-0.013	6.460	**0.007**
2 vs 3	-0.042	-0.109	0.025	1.863	0.180

Comparisons among groups (Factor 2 - Consolidation Stress)

Scheffe contrasts among pairs of means

Group vs Group (Contrast)	*Difference*	*98% Confidence Interval*		*Test Statistics*	*p-level*
1 vs 2	-0.329	-0.400	-0.258	101.095	**0.000**
1 vs 3	-0.538	-0.609	-0.467	270.460	**0.000**
2 vs 3	-0.209	-0.280	-0.138	40.846	**0.000**

DOE 3

Comparisons among groups (Factor 2 - Consolidation Stress)

Scheffe contrasts among pairs of means

Group vs Group (Contrast)	*Difference*	*98% Confidence Interval*		*Test Statistics*	*p-level*
1 vs 2	0.018	-0.008	0.044	2.707	0.107
1 vs 3	-0.030	-0.056	-0.004	7.420	**0.008**
2 vs 3	-0.048	-0.074	-0.022	19.090	**0.000**

Table 3.5-5: ANOVA and omega squared results for the eight responses: cohesion (τ_c), unconfined yield stress (UYS), major principal stress (MPS), pre-shear point (PSP), flow function coefficient (FFC), bulk density (ρ_b), effective angle of internal friction (AIFE), and angle of internal friction (AIF). The p-values that indicate a significant factor are shown in bold.

DOE 1

Source of Variation	τ_c		UYS		MPS		PSP		FFC		ρ_b		AIFE		AIF	
	p-level	ω^2	*p-level*	ω^2	*p-level*	ω^2	*p-level*	ω^2	*p-level*	ω^2	*p-level*	ω^2	*p-level*	ω^2	*p-level*	ω^2
Factor #1 (Tester)	**0.006**	0.004	0.376	0.000	**0.000**	0.014	**0.000**	0.032	**0.001**	0.043	**0.000**	0.024	**0.000**	0.268	**0.000**	0.612
Factor #2 (Stress)	**0.000**	0.098	**0.000**	0.090	**0.000**	0.927	**0.000**	0.913	**0.000**	0.084	**0.000**	0.017	**0.000**	0.134	**0.000**	0.047
Factor #3 (Material)	**0.000**	0.800	**0.000**	0.819	**0.000**	0.014	**0.000**	0.035	**0.000**	0.598	**0.000**	0.901	**0.000**	0.522	**0.000**	0.121
Factor #1 + #2	**0.025**	0.003	0.078	0.001	**0.000**	0.004	**0.000**	0.010	**0.003**	0.042	**0.000**	0.018	**0.000**	0.015	**0.000**	0.063
Factor #1 + #3	0.994	0.000	**0.001**	0.005	**0.000**	0.003	**0.001**	0.002	**0.001**	0.046	**0.000**	0.012	0.315	0.000	**0.002**	0.009
Factor #2 + #3	**0.000**	0.081	**0.000**	0.075	**0.001**	0.001	**0.000**	0.003	**0.000**	0.067	**0.000**	0.013	**0.000**	0.037	**0.000**	0.066

DOE 2

Source of Variation	τ_c		UYS		MPS		PSP		FFC		ρ_b		AIFE		AIF	
	p-level	ω^2	*p-level*	ω^2	*p-level*	ω^2	*p-level*	ω^2	*p-level*	ω^2	*p-level*	ω^2	*p-level*	ω^2	*p-level*	ω^2
Factor #1 (Tester)	**0.009**	0.019	**0.035**	0.010	**0.000**	0.002	**0.000**	0.012	0.177	0.012	**0.000**	0.671	**0.000**	0.472	**0.000**	0.689
Factor #2 (Stress)	**0.000**	0.921	**0.000**	0.949	**0.000**	0.996	**0.000**	0.984	**0.000**	0.779	**0.001**	0.077	**0.000**	0.502	**0.000**	0.153
Factor #1 + #2	**0.021**	0.020	0.155	0.006	0.085	0.000	**0.000**	0.002	**0.035**	0.060	**0.000**	0.165	0.471	0.000	**0.001**	0.091

DOE 3

Source of Variation	τ_c		UYS		MPS		PSP		FFC		ρ_b		AIFE		AIF	
	p-level	ω^2	*p-level*	ω^2	*p-level*	ω^2	*p-level*	ω^2	*p-level*	ω^2	*p-level*	ω^2	*p-level*	ω^2	*p-level*	ω^2
Factor #1 (Tester)	**0.000**	0.341	**0.000**	0.306	**0.000**	0.035	**0.000**	0.059	**0.000**	0.256	0.116	0.010	**0.000**	0.644	**0.000**	0.711
Factor #2 (Stress)	**0.001**	0.259	**0.001**	0.260	**0.000**	0.954	**0.000**	0.917	**0.000**	0.436	**0.000**	0.528	**0.000**	0.182	**0.000**	0.134
Factor #1 + #2	**0.000**	0.295	**0.000**	0.313	**0.000**	0.011	**0.000**	0.024	**0.000**	0.252	**0.000**	0.389	**0.000**	0.141	**0.000**	0.136

Table 3.5-6: Scheffe orthogonal contrast p-values for the eight responses: cohesion (τ_c), unconfined yield stress (UYS), major principal stress (MPS), pre-shear point (PSP), flow function coefficient (FFC), bulk density (ρ_b), effective angle of internal friction (AIFE), and angle of internal friction (AIF). The p-values that indicate a significant contrast are shown in bold.

DOE 1

Comparisons among groups (Factor 2 - Stress)

Group vs Group (Contrast)	τ_c	*UYS*	*MPS*	*PSP*	*FFC*	ρ_b	*AIFE*	*AIF*
1 vs 2	**0.000**	**0.000**	**0.000**	**0.000**	**0.000**	**0.000**	**0.000**	0.990
1 vs 3	**0.000**	**0.000**	**0.000**	**0.000**	**0.000**	**0.000**	**0.000**	**0.000**
2 vs 3	**0.000**	**0.000**	**0.000**	**0.000**	0.147	0.846	**0.000**	**0.000**

DOE 2

Comparisons among groups (Factor 1 - Tester)

Group vs Group (Contrast)	τ_c	*UYS*	*MPS*	*PSP*	*FFC*	ρ_b	*AIFE*	*AIF*
1 vs 2	0.199	**0.031**	**0.000**	**0.000**	*****	**0.000**	**0.000**	**0.000**
1 vs 3	**0.007**	0.412	**0.000**	**0.000**	*	0.543	**0.000**	**0.000**
2 vs 3	0.180	0.264	0.430	0.463	*****	**0.000**	0.193	**0.023**

* values not depicted since the tester type was found to be not significant to the FFC response

Comparisons among groups (Factor 2 - Stress)

Group vs Group (Contrast)	τ_c	*UYS*	*MPS*	*PSP*	*FFC*	ρ_b	*AIFE*	*AIF*
1 vs 2	**0.000**	**0.000**	**0.000**	**0.000**	**0.001**	0.296	**0.000**	**0.000**
1 vs 3	**0.000**	**0.000**	**0.000**	**0.000**	**0.000**	**0.000**	**0.000**	**0.000**
2 vs 3	**0.000**	**0.000**	**0.000**	**0.000**	**0.000**	**0.017**	**0.000**	0.672

DOE 3

Comparisons among groups (Factor 2 - Stress)

Group vs Group (Contrast)	τ_c	*UYS*	*MPS*	*PSP*	*FFC*	ρ_b	*AIFE*	*AIF*
1 vs 2	0.107	**0.000**	**0.000**	**0.000**	**0.000**	**0.000**	0.706	**0.000**
1 vs 3	**0.008**	**0.000**	**0.000**	**0.000**	**0.000**	**0.000**	**0.000**	**0.022**
2 vs 3	**0.000**	**0.000**	**0.000**	**0.000**	0.293	0.943	**0.000**	**0.000**

Chapter 4. A novel method to measure powder flow properties using a small amount of material

4.1. Introduction

Powder flow characterization, is often limited by the amount of material required for testing, often tens to hundreds of grams of material. There are instances where the material available for testing is limited, due to the cost of the material, availability of the material, safety concerns, etc. Work has been done by Hughes et al to develop a material-sparing bulk density test for use in such situations [105]. Here, the smallest sample size considered was 10mL. However, in some cases even this limited sample size can be prohibitive.

The bulk density of a material is commonly used to determine a material's flow behavior and to improve solids processing understanding. The bulk density of a material has been used to characterize the flowability of granular materials and powders [65, 106]. There have been multiple studies comparing the bulk density to other flow characteristics [41, 42, 107-109]. Surface modification of powders often employs the bulk density as a quantitative assessment for the resulting improvement in the flow [48, 49]. The bulk density has also been used to improve the understanding of several solids processing unit operations spanning industries: axial mixing [110], granulation [111, 112], capsule filling [113], fluidization [114], food powder mixing [115], and laser sintering of polymer parts [116].

The bulk density is defined as the ratio of the mass of powder sample to the volume of that powder sample:

$$\rho_b = \frac{m_{sample}}{v_{sample}}$$

where ρ_b was the bulk density, m_{sample} was the mass of the sample, and v_{sample} was the volume of the sample. By definition, the bulk density accounts for the true density of the particles (through the mass term) and the interstitial space between the particles (through the volume term) [67]. A low bulk density is observed when a given mass of particles occupies a large volume; typically observed in cohesive, poorly flowing materials. The high inter-particle forces, relative to gravity, prevent the particles from achieving a close packing arrangement. Alternatively, a high bulk density is observed when a given mass of particles occupies a relatively small volume, typically observed in free-flowing materials. The low inter-particle forces, relative to gravity, results in closer packing. The bulk density is not a constant and is greatly dependent on the packing, or consolidation, state of the material [15]. During solids manufacturing, granular materials and powders undergo processing in a variety of environments. Due to the sensitivity to the consolidation state of the material, the bulk density measurement can be used to determine a material's flowability (i.e. manufacturability) and, therefore, the extent to which the material may dilate or consolidate during manufacturing [65, 66]. Since the bulk density measurement is highly dependent on the consolidation state of the material, the bulk density is typically considered at multiple packing states. Common measurement methods include: comparing the tapped and aerated states, such as the Carr Index and Hausner ratio [68, 69]; comparing the density over a range of packing states, such as with the FT4 compressibility test [101]; and comparing the tapped and dilated states, such as with the GDR dilation test [71]. Here, the solids fractions over a range of packing states will be considered.

This chapter introduces a new method for measuring the bulk flow behaviors of cohesive and non-cohesive granular materials and powders using less than 50 mg of material. The solids fractions over a range of packing states were characterized for 12 materials with a range of flow properties. The rest of the chapter is organized as follows. The materials characterized and the experimental method used to measure the solids fractions are described. The effect of particle size and cohesion via capillary forces on the packing behavior are identified and discussed. It was found that the packing behavior of the materials could be characterized using two regimes: at very low stresses the Walker equation describes the observed behavior, otherwise the Heckel equation could be used. Due to the resolution of the small system, "catastrophic" collapsing events within the powder bed were observed. The method introduced here was validated against known and expected physics as well as a more traditional method - the FT4 compressibility test. It was found that the results were consistent with the behavior observed at larger scales.

4.2. Material and Methods

4.2.1. Materials

A set of precision grade soda-lime glass beads (Mo-Sci Specialty Products, Inc, Rolla, MO, USA) of four particle size distributions were used to study packing of granular systems in a small geometry. The four grades of glass beads had mean particle sizes of 275, 100, 50, and 5 microns (Figure 4-1). To remove any moisture acquired due to storage conditions, the glass beads were dried at 100 °C for one hour. The 275, 100, and 50 micron glass beads were observed to be relatively free-flowing. The 5 micron glass beads were observed to exhibit cohesive behaviors. The attractive forces between particles were increased via the introduction of capillary forces. De-ionized water was added at 10 and 20% by weight. By volume, 10% by weight corresponds to 12, 10, 9,

and 5% for 275, 100, 50, and 5 microns, respectively, and 20% by weight corresponds to 36, 35, 35, and 15% for 275, 100, 50, and 5 microns, respectively, as shown in Table 4-1.

4.2.2. Methods

The solids fraction as a function of applied normal stress of the twelve materials (4 particle sizes at three moisture contents) was measured using a cup and piston design (Figure 4-2). A TA Instruments ARES RDA-III rheometer was used with custom plates (the cup and piston shown in Figure 4-2). The cup was cylindrical, 5mm in diameter, and 1.5mm in depth and the piston was 5mm in diameter and 5mm in length. Material was poured into the cup until the cup was overfilled. The excess material was then scraped away. The mass of remaining material was then measured. The sample mass was dependent on the bulk density of the material, but was typically less than 50mg. The piston was subsequently lowered into the powder bed at a constant rate of 0.005 mm/s until the applied normal stress reached 1100 kPa. As a function of time, the bed height and normal force acting on the piston were recorded; sample data is shown in Figure 4-3. The bed height decreases linearly with time, as expected. The force acting on the piston was initially low and then, at a critical point, sharply increased. The horizontal separation of the stress data is due to variation in the time at which the piston first encountered the powder bed, i.e. the height of the powder bed. The largest variation in bed height observed in the data shown in Figure 4-3 is 124 microns, less than the average diameter of the particles. Thus, the difference in the powder bed height is less than one layer of particles. From this data, the solids fraction as a function of applied normal stress was calculated.

4.3. Results

An example of the measured solids fraction profiles is depicted in Figure 4-4. Specifically, three repetitions of the 275 micron beads with 0% added moisture are shown. It was observed that the beads have an initial packing state with a porosity dependent on the cohesion of the material. As the normal force was applied, the beads rearrange to a position that can support a larger normal force. That is, the solids fraction increases with increasing applied normal force. The initial state was also dependent on the loading of the material into the cup. This potential source of variability can be mitigated by exercising care on the part of the user while loading the material. In addition to the initial variability, during each repetition the repackaging occurs in a slightly different manner. As such, each repetition was considered an individual event, instead of as an average, to preserve the information from each repacking path.

4.3.1.Effect of particle size

The effect of particle size on the solids fraction profiles measured in the small geometry was determined. The glass beads with zero added moisture were characterized; the results are shown in Figure 4-5. It is known that as particle size decreases, cohesion due to van der Waals forces increases [17]. As a result, smaller particles tend to have lower bulk densities and have poorer flow properties. The general shape and magnitude of profiles for the three largest sizes studied here (275, 100, and 50 microns) are similar to one another. At low stress, the solids fraction varied from 0.55 to 0.65 and rose to 0.6 to 0.75 at higher stresses. The profiles were relatively flat and smooth, and as such, the solids fraction was not a strong function of the applied normal stress. These features of the profiles are indicative of freely flowing powders with low to zero cohesion. As observed from Figure 4-5, the profiles of the 5 micron beads were markedly different from the other beads. At low applied normal stress, the solids fraction varied from 0.3 to

0.35, less than that of the larger particle sizes, and rose to 0.5 to 0.7 at higher stresses, similar to that of the larger particle sizes. The 5 micron profiles reflect a larger change in solids fraction with an increase in applied normal stress. In addition, these profiles were less smooth. These aspects are indicative of a cohesive material. In the small geometry studied here, it was observed that the measurements of glass beads 50 microns in diameter and larger have attributes typically indicative of freely-flowing materials while those for the 5 microns beads have attributes typically indicative of cohesive powders.

4.3.2.Effect of capillary forces

As previously discussed, water was added to the glass beads at 10 and 20% by weight. This was done in order to alter the cohesive forces between beads without changing the particle size. The addition of liquid to the system introduced capillary forces between the beads. The solids fraction profiles for each particle size (275, 100, 50, and 5 microns) at each moisture content (0, 10, 20% by weight) are shown in Figure 4-6. Three repetitions are shown for each particle size at each moisture content. The profiles corresponding to the 275 micron beads (Figure 4-6A) show a reduction in solids fraction upon the addition of 10% water and a subsequent increase in solids fraction upon the addition of 20% water. The moisture content at 10% is sufficient to create liquid bridges between particles. This increase in attractive force manifests itself as an increase in cohesion and results in a more loosely packed powder. However, at 20% moisture, the amount of liquid in the system is enough to create a paste-like material. The amount of water in between glass beads at this point is sufficient to entirely coat the particles. The layer of water lubricates the interaction between the beads, the result being an observed decrease in cohesion and an increase in the packing density of the material. The magnitude of the attractive forces between the glass beads goes through a maximum at some point between

10 and 20% liquid added. Similar behavior was observed for the 100 (Figure 4-6B) and 50 micron (Figure 4-6C) particle sizes at each water content level.

The profiles for the 5 micron glass beads are shown in Figure 4-6D. The addition of water had a lesser impact on their packing behavior. This is likely largely due to the difference in surface area coverage between the particle sizes. The surface area to volume ratio of the 5 micron beads is much larger, therefore the same amount of water added by weight results in less coverage. In the small geometry studied here, it was observed that for the glass beads 50 microns in diameter and larger the cohesion increases with the addition of 10% water and subsequently decreases with the addition of 20% water. Once again, the 5 micron glass beads exhibited markedly different behavior.

4.3.3. Additional Observations

In addition to the effects of particle size and capillary forces, two other observations were made regarding the solids fraction profiles. The first was that the repacking occurred in two distinct regimes. The second observation was that the repacking was not always smooth. These observations are discussed in greater detail below.

The Heckel equation is often used to describe compaction profiles of granular materials and powders, for example those that describe tabletting processes [117]:

$$\ln\left(\frac{1}{1-\frac{V_s}{V}}\right) = KP + A$$

where V_s/V was the solids fraction, P was the applied normal stress, and K and A were fitted parameters. The left hand side of the Heckel equation was graphed along the y-axis and the stress was graphed along the x-axis (Figure 4-7). As a result, the solids fraction

profiles are linear in the range that is described by the Heckel equation. A linear fit to the profile yields values for the parameters K and A as the slope and y-intercept, respectively. The y-intercept (A) reflects the porosity (including liquid volume fraction in the cases where liquid is present) at zero applied normal stress, e.g. the conditions during die filling and particle rearrangement before deformation of the particles occurs. The slope (K) reflects the reduction in porosity (including liquid volume fraction in the cases where liquid is present) as a function of applied normal stress. It was found that past a critical packing state, the Heckel equation fit the solids fraction profiles measured here reasonably well. The profiles corresponding to the 275 micron glass beads with 0% added moisture are shown in Figure 4-7 with I, II, and III each denoting a repetition. For this material, the critical packing state where the Heckel equation begins to describe the repacking behavior occurs at around 50 kPa. A linear fit to the profile labeled as "I" has a slope (K) of 0.0002 and a y-intercept (A) of 0.9361 with a coefficient of determination (R^2) of 0.9995 and p-value less than 0.001. Similar observations were made for each of the 12 materials studied here.

However, in the low stress range, the Heckel equation does not describe the repacking behavior. This has been observed previously in the literature. The Walker equation, although used less frequently to describe compaction profiles, had some success in describing behavior at low stresses in our experiments:

$$\frac{V}{V_s} = a - Kln(\frac{P}{P_0})$$

where Vs/V was the solids fraction, P/P_0 was the stress normalized by the unit stress, and *a* and K were fitted parameters. The inverse of the solids fraction was graphed as a

function of the natural log of the normalized stress by a reference. Profiles that can be described using the Walker equation become linear. A linear fit to the profile yields values for the parameters K and *a* as the slope and y-intercept, respectively. The y-intercept is the measured solids fraction at an applied normal stress of 1kPa (the reference applied normal stress). The slope describes the curvature of the solids fraction profile. It was found that prior to the critical packing state at which the Heckel equation begins to describe the repacking behavior, there existed a first regime of repacking behavior. For this first regime at low stresses, the Walker equation fit the solids fraction profiles measured here reasonably well. The profiles corresponding to the 275 micron glass beads with 0% added moisture are shown in Figure 4-8 with I, II, and III each denoting a repetition. The maximum stress considered here is 50 kPa as this was identified as the critical transition point between the Heckel and Walker equations for this material. A linear fit to the profile labeled as I has a slope (K) of -0.0204 and a y-intercept (*a*) of 1.7412 with a coefficient of determination (R^2) of 0.986 and p-value of 0.005.

Similar observations were made for each of the 12 materials studied here. The average value for the slope and y-intercept parameters from the Walker equation fit to each of the 12 materials is shown in Figure 4-9. The value of *a* denotes the y-intercept of the Walker equation and represents the solids fraction at a reference applied normal stress of P_0, taken to be 1kPa here.

The value of *a* for 0% moisture content was similar for the 275, 100, and 50 micron beads; thus they each approach a similar solids fraction at the reference applied normal stress. This would be expected since they are all fairly mono-dispersed glass particles that are roughly spherical and non-cohesive. The *a*-value for the 5 micron beads at 0%

moisture content was much larger and different from the three other particle sizes. Again, this would be expected since the 5 micron particles are cohesive and it would then be expected that they would reach a lower solids fraction than the non-cohesive beads at the same reference applied normal stress. The value of K describes the curvature of the solids fraction profile. The value of K for 0% moisture content was similar and small in magnitude for the 275, 100, and 50 micron beads; thus the profiles each have a similarly flat shape, i.e. the solids fraction was relatively independent of applied normal stress. Again, this would be expected since the particles are fairly mono-dispersed, spherical, and non-cohesive. The K-value for the 5 micron beads at 0% moisture content was much larger and different from the three other particle sizes. Again, this would be expected since the 5 microns particles are cohesive and it would be expected that the solids fraction would increase as a function of applied normal stress.

Revisiting the *a*-values (y-intercepts), the addition of 10% liquid led to a relatively large increase in *a*-value of similar magnitudes for the 275, 100, and 50 micron particles. This is to be expected since the addition of liquid increases the cohesion of the system and leads to a lower solids fraction at the reference applied normal stress (the Walker equation is inversely proportional to the solids fraction). The addition of 10% liquid to the 5 micron particles also led to an increase in *a*-value, but the increase was smaller in magnitude. As discussed previously, this may be due to the difference in surface area between the particle sizes. The 5 micron particles have a much larger surface area to volume ratio and as a result the same amount of liquid added by mass results in lower surface area coverage (or much thinner coverage). From Figure 4-9, it was observed that adding 20% liquid by mass results in a decrease in cohesion of similar magnitudes for the

275, 100, and 50 micron particles. This was to be expected since the addition of 20% liquid created a paste-like material. The surface coverage of the water was sufficient to lubricate the particles increasing the packing density of the particles. The addition of 20% liquid to the 5 micron particles also led to a decrease in *a*-value, but the decrease was smaller in magnitude; again potentially due the difference in surface area coverage between the particle sizes. As observed from Figure 4-9, the effect of the moisture content on the slope parameter of the Walker equation (the value of K) was similar to that observed for the y-intercept (the value of *a*).

It was observed that the effect of the moisture content was more clearly visible than the effect of the particle size on the slope (K) and y-intercept (a). The error of the parameter fits was calculated as the standard deviation of the results of the three repetitions for each material. The error of the slope fit (Figure 4-9, bottom) was much higher than the y-intercept fit (Figure 4-9, top). There was a certain amount of error in filling the small geometry with cohesive beads; the main source in the variability of the solids fraction at 1 kPa, the reference applied normal stress. Additionally, the path of repacking was highly variable, especially in the initial states. As a result, the shape of the solids fraction profile - characterized by the slope of the Walker equation - was highly variable, indicated by the large error bars of the slope measurement.

The second additional observation was that the repacking was not always smooth. In fact, horizontal features appear in several of the measured solids fraction profiles. An example of these features occurring in a solids fraction profile measured for the 100 micron beads with 20% by weight added moisture is depicted in Figure 4-10. In some instances, the stress on the piston suddenly decreases. As the piston descends into the

powder bed, meta-stable structures (rings, arches, etc) within the bed that can withstand a load can form. Once the force applied to the structure exceeds that load, one or more particles "snap" through the formation. When one of these structures breaks, a sudden “catastrophic” event, the bed experiences a dramatic repacking and reduction in void space. These events have been described in the literature as "snap-through buckling" [118]. The size and frequency of these events may be dependent on how easily the structures form and how strong the structures are once formed. This may be related to the material's cohesion. The size and frequency of these events have also been observed to be highly variable so a large number of experiments and/or simulations would be required to obtain statistically representative results.

4.3.4. Validation of method

The solids fraction profiles (shown in Figure 4-6) and parameters from the Walker equation (shown in Figure 4-9) follow trends previously observed for bulk materials. One might expect that as the particle size decreases, the cohesion of the system to increase due to van der Waals forces. This is, in fact, what was observed. The increase in cohesion in the 5 micron beads resulted in lower packing fractions and a steeper solids fraction profile. It has been previously shown in the literature that the addition of moisture, with the formation of capillary “necks”, into a powder initially increases the cohesion in the system and lowers the observed packing fractions. As the moisture content increases further, the particles become lubricated, resulting in an increase in the packing fraction. This effect was also observed here, in the small geometry. The general behavior that one might expect to observe based on experience and physics known at larger scales is in fact also observed in the small geometry used here.

The solids fraction profiles measured in the small geometry were validated against a solids fraction profile measurement at a larger scale, the compressibility test, obtained using the FT4 from Freeman Technology. The measurements obtained using the small geometry were compared to measurements taken using the Freeman Technology FT4. The 25 mm x 10 mL cell was used to measure the compressibility of each of the 12 materials in the FT4. A conditioning step was not used at the small scale; therefore, the conditioning step was not used during the FT4 testing. The compressibility test carried out using the FT4 had a maximum applied normal stress of 15kPa; two orders of magnitude less than with the small scale system.

It might be expected that the FT4 system would not capture all the relevant physics occurring at the small scale. The effect of the walls on the repacking of the material would be much more significant at the small scale as a larger portion of the particles in the system would interact with the boundary of the geometry. Additionally, by nature of the small scale, the breaking of the formed meta-stable structures within the bed could be resolved. At larger scales, these events occur more frequently and thus their effect would be averaged and single events would be less likely to be resolved. Conversely, some emerging behaviors taking place at large scales might not be observed in the small scale system.

Nonetheless, for the sake of comparison, the Walker equation was fit to the profiles measured using the FT4 and the slope and y-intercept parameters were extracted. The values for the parameters measured by each system were compared using parity plots (Figures 4-11 and 4-12). The linear regression obtained between the y-intercept parameter values from each system had a regression equation of $y=0.7164x+0.6706$ with

a coefficient of determination of 0.77 and p-value less than 0.001 (Figure 4-11). It was observed that the error in the measurement of the y-intercept, *a*, (calculated as the standard deviation of three measurements and depicted as error bars) using the FT4 and the small scale system was similar. The linear regression obtained between the slope parameter values from each system had a regression equation of y=0.2055x+0.0742 with a coefficient of determination of 0.51 and p-value of 0.009 (Figure 4-12). It was observed that the error in the measurements of the slope, K, obtained using the small scale system were much larger than those obtained by the FT4. This was expected since, as previously discussed, the slope captured the curvature of the solids fractions profile and this was highly variable. The coefficient of determination values represent the amount of explained variance. These results can be interpreted as 77% and 51% of the variability in the y-intercept and slope, respectively, measured at the small scale was also observed at the larger scale. These values indicate that the FT4 captured a statistically significant portion of the physics occurring during the repacking at the small scale. The remainder of the variance was likely due to the wall effects and catastrophic repacking. Overall, there was good qualitative agreement between methods.

4.4. Conclusions

In this study, a characterization method capable of capturing bulk behaviors using fractions of a gram of material has been developed. The solids fraction profiles of 12 materials with a range of flow properties were measured. It was found that the packing fractions decreased with decreasing particle diameters. It was also found that the effect of moisture addition initially increases the cohesive forces between particles due to capillary forces, but as the moisture content increases the moisture lubricates the particles

and results in an increase in the packing fraction. These observations were consistent with expectations derived from the behavior of these materials at a larger scale. The packing of the materials occurred in two regimes: the Walker equation describes the packing behavior at very low stresses and the Heckel equation describes the packing behavior at higher stresses. During the packing, metastable structures were formed and then broken within the powder bed. Due to the resolution of the small scale system, these collapses in the powder bed were able to be resolved. The measurements obtained at the small scale were validated against known and expected physics as well as against a traditional method, the Freeman Technology FT4 compressibility test. Additional effects, such as the wall effects and the collapsing events were captured by the small scale system. For the physics captured by both systems, good qualitative correlation between the small scale system and traditional measurement was observed.

These results are based on a limited number of repetitions. Further work, i.e. additional repetitions through simulations and/or extensive experimentation, is needed to describe and characterize the breaking of the meta-stable structures formed during packing in a statistically meaningful manner. This chapter demonstrates that bulk flow properties can be observed using less than 50mg of material. This is an important development and has applications in situations where the amount of material available for testing is restricted.

4.5. Figures for Chapter 4

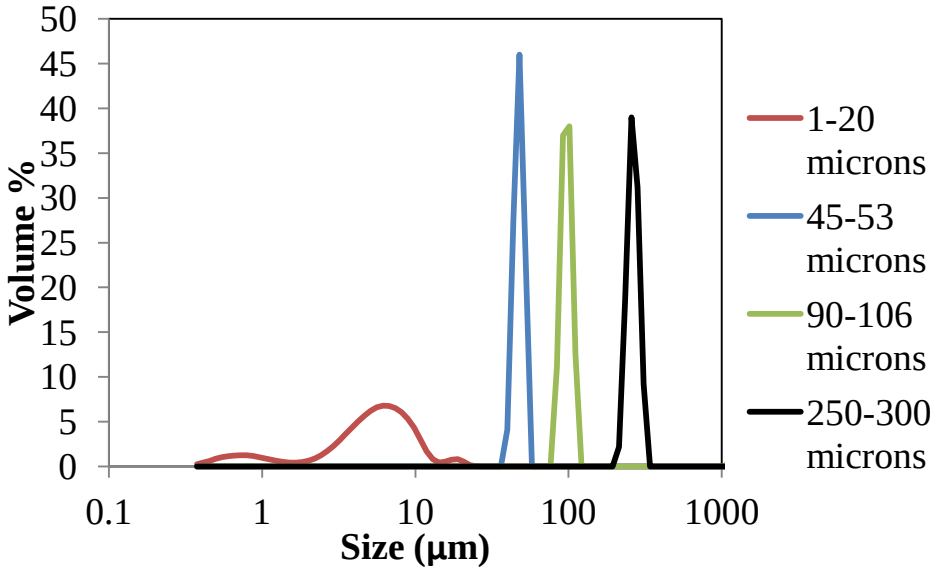

Figure 4-1: Particle size distribution of glass beads, d_{50} in microns listed in legend

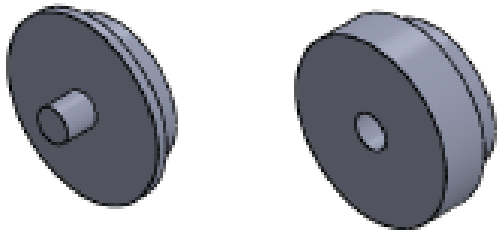

Figure 4-2: Schematics of cup and piston

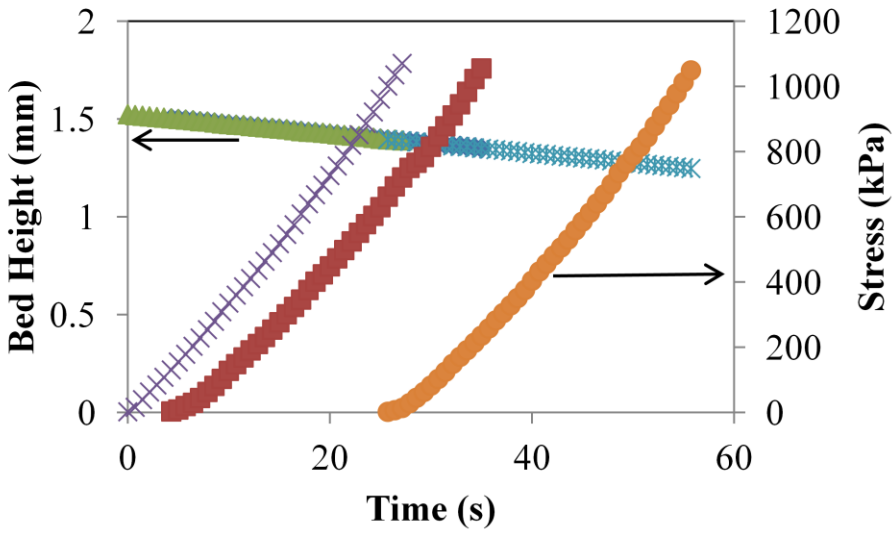

Figure 4-3: Example of data gathered using the small scale compressibility method; three repetitions for 275 micron glass beads with 0% water addition are shown.

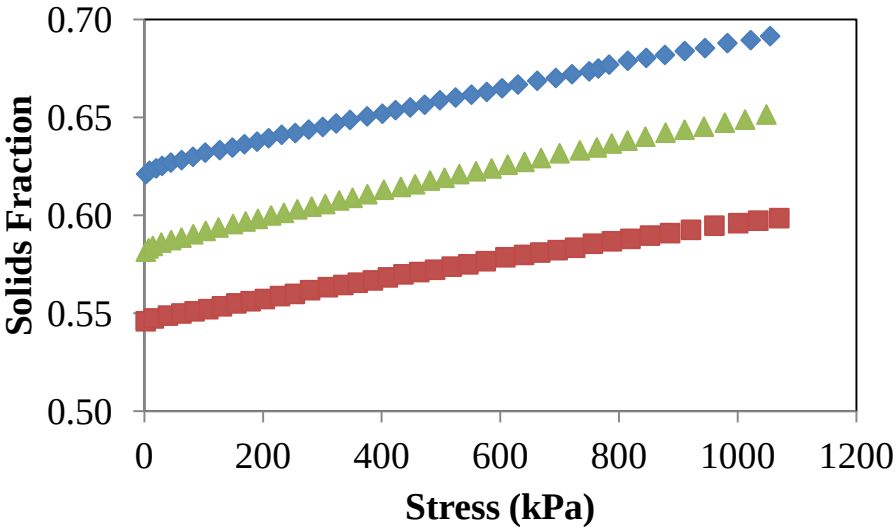

Figure 4-4: Example of compressibility profiles, three repetitions of 275 micron glass beads are shown

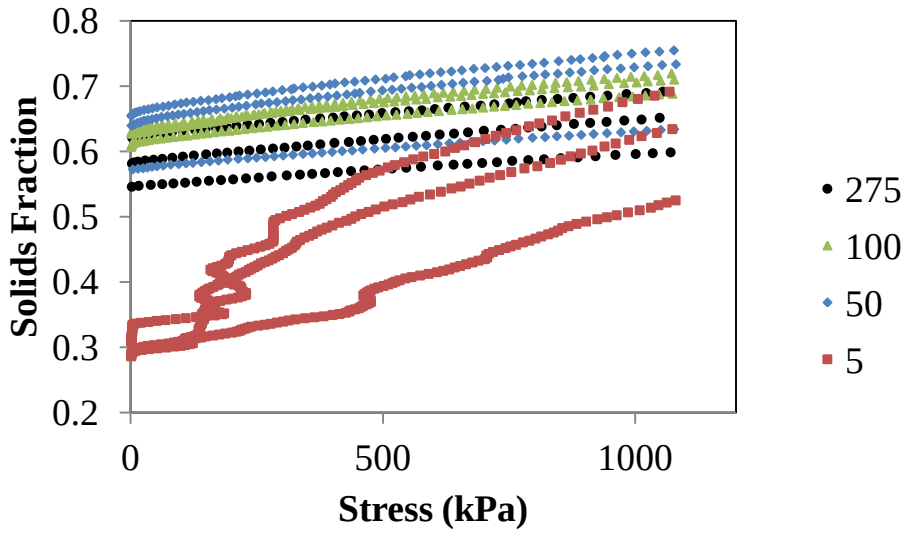

Figure 4-5: Effect of particle size on measured compressibility profiles; d_{50} in microns listed in legend

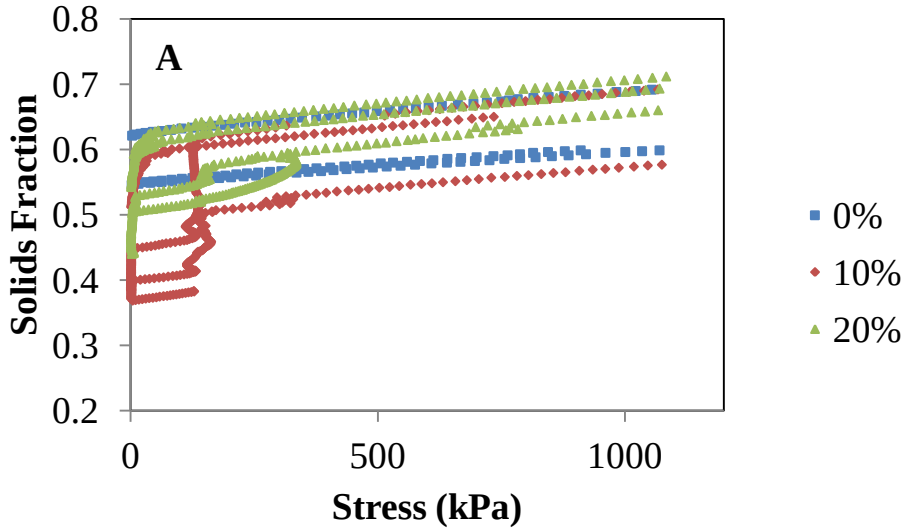

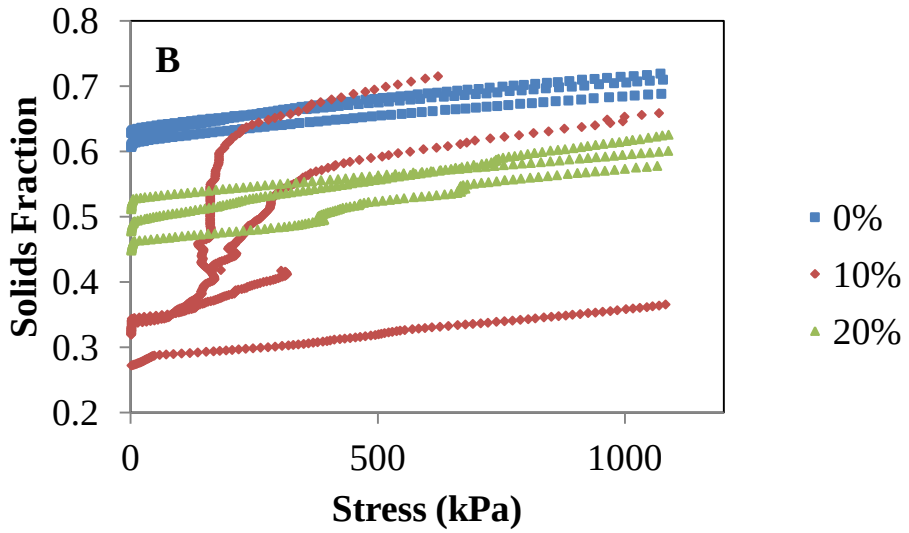
B
Solids Fraction
0.8
0.7
0.6
0.5
0.4
0.3
0.2
0
500
1000
Stress (kPa)
0%
10%
20%

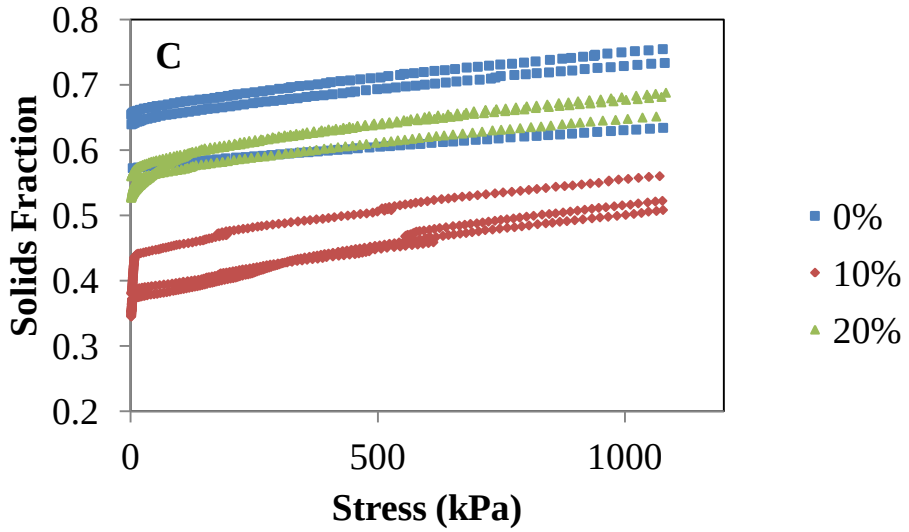
C
Solids Fraction
0.8
0.7
0.6
0.5
0.4
0.3
0.2
0
500
1000
Stress (kPa)
0%
10%
20%

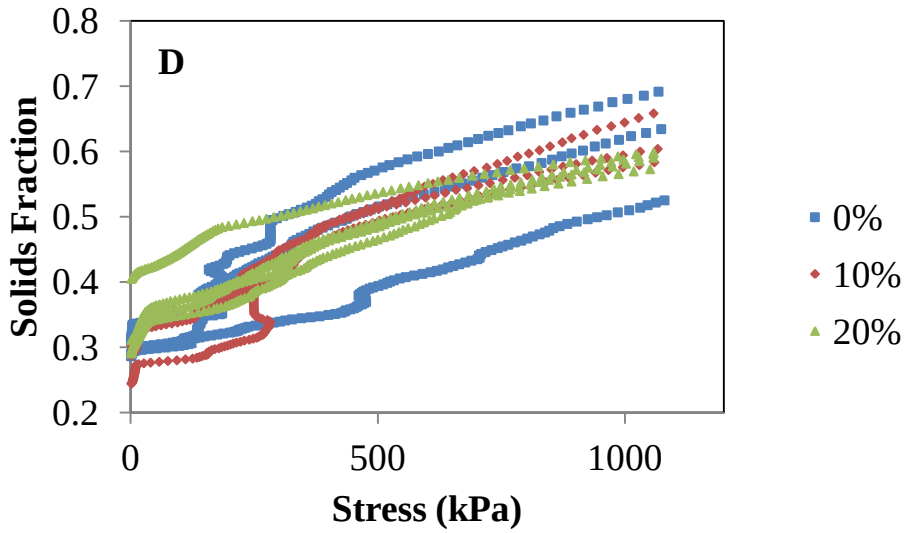

Figure 4-6: Effect of moisture content on (A) 275, (B) 100, (C) 50, and (D) 5 micron beads

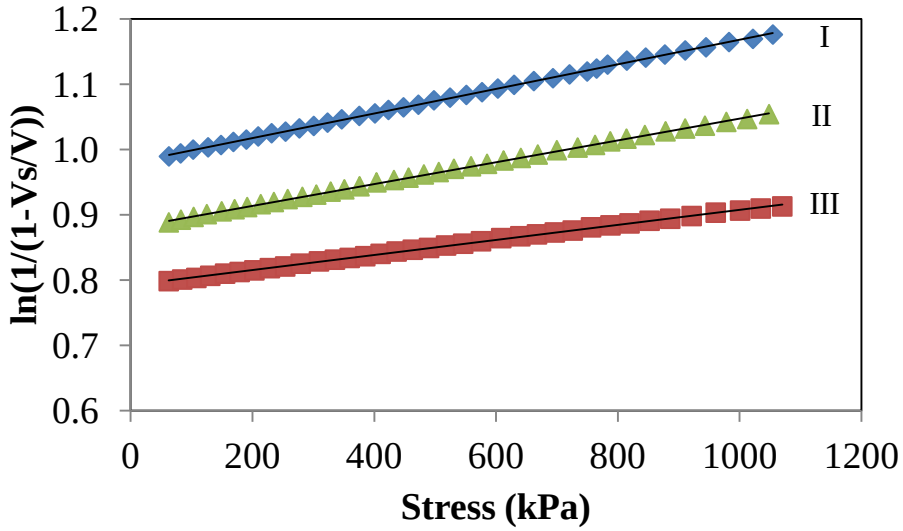

Figure 4-7: Example of fitting Heckel equation to the compressibility profiles at stresses larger than 50kPa, 275 micron at 0% added water shown. The regression statistics for the fits are as follows: (I) R^2 = 0.9995 with p-value <0.001, (II) R^2 = 0.0006 with p-value < 0.001, and (III) R^2 = 0.9992 with p-value < 0.001.

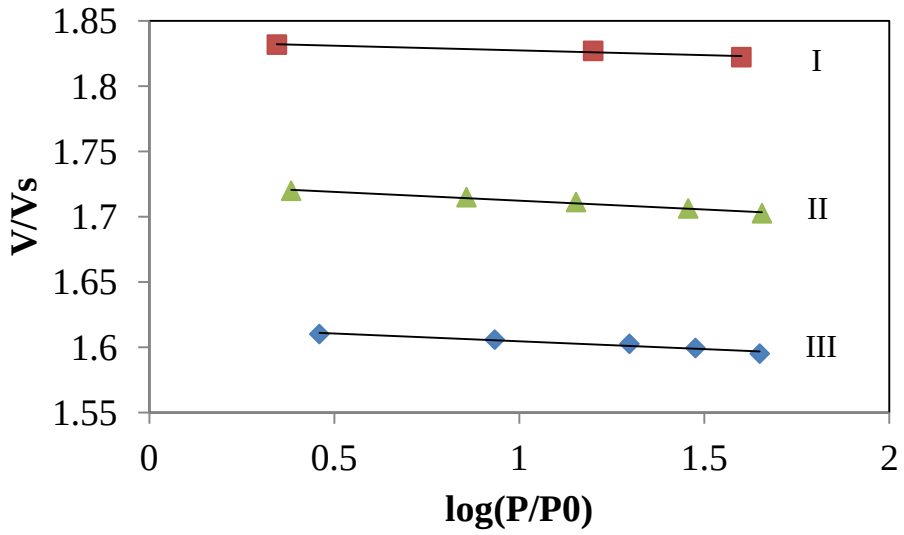

Figure 4-8: Example of fitting Walker equation to the compressibility profiles at low stresses (less than 50kPa), 275 micron at 0% added water shown. The regression statistics for the fits are as follows: (I) R^2 = 0.9582 with p-value = 0.005, (II) R^2 = 0.9850 with p-value = 0.001, and (III) R^2 = 0.9494 with p-value = 0.131

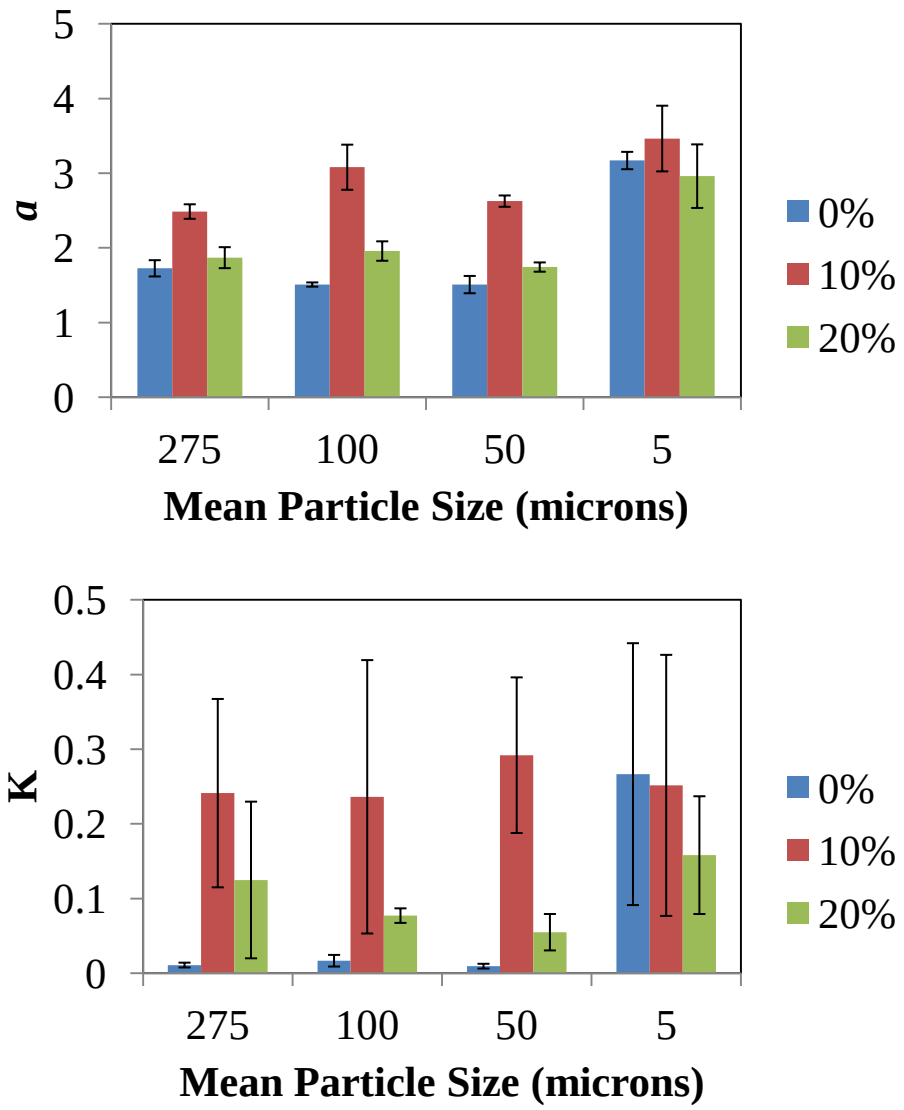

Figure 4-9: Parameter fits of the Walker equation (y-intercept, top; slope, bottom) to measured compressibility profiles up to 50kPa

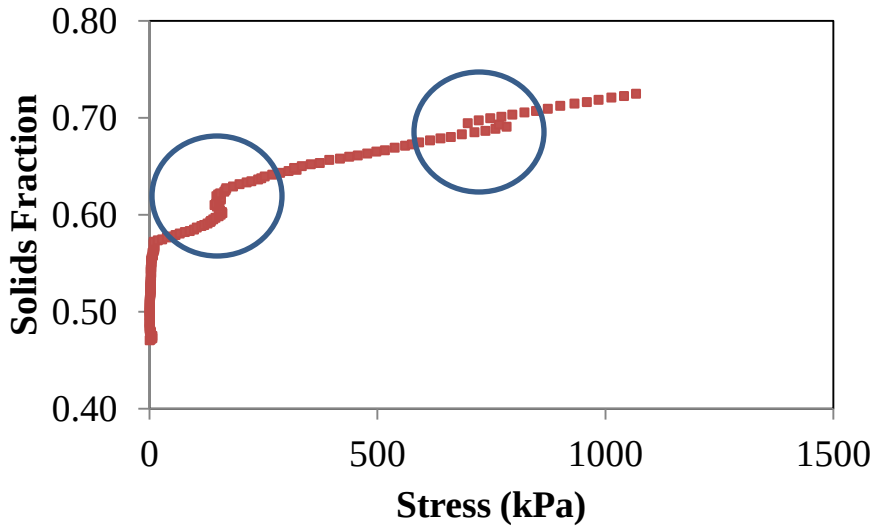

Figure 4-10: Example of horizontal features in a measured profile of 100 micron beads with 20% added moisture.

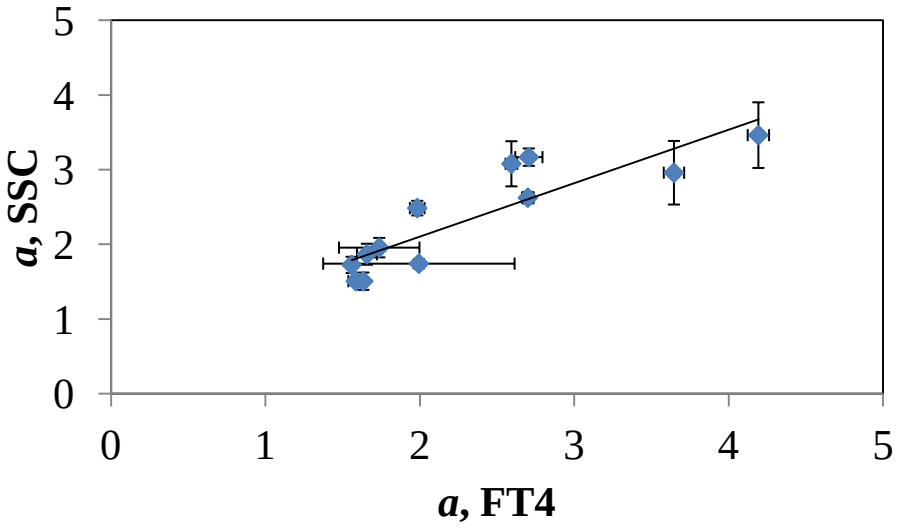

Figure 4-11: Y-intercept from Walker equation fit of small scale compressibility and FT4 for each material. The regression equation was y=0.7164x+0.6706 and had an R^2 of 0.771 and p-value less than 0.001.

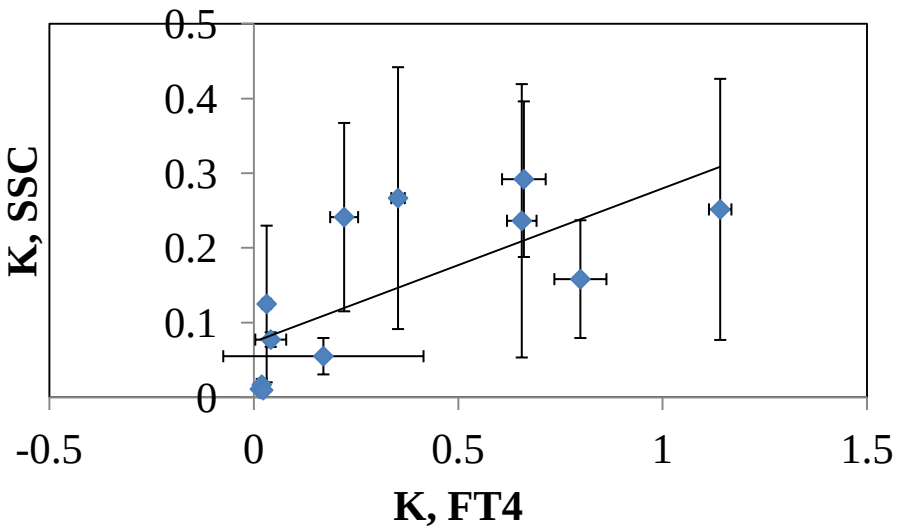

Figure 4-12: Slope from Walker equation fit of small scale compressibility and FT4. The regression equation was y=0.2055x+0.0742 and had an R^2 of 0.511 and a p-value of 0.009.

4.6. Tables for Chapter 4

Table 4-1: Liquid added by volume percent as a function of particle size and liquid added by mass percent

	275 microns	100 microns	50 microns	5 microns
10% by mass	12%	10%	9%	5%
20% by mass	36%	35%	35%	15%

Chapter 5. Measurement of the axial dispersion coefficient of granular materials in a rotating cylinder: dependence on bulk flow properties

5.1. Introduction

The horizontal rotating drum is commonly used for processing powders. It is used across industries and in processes as rotary kilns, impregnators, cement mixers, coaters, blenders, etc. For batch operations the drum or cylinder is placed perfectly horizontal and rotated about its axis. For continuous operations the drum is inclined, typically by a few degrees, loaded through the upper end and discharged through the lower one [119]. There are two main observations that have informed current studies of axial mixing of powders and granular materials: that Fick's second law can be used to describe the axial dispersive mixing [120] and that the axial dispersion coefficient can be related to the residence time distribution via the Peclet number, known as the Taylor dispersion model [121-123]. As a result, the axial dispersion coefficient in batch systems can be related to that in continuous flow systems. These observations have been utilized by many authors to study horizontal rotating drums. Rotary kilns have been the focus of many recent studies [124-126] as have continuous blenders [51, 127-129].

As mentioned, the axial dispersion coefficient has been measured in rotating drums to characterize axial mixing using Fick's second law [130]. Experimentally, tracer particles are introduced and their distribution throughout the bed is monitored as a function of time to yield a measurement of the axial dispersion coefficient. Several initial conditions can be used. Parker *et al* [131] tracked the movements of a single radioactively labeled tracer particle. Hogg *et al* [132], Rao *et al* [133], Cahn and Fuerstenau [134], Carley-Macauly and Donald [135], and Wightman and Muzzio [136] detail studies where one half of the

drum was initially filled with tracer particles. Hogg *et al* [137] began experiments with a thin band of tracer particles at one end of the drum and Shoji *et al* [138] used a thing band near the center of the drum. Signh, on the other hand, started with the tracer particles in a wide band at the center of the drum [139]; this is the initial condition that will be used in this work. These methods have been used to study the effect of several process parameters on the axial dispersion coefficient in a rotating drum, including the rotation rate, fill level, and the incline of the drum. In batch systems, it has been found that the axial dispersion coefficient increases with increasing rotational speed [133, 140] and an inverse relationship between the fill level and axial dispersion coefficient, where the coefficient decreases with increasing fill level [140], has been observed. Abouzeid *et al* [141] and Hehl *et al* [142] have studied the effect of process parameters in continuous flow systems.

The effect of particle and bulk flow properties have been considered in several published works. Some of these studies focused on particle properties such as particle size, shape, and roughness. Studies on the effect of particle size report conflicting results [129, 133, 139, 141]. Rutgers found that needle-like particles give lower axial dispersion coefficients than spherical particles [140]. Rao et al [133] found that increasing surface roughness results in larger coefficients. The ratio of particle-particle friction to particle-wall friction was related to the mixing time by Woodle and Munro [143]. In high dilution mixing in systems with a tracer different from the bulk material, Orr and Shotten found that the ability to mix is dependent on the tensile strength [144]. There have also been equations developed based on continuous flow experiments that relate the axial dispersion coefficient to the angle of repose and bulk density [145, 146]. However, these

equations predict an axial dispersion coefficient of zero in no-flow, i.e. batch, systems; which is contrary to experimental observations. However, as of yet, there has not been a systematic study on the effect of inter-particle forces, characterized by bulk properties, on the axial dispersion coefficient.

This chapter examines the effect of bulk flow properties on axial mixing. The axial dispersion coefficient was measured for five materials with a range of flow properties. The rest of the chapter is organized as follows. The materials characterized and the experimental method used to measure the axial dispersion coefficient are described. Then results are presented for the axial dispersion coefficient as a function of flow properties. The results include statistical analysis used in determining the statistical significance of the material type. It was found that the effect of the material type was statistically significant. Using partial least squares regression, it was also found that, for the materials studied here, the variation in the axial dispersion coefficient can be mostly explained by measurements from three flow property characterization methods: particle size, compressibility, and the shear cell.

5.2. Materials and Methods

5.2.1. Materials

The axial dispersion coefficient of five powders was measured: Lactose Monohydrate N.F. Regular (Forremost, Rothschild, WI, USA), Vivapur 102 (JRS Pharma, Rosenburg, Germany), Compap L APAP (Mallinckrodt, Greensville, IL, USA), Zeolite Y (Zeolyst International, Conshohocken, PA, USA), and fluidized cracking catalyst (W.R. Grace & Co., Columbia, MD, USA). These powders were chosen as they are industrially relevant and represent a wide range in flow behavior. The materials and their properties are listed

in Table 5-1. The particle size distribution was measured using a Beckman-Coulter LS 13 320 series laser diffraction particle size analyzer (Pasadena, CA, USA). The cohesion, flow function coefficient, compressibility, conditioned bulk density, and permeability were measured using the FT4 powder rheometer (Freeman Technology, Tewkesbury, Gloucestershire, UK). The FT4 methods are described in detail by Freeman [77, 101] and have been introduced in previous chapters. The cohesion and flow function coefficient were measured using the shear cell at an initial consolidation stress of 3kPa. The compressibility (percent volume change upon compression) and permeability (in terms of pressure drop) were measured using the vented piston at an applied normal stress of 15kPa, as is typical for these characterization techniques. The flow index was measured using the gravitational displacement rheometer (GDR) as detailed by Alexander *et al* [57] and Faqih *et al* [50, 58, 71]. A smooth acrylic cylinder was used for each material, except for the fluidized cracking catalyst, where a ribbed cylinder was used to mitigate slumping (which is further discussed in Section 5.3).

5.2.2.Methods

5.2.2.1. Visible Light Spectroscopy

This work utilized a tracer material to measure the axial mixing behavior, as is typical of this type of study. In this case, the self-diffusion was of interest and so the material being studied, dyed to a darker color, served as the tracer. The concentration of the dyed material in a sample was measured using a color probe (X-Rite VeriColor Spectro 450, Grand Rapids, MI), i.e. visible light spectroscopy. The surface of a sample with an unknown concentration of dyed material was exposed to light in the visible spectrum. The intensity of the light reflected from the sample surface was proportional to the

concentration of dyed material in the sample. Using a calibration curve, the concentration of dyed material in samples was determined. The calibration curve for lactose monohydrate is shown in Figure 5-1. The experimental points were fitted with a 4^{th} order polynomial to obtain the calibration curve. The following equation describes the calibration curve with a coefficient of determination of 0.9982 and p-value less than 0.01.

$$c = 5x10^{-7}R^4 - 3x10^{-4}R^3 + 6.4x10^{-2}R^2 - 5.1R + 153.2$$

where c was the mass concentration of dyed material in percent and R was the reflectance. Similar calibration curves were obtained for the other materials.

5.2.2.2. Experimental Setup

The particle mixing dynamics within a rotating cylinder was characterized in terms of the axial dispersion coefficient. An acrylic cylinder 30 cm long with an inner diameter of 9.5 cm was used. The cylinder was loaded to a 35% fill level with a wide band initial condition, as illustrated in Figure 5-2. The cylinder was divided into thirds along the axial dimension using physical dividers: the first third was loaded with undyed material, the second third with dyed material (acting as the tracer), and the final third with undyed material. After filling to 35% by volume, the dividers were removed. Variability in the initial loading of the cylinder was a potential source of error in the experiment. Error in the placement of the physical dividers may translate to error in the width and lateral position of the band of dyed material. Further, the level of fill may vary between the dividers, which could translate to error in the ratio of dyed to undyed material. The cylinder was placed on rollers and rotated at 25 rpm for a total of 30 minutes. Samples, 2.5 mL in volume, were taken every 3 cm along the axial dimension at 5, 10, 15, 20, 25,

and 30 minutes of mixing. The samples were collected by opening a portion of the end of the cylinder (so as to not disturb the powder) and then using a scoop to sample the powder. As samples were removed from the cylinder, the fill level was effectively decreasing. Sampling ceased once 10% of the initial volume was removed, tempering the effect of the change in fill level. This occurred after three time points, therefore two cylinders were used for each experimental run. The first cylinder was sampled at 5, 10, and 15 minutes. A fresh cylinder was then initially rotated for 20 minutes and sampled at 20, 25, and 30 minutes of mixing. This was repeated three times for each material.

The visible light spectroscopy method described in Section 2.2.1 was used to measure the concentration of dyed material in each sample. Concentration profiles as a function of axial position for each time point sampled were subsequently generated.

5.3. Results

5.3.1. Concentration profiles

Concentration profiles for each time point sampled for lactose monohydrate are presented in Figure 5-3. As observed from Figures 5-3, the concentration of dyed material is higher in the center of the cylinder than at the edges. This was expected since the initial wide band of dyed material was centrally located along the axial dimension of the cylinder. This figure shows the evolution of mixing with time. As time progresses, the maximum concentration (located at about 15cm) decreases while the concentration at the ends of the cylinder (0 and 30cm) increases. If mixing continued to a well-mixed state, the profile would approach a flat line at a concentration of 0.33. Analogous results are presented in Figure 5-4 for Compap L APAP. Differences in mixing behavior were also observed from the concentration profiles over time. For example, when comparing the lactose

monohydrate (Figure 5-3) and Compap L APAP (Figure 5-4) results, the profiles for lactose monohydrate were flatter than those for Compap L APAP at the same time point. From this observation, it can be concluded that the lactose monohydrate would reach a well-mixed state at a shorter time than the Compap L APAP. As the axial dispersion coefficient describes the rate at which a system mixes, it would be expected that the axial dispersion coefficient for lactose monohydrate would be greater than that for Compap L APAP. As detailed below, this was the case. Concentration profiles as a function of axial position for 5, 10, 15, 20, 25, and 30 minutes were measured for the three other materials (not shown). Similar features to those observed in Figures 5-3 and 5-4 were observed for the other materials.

5.3.2. Axial dispersion coefficient

As previously discussed, it has been suggested that the axial mixing of cohesion-less spheres in a rotating cylinder can be described using the functional form of Fick's second law [120].

$$\frac{\partial c}{\partial t} = D_{ax} \frac{\partial^2 c}{\partial x^2}$$

where c was the concentration of tracer (in this case, dyed material), t was the time, x was the axial position, and D_{ax} was the axial dispersion coefficient. The applicability of this approach to cohesive powders is investigated here. This equation was solved numerically using the wide band initial condition and no-flux boundary conditions using finite differences as done by Singh [139]. To further mitigate some of the error introduced in the initial loading of the cylinder, the initial axial position and width of the wide band were allowed to float. The wide band location and width that minimized the residual

between the experimental concentration profile and numerical solution at 5 and 20 minutes of mixing, corresponding to the first time point in each cylinder, was found. Using this initial band location and width, the axial dispersion coefficient that minimizes the residual sum of squares between the experimental concentration profile and numerical solution (Eqn. 2) was identified for each time point for which samples were taken (every 5 minutes up to 30 minutes of mixing).

$$ss_{res} = \sum_{i} (y_i - f_i)^2$$

where ss_{res} was the residual sum of squares, y_i were the experimental values, and f_i were the numerical values.

The numerical solutions minimizing the residual sums of squares to the experimental concentration profiles of lactose monohydrate and Compap L APAP (Figures 5-3 and 5-4, respectively) are shown here in Figures 5-5 and 5-6, respectively, as typical results. The numerical fits are in reasonably good agreement with the experimental data capturing the evolution of mixing over time as well as the difference in mixing dynamics between materials. Similar observations were made for all experiments executed for each material.

The D_{ax} values corresponding to the numerical fits for lactose monohydrate shown in Figure 5-5 are 0.023, 0.021, and 0.02 cm^2/s at 20, 25, and 30 minutes of mixing, respectively. The D_{ax} values corresponding to the numerical fits for Compap L APAP shown in Figure 5-6 are 0.012, 0.012, and 0.012 cm^2/s at 20, 25, and 30 minutes of mixing, respectively. As expected from comparing the concentration profiles of the

lactose monohydrate and Compap L APAP, the D_{ax} values of the lactose monohydrate were higher than those for Compap L APAP, indicating faster mixing. It is observed that Fick's second law can be used to describe the dispersive mixing in cohesive systems.

5.3.3. Axial dispersion coefficients for cohesive materials

The axial dispersion coefficient was measured for each of the five materials studied here: Zeolite, lactose monohydrate, Compap L APAP, Vivapur 102, and FCC. The values obtained at each of the six time points for an experiment were averaged. Each experiment was repeated three times and an overall average axial dispersion coefficient for each material was computed. These results, the averages and standard deviation of the 18 measurements (six time points and three repeats), are tabulated in Table 5-2. The axial dispersion coefficients range from 0.016 to 0.083 cm^2/s, which is in agreement with values previously reported for granular materials. In the review by Sherritt et al. experimental results for the axial dispersion coefficient ranged from 1e-07 to 1e-03 m^2/s, or 0.001 to 10 cm^2/s [130]. These coefficients are on the same order of magnitude of many diffusion coefficients of gases diffusing into gases and larger than many liquid into liquid diffusion coefficients [147]. FCC had the smallest coefficient, 0.016 cm^2/min, and Zeolite had the largest coefficient, 0.083 cm^2/min, a five-fold increase over that for FCC.

The relationships between the axial dispersion coefficients and the various material properties in Table 5-1 were investigated. In Figure 5-7, the axial dispersion coefficient is plotted as a function of the flow function coefficient (FFC), measured using the shear cell. The flow function coefficient is often used to characterize the flowability of a material, where a larger flow function coefficient corresponds to a more free-flowing

material. The materials can be ranked in terms of flow function coefficient from lowest to highest as follows: Zeolite, lactose monohydrate, Compap L APAP, Vivapur 102, and FCC. Perhaps contrary to intuition, Figure 5-7 shows that as the flow function coefficient increases, corresponding to an increase in flowability, the axial dispersion coefficient *decreases*. It can be seen that the error bar for the axial dispersion coefficient of the poorest flowing material (Zeolite) is the largest. The next material in terms of flowability is lactose monohydrate. A relatively large decrease in axial dispersion coefficient and standard deviation is observed. The next material in terms of flowability is Compap L APAP. There is less of a decrease in axial dispersion coefficient and standard deviation. The next two materials in terms of flowability are Vivapur 102 and FCC and these materials show a much smaller decrease in axial dispersion coefficient. The results for axial dispersion can be separated into two groups: the poorest flowing materials (Zeolite and lactose monohydrate) and the better flowing materials (Compap L APAP, Vivapur 102, and FCC). It is interesting that in spite of the fact that Compap L APAP, Vivapur 102, and FCC have quite different flow function coefficients, their axial dispersion coefficients are relatively similar.

In Figure 5-8 the axial dispersion coefficient is shown as a function of compressibility percent at an applied normal stress of 15kPa, measured using the FT4 compressibility test. Typically, a lower compressibility percent corresponds to a material with lower cohesion and better flowability. Behavior similar to that observed previously for the FFC in Figure 5-7 was observed for the compressibility percent in Figure 5-8, however, the relative order of Compap L APAP and Vivapur 102 reversed. In Figure 5-8, it can be

seen that all the materials have significant differences in compressibility and again fall into two groups in terms of axial dispersion coefficient.

The particle size, in terms of d_{10} and d_{50}, also correlates with the axial dispersion coefficient, as seen in Figures 5-9 and 5-10. Smaller particle sizes often exhibit larger cohesive forces and worse flowability. It is observed in Figures 5-9 and 5-10 that the axial dispersion increases with decreasing average and fines particles sizes. Behavior similar to that described above for the FFC in Figure 5-7 and compressibility percent in Figure 5-8 was observed for d_{10} and d_{50}. However, the relative order of Compap L APAP, Vivapur 102, and FCC varied. In Figures 5-9 and 5-10, it can be observed that all materials have significant differences in d_{10} and d_{50} and again fall into two groups in terms of axial dispersion coefficient. Zeolite and lactose monohydrate fall into the same group (in terms of axial dispersion coefficient) and appear in the same order for the flow function coefficient, compressibility percent, d_{10}, and d_{50}. Vivapur 102, Compap L APAP, and FCC belong to the same group but appear in different orders. Not every material property correlates with the axial dispersion coefficient, however. For example, the permeability does not exhibit a clear relationship with the axial dispersion coefficient as seen in Figure 5-11. While only some of the material properties have a relationship to the axial dispersion coefficient, the ones that do exhibit the same relationship. Summarily, the flow function coefficient, d_{10}, and d_{50} decrease with increasing axial dispersion coefficient while the compressibility percent increases with increasing axial dispersion coefficient. That is, as the flow properties worsen, the axial dispersion coefficient increases. Put another way, cohesive, poorly flowing materials mix more quickly than less cohesive materials.

This is likely due to the manner in which cohesive granular material flows in a rotating cylinder. The experimental conditions were chosen such that the type of bed motion exhibited in each of the experiments was in the cascading regime. As described by Mellman, powder bed motion in which the bed does not slip at the drum wall, circulates continuously, and has an arched bed surface can be classified as cascading motion [148]. There is an active surface layer and a relatively inactive core. Particles against the drum wall move with the wall until the maximum height of the bed is reached. The particles then fall down the free surface of the bed. Cohesion-less particles tend to fall individually down the free surface. However, in cohesive systems, the particles do not fall individually, but as assemblies or "chunks" of material. The size of the particle assemblies is dependent on the inter-particle surface forces, the larger the attraction between particles, the larger the assemblies that can form. Therefore, the relevant characteristic length may not be the particle diameter, but instead the size of the formed assemblies. Since the cohesive, poorly flowing materials, which would form larger assemblies and therefore have a larger effective length, exhibit larger axial dispersion coefficients, these results follow the trend observed previously in the literature of surface velocities and axial dispersion coefficient increasing with particle diameter [129, 149].

To verify the above concept, flow index measurements taken using the Gravitational Displacement Rheometer (GDR) were compared to the axial dispersion coefficient measurements. The GDR measures the size of the avalanches, or "chunks," that fall during flow of a granular material in a rotating drum [57]. A larger flow index indicates larger avalanches. From the above discussion, it would be expected that the axial dispersion coefficient would increase with increasing flow index. Behavior similar to

that observed previously for the FFC, compressibility percent, d_{10}, and d_{50} (Figures 5-7-10) was observed for the flow index. In Figures 5-12, it can be observed that the materials have significant differences in flow index and again fall into two groups with respect to the axial dispersion coefficient. The three left-most points are Vivapur 102, Compap L APAP, and FCC, forming the same group as observed for the FCC, compressibility percent, d_{10}, and d_{50}. While their respective flow index values are different, they had similar axial dispersion coefficient values. The lactose monohydrate had a larger axial dispersion coefficient and belongs to the second group of poorly-flowing materials. As mentioned previously, the flow index is typically measured in a smooth, acrylic cylinder. However, during the testing for the fluidized cracking catalyst, the particles flowed in the surging regime. Due to a low coefficient of wall friction, the powder bed would travel up with the cylinder wall to a critical angle and then slide down as a whole. This sliding movement registered as an avalanche. For this material, a ribbed cylinder was used to mitigate the slumping. The ribs increased the wall friction and prevented the bed as a whole sliding against the wall. The flow index of the fluidized cracking catalyst measured using the ribbed cylinder is shown in Figure 5-12. The flow index measurement for the Zeolite, 16.34, was lower than expected. It was observed during testing that the Zeolite particles would form spherical agglomerates, as seen in Figure 5-13. The material prior to testing is shown on the left and after testing on the right. The agglomerates likely formed due to electrostatic forces. Agglomerates were not observed during the axial dispersion measurement. Therefore, agglomeration is a phenomenon introduced by the flow index measurement technique that does not occur during the other experiments. Due to the inaccurate measurement caused by the

electrostatic forces, the flow index measurement for Zeolite was not included in Figure 5-12. For the cases studied here, the flow index measurements support the concept that the relevant characteristic length for the axial mixing in cohesive systems should be the avalanche size as opposed to the particle diameter.

5.3.4.PLS regression

It is clear that the material has a statistically significant effect on the axial dispersion coefficient. It has also been observed that, for the materials studied here, some material properties correlate with the axial dispersion coefficient while some do not. A statistical approach to identifying the flow property or properties whose variation best predicts changes in the axial dispersion coefficient was explored. This approach may lead to a reduced number of material flow properties that are needed for the characterization of future materials and/or experimental conditions, saving time, money, and resources as well as demonstrate understanding of the axial mixing dynamics in a rotating cylinder. The statistical approach used here was partial least squares (PLS) regression.

The PLS regression technique, also known as “projection to latent structures”, can be useful in situations where the goal is to identify and quantify relationships between predictors and observations; particularly in cases where the predictors are collinear and their number exceeds that of the observations. Here, there was a set of nine material flow properties acting as the predictors and one observation, the axial dispersion coefficient. While each property is measured in a different manner, they are all measurements of the inter-particle surface forces. It would then be expected that a set of material properties would be highly collinear. Therefore, PLS regression was a suitable method to employ here.

A two factor non-hierarchal PLS model was fitted to the x-block data consisting of nine material properties for the five materials and the single y-variable, the axial dispersion coefficient. The data were mean-centered and scaled. The cumulative percent variance explained by the two factors was 94%, shown in Figure 5-14. The first factor explained 90% and the second factor explained an additional 4%. Good parity was observed between the predicted and actual y-values (axial dispersion coefficients), as shown in Figure 5-15. The root mean square error was 0.09. The regression coefficients are depicted in Figure 5-16. The coefficients represent the contribution of each material flow property to the prediction of the axial dispersion coefficient, with higher coefficients indicating larger contributions. Positive coefficients indicate a positive correlation and negative coefficients indicate an inverse proportionality. Those with little or no weight are not very useful in the prediction. The material property with the largest contribution was the compressibility. The properties with the smallest contributions were the permeability and the flow index. It was expected that the flow index would be a poor predictor of the axial dispersion coefficient due to the smaller than expected measurement for the Zeolite. To verify that these two independent measurements could be removed from the model without losing predictive capability a new PLS regression model was fitted using the remaining seven material flow properties. The cumulative percent variance explained by two factors was 95%. The first factor explained 91% and the second factor an additional 4%. The root mean square error of the predicted versus actual y-values remained 0.09. The coefficient weights, as depicted in Figure 5-17, also remained similar. The compressibility had the largest weight. The compressibility and cohesion were positively correlated with the axial dispersion coefficient while the d_{10},

d_{50}, d_{90}, conditioned bulk density, and flow function coefficient were negatively correlated. Therefore, it can be concluded that the axial dispersion coefficient can be described using these seven material flow properties. These material flow properties are measured by three characterization methods. The d_{10}, d_{50}, and d_{90} are particle size parameters. The conditioned bulk density and compressibility at 15kPa are both measured using the FT4 compressibility test. The cohesion and flow function coefficient are measured by the FT4 shear cell. The parameters obtained using these three characterization methods can predict 95% of the variation observed in the axial dispersion coefficient.

5.4. Conclusions

In this study, the axial mixing of cohesive systems was examined. The self-mixing dynamics of five materials with a range of flow properties was characterized in terms of the axial dispersion coefficient. It was found that Fick's second law can be used to describe the dispersive mixing in cohesive systems. The coefficients for the five materials varied five-fold and were within the range observed by previous work reported in the literature. Keeping the experimental conditions constant, it was also found that the material type had a statistically significant effect on the axial dispersion coefficient. That is, the strength of the inter-particle surface forces effects how quickly a cohesive system mixes. Analysis of the material properties revealed that the axial dispersion coefficient was correlated to the inter-particle surface forces. More cohesive, poorly flowing materials mix more quickly than less cohesive materials. This is likely due to the "chunks" formed as the material flows (supported by the flow index measurements). For the materials studied here, measurements from three characterization methods, particle

size distribution, compressibility, and shear cell, can predict 95% of the variation observed in the axial dispersion coefficient.

These results are based on five materials at a single experimental condition. Thus, further work is needed at additional experimental conditions to generalize our results across multiple scales. A better understanding of axial mixing behavior in rotating drums is important to the successful design and scale up of processes that contain a mixing component, e.g. mixing, calcination, coating, etc. This paper also demonstrates a statistical approach for identifying relevant material flow properties for specific processes. The approach can easily be generalized and applied to additional material properties and unit operations.

5.5. Figures for Chapter 5

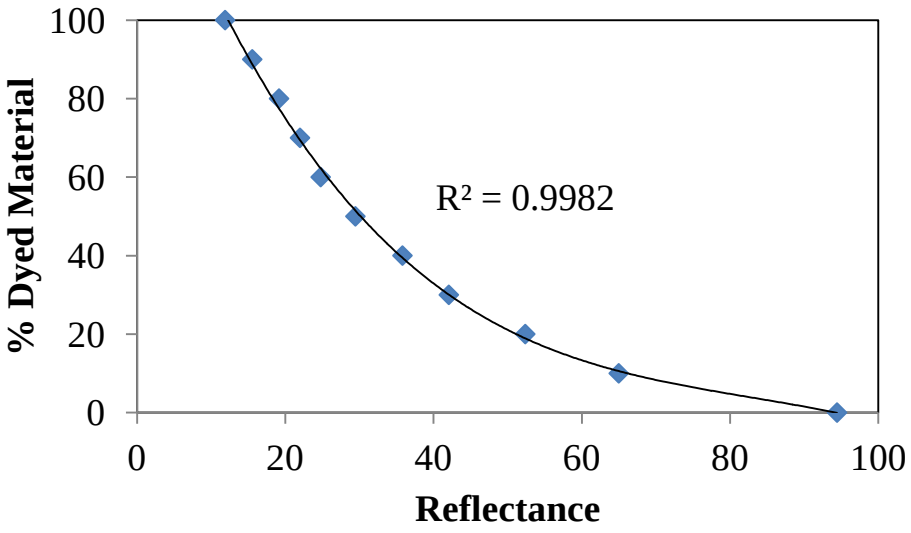

Figure 5-1: Calibration curve for lactose monohydrate with a 4th-order polynomial fit.

Figure 5-2: Initial loading condition of cylinder: 1/3 of the length loaded with undyed material, 1/3 with dyed material (tracer), and 1/3 with undyed material

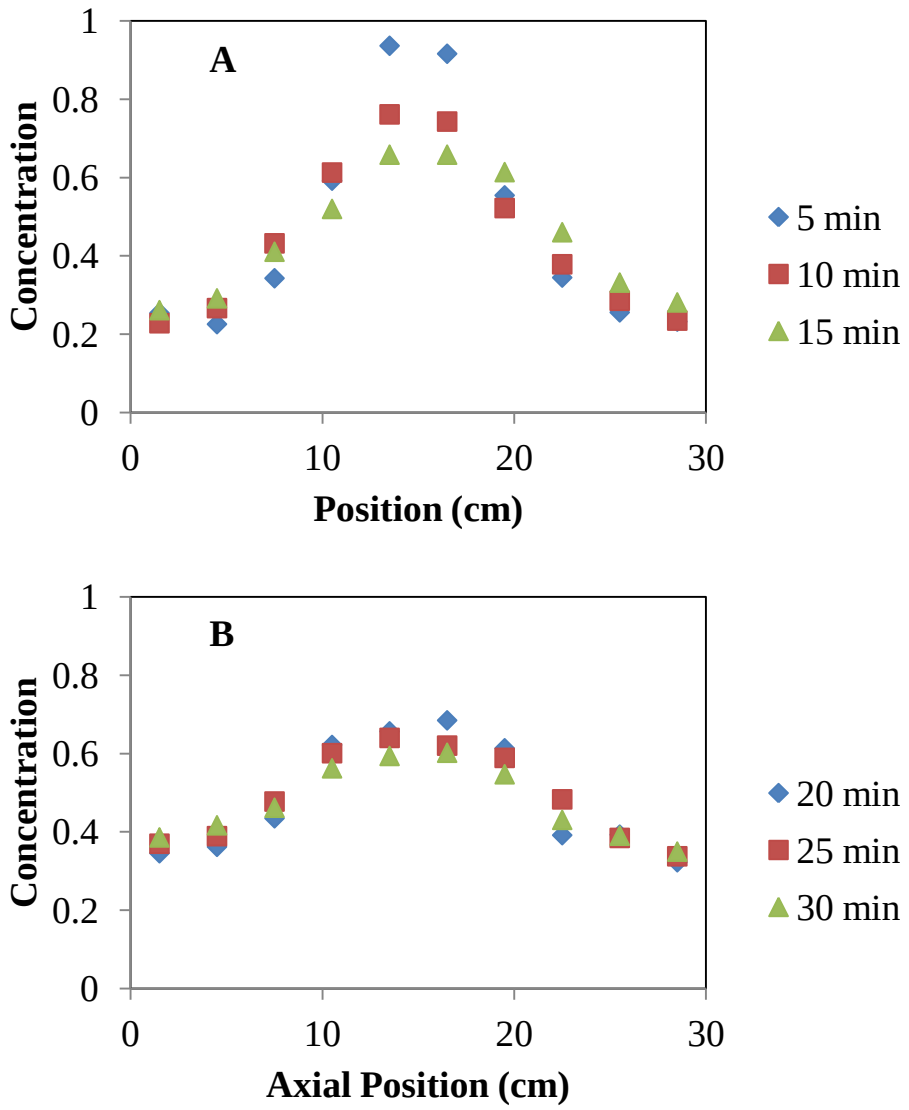

Figure 5-3: Concentration profiles of dyed lactose monohydrate at (A) 5, 10, and 15 minutes and (B) 20, 25, and 30min of mixing.

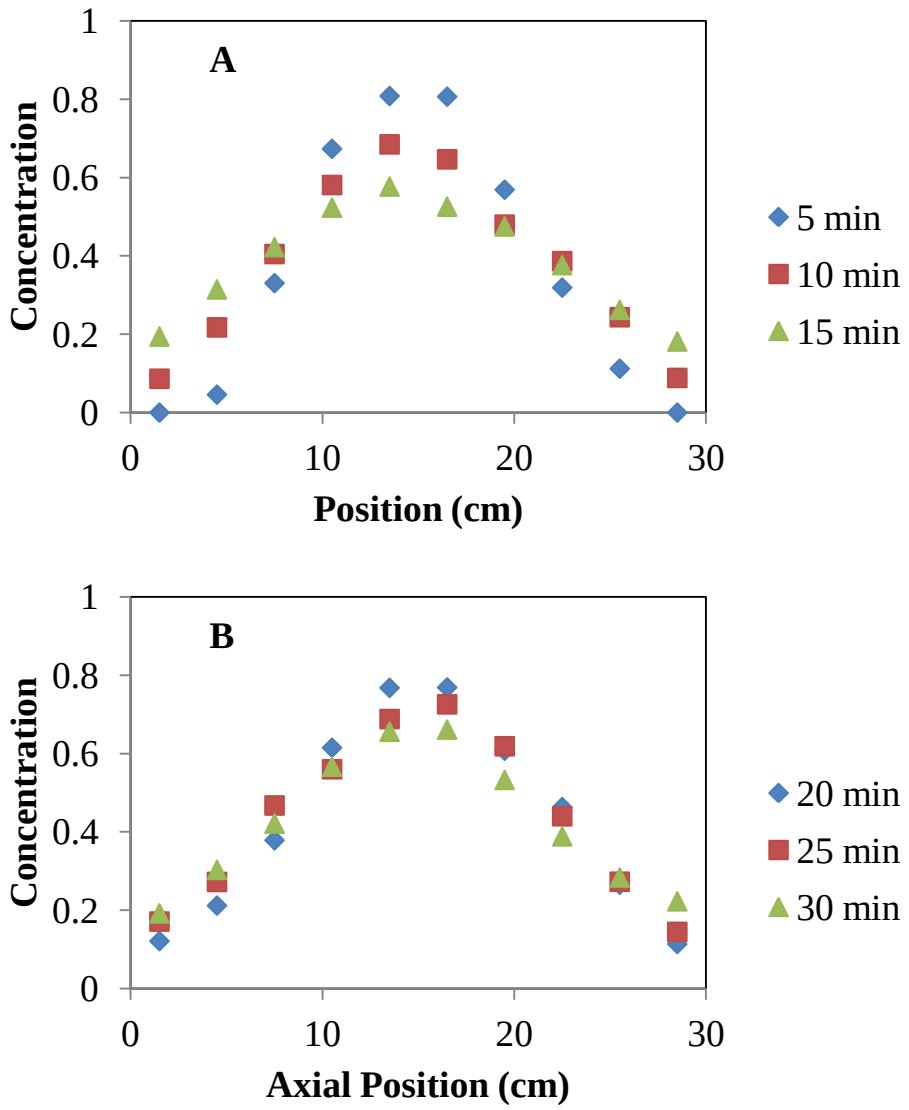

Figure 5-4: Concentration profiles of dyed Compap L at (A) 5, 10, and 15 minutes and (B) 20, 25, and 30 minutes of mixing.

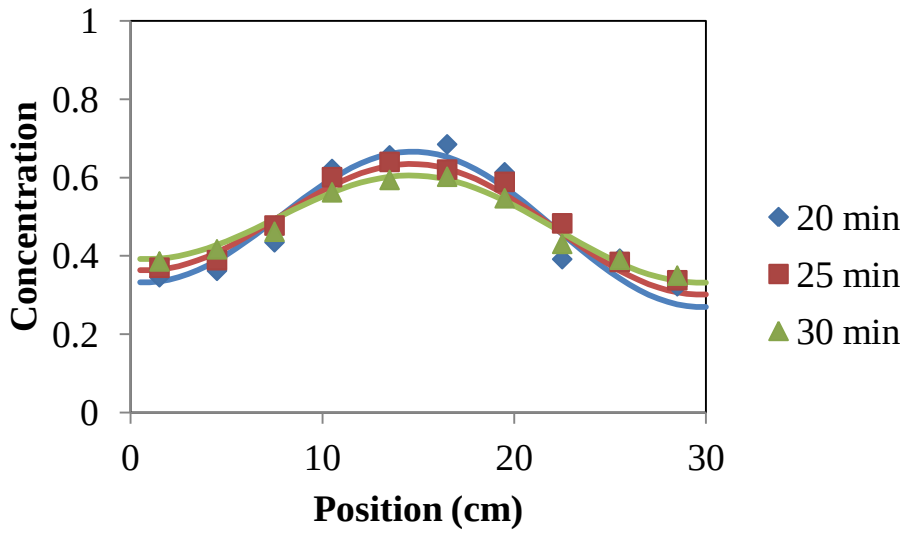

Figure 5-5: Experimental concentration profile (shown as points) of dyed lactose monohydrate and the optimal numerical solution of Fick's Second Law (shown as lines) at 20, 25, and 30min of mixing.

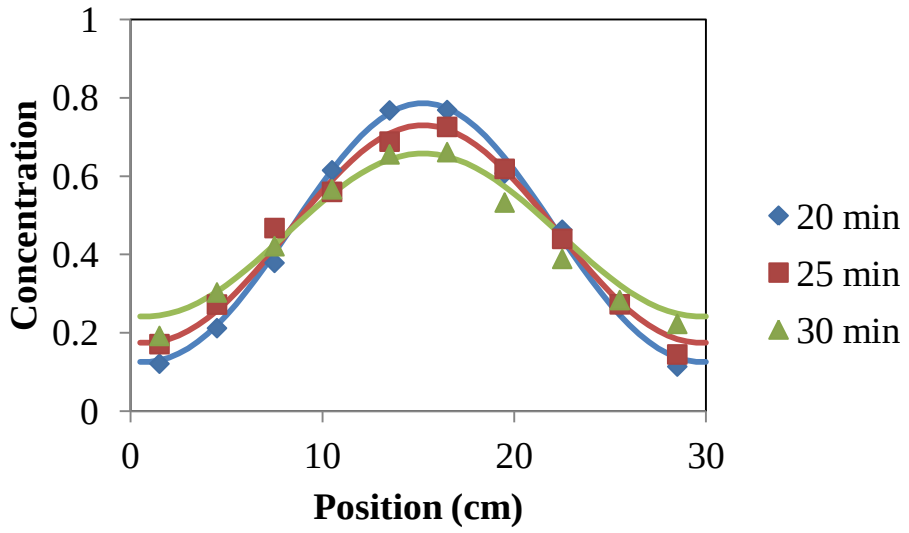

Figure 5-6: Experimental concentration profile (shown as points) of dyed Compap L and the optimal numerical solution of Fick's Second Law (shown as lines) at 20, 25, and 30min of mixing.

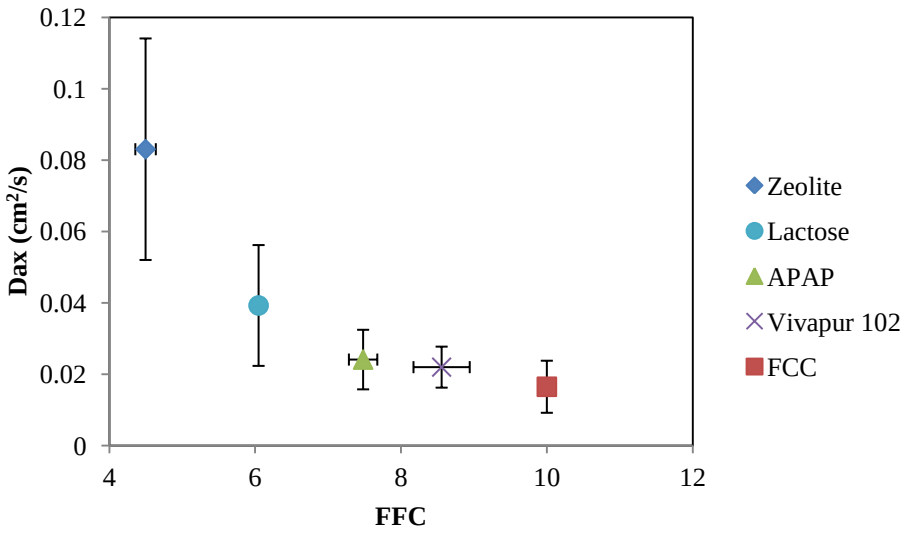

Figure 5-7: The axial dispersion coefficient as a function of the flow function coefficient as measured by the FT4 shear cell.

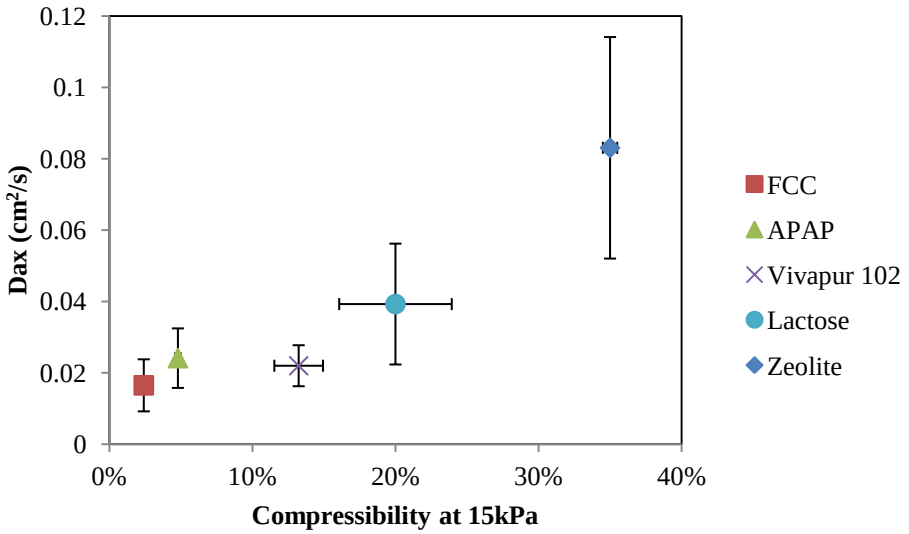

Figure 5-8: The axial dispersion coefficient as a function of the compressibility at an applied normal stress of 15kPa as measured by the FT4 powder rheometer.

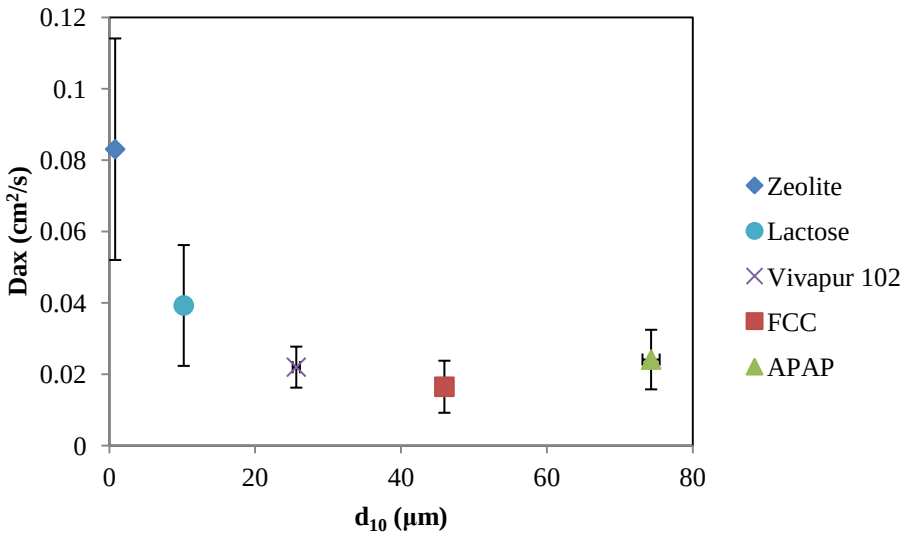

Figure 5-9: The axial dispersion coefficient as a function of d_{10}.

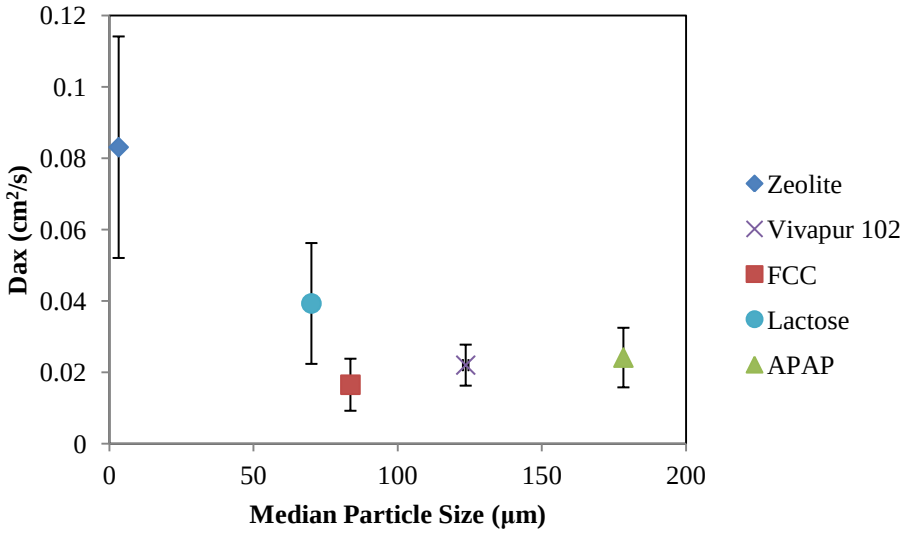

Figure 5-10: The axial dispersion coefficient as a function of d_{50}.

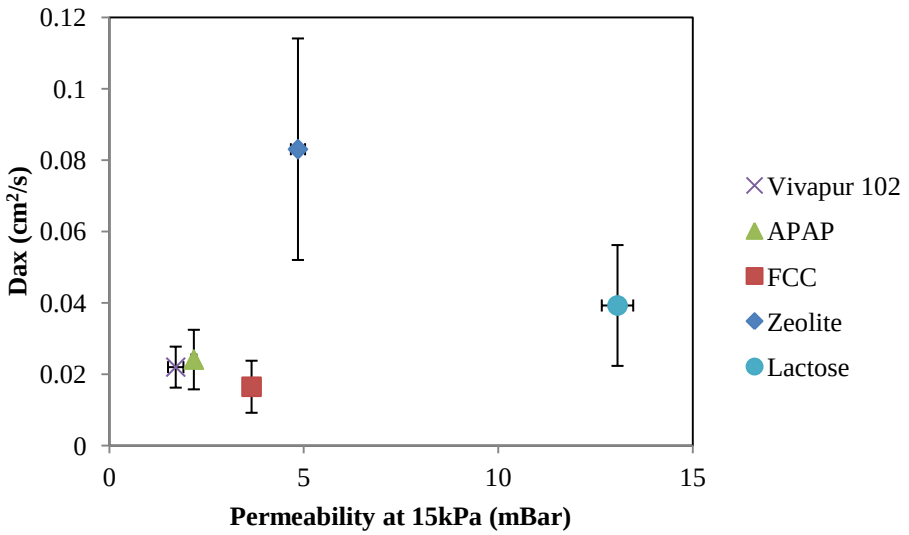

Figure 5-11: The axial dispersion coefficient as a function of the permeability at an applied normal stress of 15kpa as measured by the FT4 powder rheometer.

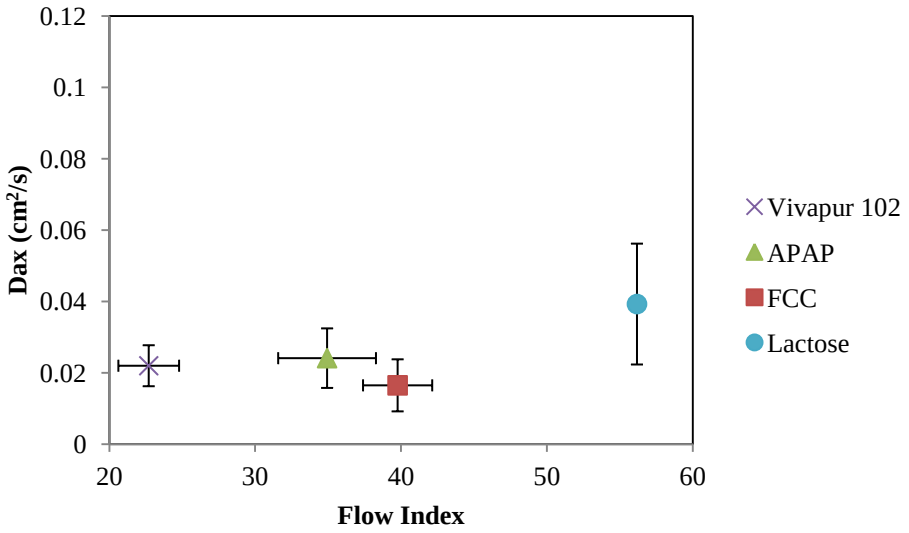

Figure 5-12: The axial dispersion coefficient as a function of the flow index as measured by the GDR.

Figure 5-13: Zeolite before GDR testing (left) and after GDR testing (right).

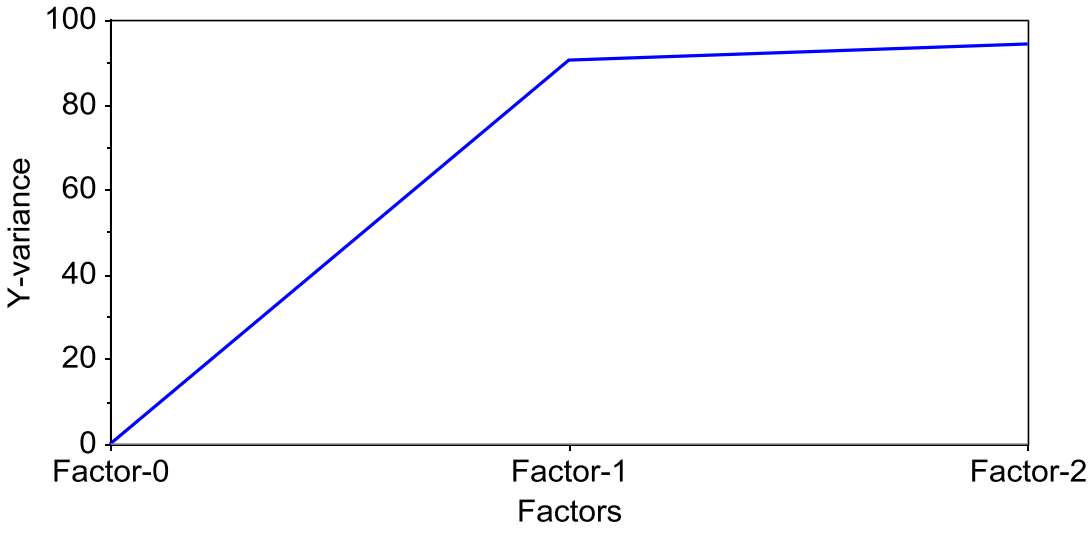

Figure 5-14: Cumulative percent explained variance by PLS model.

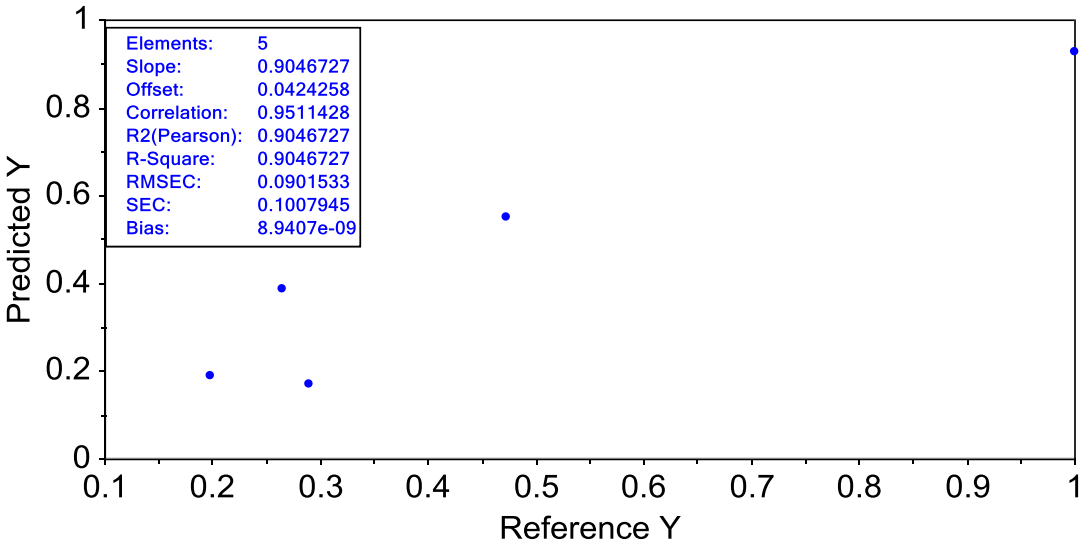

Figure 5-15: Predicted versus reference parity plot for the axial dispersion coefficient

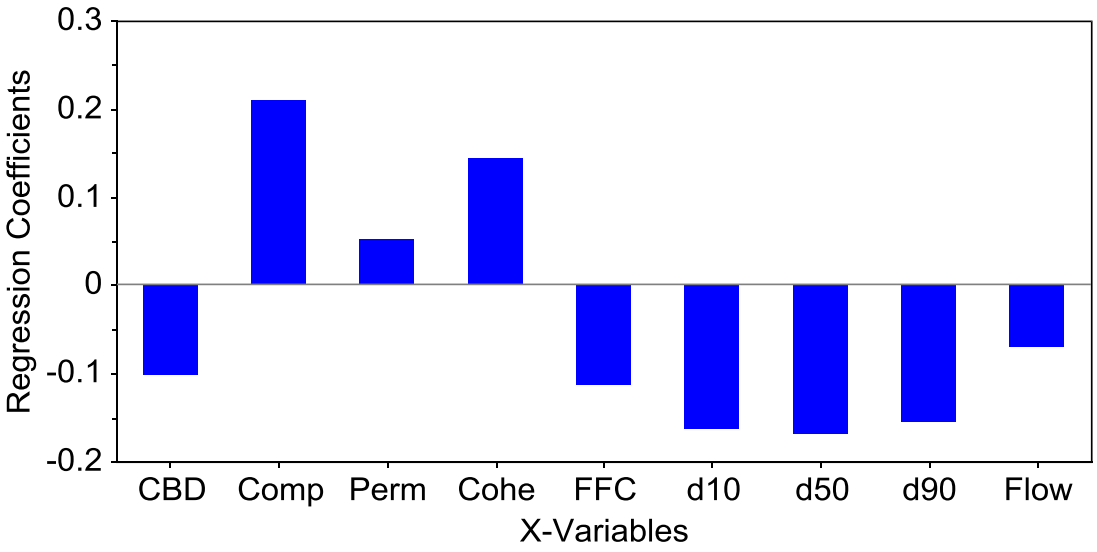

Figure 5-16: Regression coefficients of PLS model

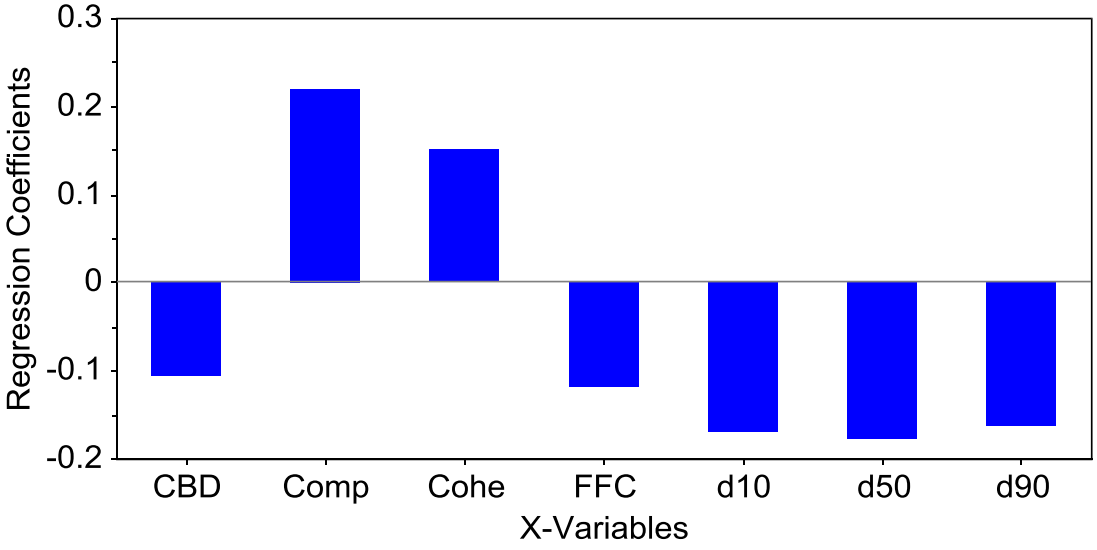

Figure 5-17: Regression coefficients of reduced PLS model

5.6. Tables for Chapter 5

Table 5-1: Particle size and flow properties

Material	d_{10} (µm)	d_{50} (µm)	d_{90} (µm)	Compressibility @ 15kPa	Permeability @ 15kPa	FFC	Flow Index
Zeolite	0.80	3.23	11.51	0.35	4.85	4.50	16.34
FCC	45.95	83.61	139.12	0.02	3.66	10.00	39.77
Compap L APAP	74.29	178.29	316.37	0.05	2.17	7.48	34.93
Vivapur 102	25.64	123.59	198.93	0.13	1.71	8.56	22.70
Lactose monohydrate	10.20	70.07	150.73	0.20	13.07	6.05	56.18

Table 5-2: Axial dispersion coefficients for each material tested

Material	Dax (cm^2/s)	Standard Deviation
FCC	0.016	0.007
Vivapur 102	0.022	0.006
Lactose Monohydrate	0.039	0.017
Zeolite	0.083	0.031
Compap L APAP	0.024	0.008

Chapter 6. Conclusions and recommendations

The work presented in this dissertation focused on using statistical methods to optimize powder flow measurements and to predict powder processing performance. A PCA method was introduced to analyze databases of raw material properties. Commonly used techniques, and those identified as capable of distinguishing most between raw materials, were investigated in detail. Namely, the fundamentals of the shear cell and compressibility test were studied. Finally, the material characterization and the statistical method for analyzing databases were applied to a case study - axial mixing. This chapter summarizes the work presented in the dissertation and outlines recommendations for future work.

6.1. Conclusions

The first specific aim focused on the development of a statistically-based method for analyzing databases of raw material properties. Chapter 2 of the dissertation details the material properties typically considered in solids processing as well as the PCA method for the database analysis. The PCA method was demonstrated using a case study of a database of raw materials. Two different questions were considered: 1) what is the minimum set of material properties that retain the same predictive capability as the original data set and 2) if only a limited number of tests could be completed, for example 3, which properties should be measured such that the predictive capability is maximized. It was found that the original 25 material properties could be reduced to 14 without losing predictive power. The three characterization tests that maximize the modeling capability were found to be the shear cell, compressibility test, and the particle size.

The second specific aim focused on studying the shear cell (Chapter 3) and compressibility tester (Chapter 4) in more detail. These techniques are commonly used and were also identified as maximizing the information for describing the differences in the materials studied in Chapter 2. The differences between the measurements taken using three commercially available rotational shear cells were studied. Two materials, a free-flowing alumina and a cohesive alumina, were used to compare measurements from three commercially available rotational shear cells. Results were collected and compared for cohesion, unconfined yield stress, major principal stress, pre-shear stress, flow function coefficient, and bulk density. ANOVA methods were used to determine the statistical significance and relative size of each of these effects. This work has found that while, as expected, the material type has the largest effect on the shear cell results, the consolidation at which the material was tested and the tester type are also statistically significant effects. These results indicate that care should be taken when comparing the results between different shear cells.

Many characterization tests require a large powder sample on the order of tens to hundreds of grams, however, many applications have limited sample availability, due to cost, material availability, safety concerns, etc. Therefore, a method that uses less material was of interest. This work introduced a novel compressibility method that uses less than 50mg of material. The effect of particle size and cohesion due to capillary forces were determined. As the particle size decreased, the packing fractions decreased. At the initial introduction of capillary forces, the packing fractions initially decreased, but at some critical point between 10 and 20% water by weight, the packing fractions increased. It was found that the packing of the powder bed occurred in two regimes that

can be described using the Walker and Heckel equations. This method was validated against known physics and the FT4 compressibility test. The bulk properties measured at a larger scale were also observed and measured using only 50mg of material.

The third specific aim focused on a case study of axial mixing (Chapter 5). Rotating drums are encountered in numerous industrial applications, e.g. calciners, impregnators, coaters, cement mixers, etc. In all of these devices, the rotation of drum is used to engender mixing of the granular material in the radial direction. Axial mixing, despite its significantly lower rate, can also have an impact on the process performance, especially when residence time control is essential. Typically, the particle dynamics in rotating drums are quantified as a function of process conditions, such as rotation speed, fill level, and cylinder size, as well as particle properties – usually limited to the characterization of particle size. In this work, the quantification of the axial particle dynamics was expanded to include bulk flow properties. Fick's second law was found to describe the axial dispersion behavior of cohesive particles. Therefore, changes in behavior can be characterized using the axial dispersion coefficient. The effect of the material was found to be statistically significant and the strength of the inter-particle surface forces was directly proportional to the axial dispersion coefficient. Partial least squares was used to determine that 95% of the variation observed in the axial dispersion coefficient measurement can be explained using particle size, compressibility, and shear cell measurements. This was a successful application of the statistical methods to identify the most relevant material properties for a given circumstance, in this case that is axial mixing.

6.2. Recommendations for future work

Based on the work presented in this dissertation, there are several potential areas of future study. Three specific directions are detailed here.

6.2.1. Application of statistical analysis of material property databases to continuous manufacturing

The database approach developed here, in Chapter 2, is flexible and can easily be applied to additional unit operations. The PLS method, discussed in Chapter 5, is particularly suitable for application to continuous manufacturing processes. The pharmaceutical industry has traditionally operated on a batch basis. Recently, however, there has been a movement towards continuous manufacturing. Operating on a continuous basis can have many advantages, including smaller equipment footprint, elimination of scale up, as development can sometimes be carried out at the manufacturing scale, and more meaningful PAT, where a large fraction of the product stream is assayed online. At the same time, material properties are critical in continuous manufacturing. For example, many of the remedies for flow problems during batch processing, such as stopping the process and manually disturbing material to encourage flow, are simply not practical during continuous processing, where achieving and maintaining steady operation is essential. When designing and operating a continuous process, careful consideration of material properties is therefore paramount. The operation of a continuous manufacturing process produces large amounts of information. Compiling the data into a database organizes the data and enables a systematic, statistically based analysis of the data. Predictive models can be developed that predict intermediate blend and final product properties based on raw material properties, mixing ratios, and operating conditions. A

potential method for developing the predictive models is a multi-block partial least squares approach.

A small scale feasibility study has been performed as a proof of concept. The continuous process considered included two feeders, a comill, and a mixer (Figure 6-1). A fractional factorial DOE was executed; the excipient type, API concentration, feedrate, mill speed, and mixer speed were varied. The material properties of the raw materials, samples taken after the mill, and samples taken after the mixer were measured. Particle size, compressibility, shear cell, and permeability techniques were used. A predictive model was developed using multi-block PLS statistics. The results are shown in Figure 6-2 as parity plots that compare the predicted to measured material properties. Each subplot represents an experimental condition, 17 in total. The results for the intermediate blends after the mill are on the top and for those after the mixer are on the bottom. As can be observed from the parity plots, some of the predictions are better than others. This feasibility study shows that this approach can be used to analyze continuous processes. With the addition of further experimental results, including materials and operating conditions, the predictive capability of the model can be improved. Moreover, this approach can be used to track the evolution of material properties throughout the process. The effect of material properties on the process performance as well as the effect of the processing on the material properties can be determined.

6.2.2. Small scale compressibility: DEM to study physics of the system

The work presented in Chapter 4 introduced a novel method for measuring powder flow properties using a small scale system. It was found that metastable structures within the powder bed could be observed as they were breaking. However, due to the nature of the

system, the frequency and size of the breaking events (i.e. the magnitude of the repacking) was highly variable. Discrete element modeling (DEM) would be useful for studying the physics of this system further. Due to the small size, the system could be studied at scale. The formation and subsequent breaking of the metastable structures could be observed for a number of initial packing arrangements. The force distribution throughout the bed over the entire compression could also be monitored. The characteristics of the metastable structures could be correlated to material properties and bulk behavior.

6.2.3. Scale up of axial mixing systems incorporating effects of material properties

The axial dispersion coefficient was found to be dependent on material properties, as discussed in Chapter 5. This result has some interesting implications for the scale-up of mixing unit operations involving cohesive granular systems. The scale-up of cohesion-less systems has been studied and the Froude number is typically used. However, the Froude number does not account for differences between the cohesive forces of materials and so provides an incomplete prescription for the scale up of mixing processes. The inclusion of the material properties in the scale-up should be studied. One potential avenue is the use of the granular bond number, the ratio of attractive surface forces to gravitational forces. The combination of the Froude number and the Bond number could be used to determine how to scale-up a given system.

6.3. Figures for Chapter 6

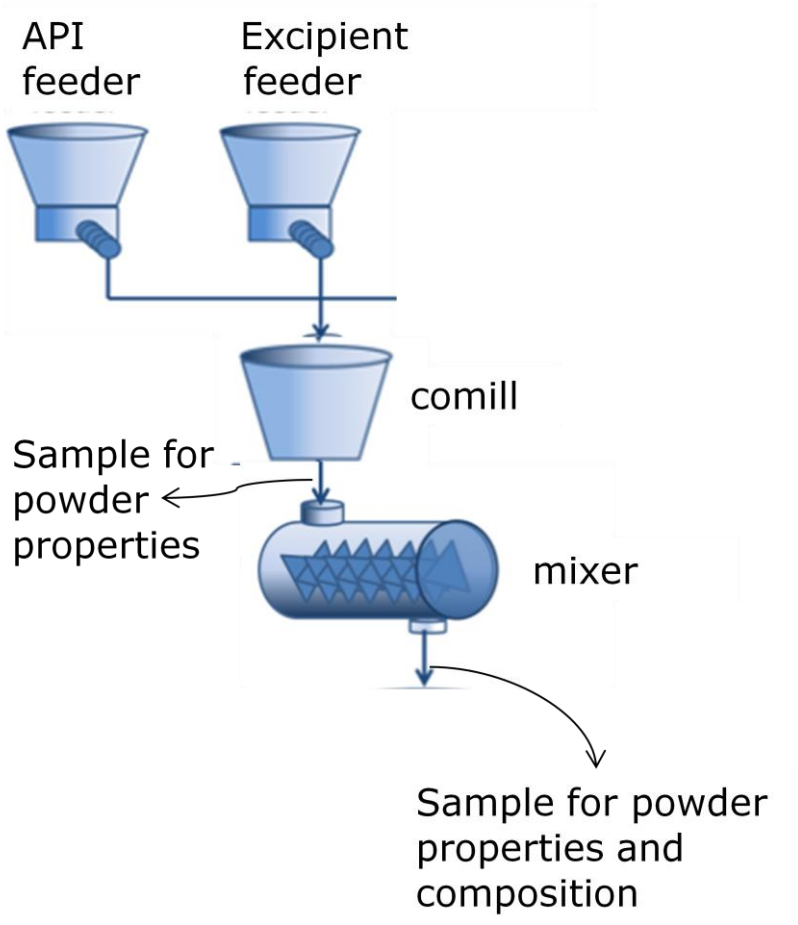

Figure 6-1: Schematic of continuous process

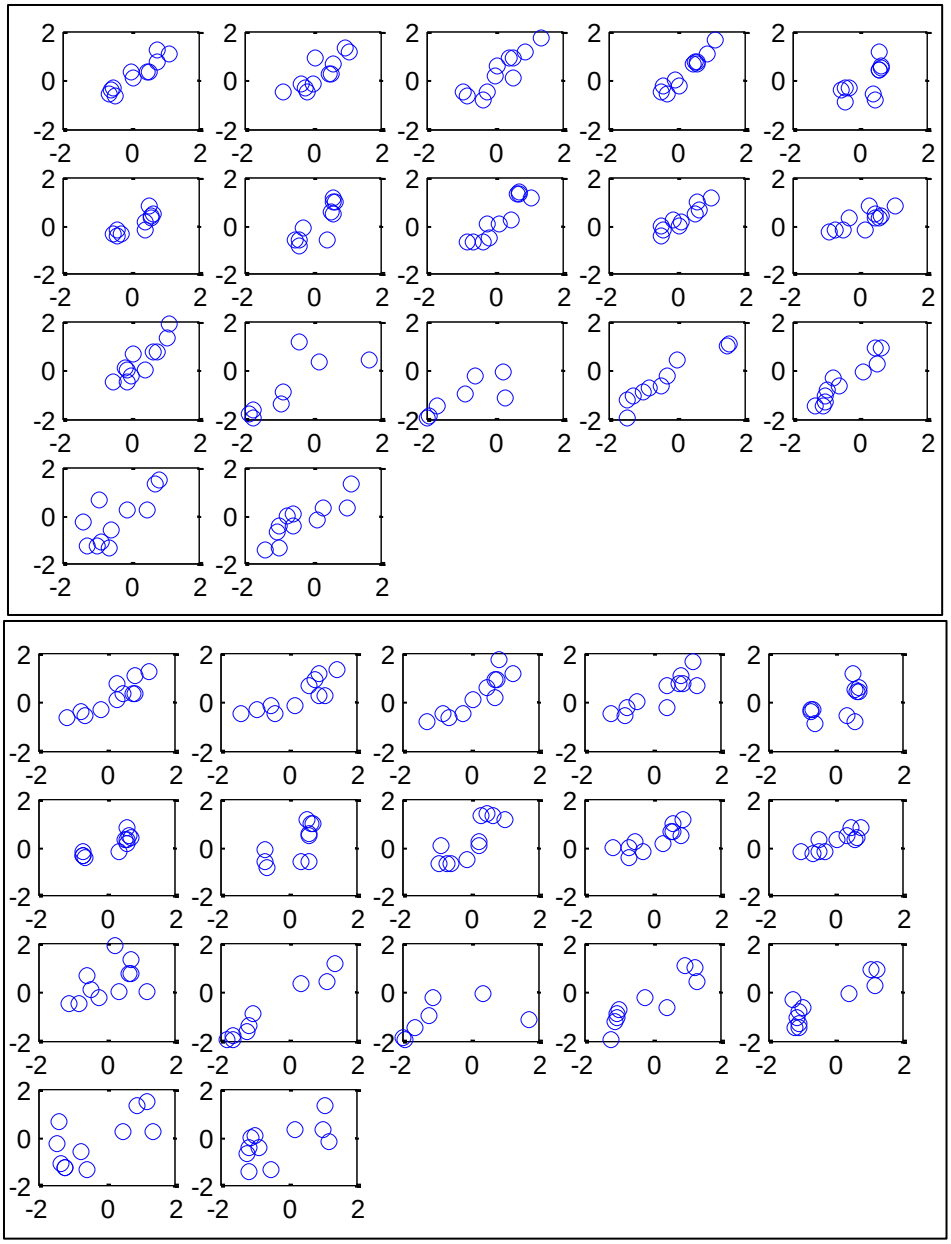

Figure 6-2: Parity plots for results from multi-block PLS predictive model

References

1. Shinbrot, T., K. LaMarche, and B.J. Glasser, *Triboelectrification and Razorbacks: Geophysical Patterns Produced in Dry Grains.* Physical Review Letters, 2006. **96**(17): p. 178002.
2. Geldart, D., *Powder Processing - The Overall View*, in *Principles of Powder Technology*, M.J. Rhodes, Editor. 1991, Wiley. p. 1-7.
3. Bates, L., *The Need for Industrial Education in Bulk Technology.* Bulk Solids Handling, 2006. **26**(7): p. 464-475.
4. Bridgewater, J., *The dynamics of granular materials – towards grasping the fundamentals.* Granular Matter, 2003. **4**(4): p. 175-181.
5. Ennis, B.J., Green, J., and Davies, R., *Partcle Technology - The legacy of neglect in the U.S.* Chemical Engineering Progress, 1994. **90**: p. 32-43.
6. Poux, M., Fayolle, P., Bertrand, J., Bridoux, D., Bousquet, J., *Powder mixing: Some practical rules applied to agitated systems.* Powder TEchnology, 1991. **68**(3): p. 213-234.
7. Wang, Z.L., et al., *Powder formation by atmospheric spray-freeze-drying.* Powder Technology, 2006. **170**(1): p. 45-52.
8. Prescott, J.K., *Powder handling*, in *Pharmaceutical Process Scale-Up*. 2011, Informa Healthcare. p. 195-209.
9. Muzzio, F.J., et al., *Solids Mixing*, in *Handbook of Industrial Mixing*. 2004, John Wiley & Sons, Inc. p. 887-985.
10. Radl, S., et al., *Mixing characteristics of wet granular matter in a bladed mixer.* Powder Technology, 2010. **200**(3): p. 171-189.
11. Remy, B., B.J. Glasser, and J.G. Khinast, *The effect of mixer properties and fill level on granular flow in a bladed mixer.* Aiche Journal, 2010. **56**(2): p. 336-353.
12. Lamberto, D.J., et al., *Laboratory methods for assessing API sensitivity to mechanical stress during agitated drying.* Chemical Engineering Science, 2011. **66**(17): p. 3868-3875.
13. Galarraga, C., E. Peluso, and H. de Lasa, *Eggshell catalysts for Fischer-Tropsch synthesis: Modeling catalyst impregnation.* Chemical Engineering Journal, 2001. **82**(1-3): p. 13-20.
14. Liu, X., J.G. Khinast, and B.J. Glasser, *A parametric investigation of impregnation and drying of supported catalysts.* Chemical Engineering Science, 2008. **63**: p. 4517-4530.
15. Vasilenko, A., et al., *Role of consolidation state in the measurement of bulk density and cohesion.* Powder Technology, 2013. **239**(0): p. 366-373.
16. Rietema, K., *Powders, what are they?* Powder Technology, 1984. **37**(1): p. 5-23.
17. Schulze, D., *Powders and Bulk Solids: Behavior, Characterization, Storage and Flow*. 2008, Berlin: Springer-Verlag
18. Campbell, C.S., *Granular material flows - An overview.* Powder Technology, 2006. **162**(3): p. 208-229.
19. CAMPBELL, C.S., *Granular shear flows at the elastic limit.* Journal of Fluid Mechanics, 2002. **465**: p. 261-291.
20. Campbell, C.S., *Elastic granular flows.* International Journal of Chemical Reactor Engineering, 2004. **2**(1).
21. Campbell, C.S., *Stress-controlled elastic granular shear flows.* Journal of Fluid Mechanics, 2005. **539**: p. 273-297.
22. Goldhirsch, I., *RAPID GRANULAR FLOWS.* Annual Review of Fluid Mechanics, 2003. **35**(1): p. 267-293.
23. Janssen, H.A., *Versuche uber getreidedruck in silozellen.* Ztg. Ver. Dt. Ing. , 1895. **39**: p. 1045-1049.

24. Jenike, A.W., *Storage and flow of solids.* Utah Engineering Experimental Station Bulletin, 1964. **123**: p. 1–194.
25. Jenike, A.W., *Gravity flow of bulk solids.* Utah Engineering Experimental Station Bulletin, 1961. **108**: p. 1–294.
26. Muzzio, F.J., T. Shinbrot, and B.J. Glasser, *Powder technology in the pharmaceutical industry: the need to catch up fast.* Powder Technology, 2002. **124**(1-2): p. 1-7.
27. Wibowo, C. and K.M. Ng, *Operational issues in solids processing plants: Systems view.* AIChE Journal, 2001. **47**(1): p. 107-125.
28. MiDi, G.D.R., *On dense granular flows.* European Physical Journal E, 2004. **14**(4): p. 341-365.
29. Prescott, J.K. and R.A. Barnum, *On Powder Flowability.* Pharmaceutical Technology, 2000: p. 60-84.
30. Schwedes, J., *Review on testers for measuring flow properties of bulk solids.* Granular Matter, 2003. **5**(1): p. 1-43.
31. Teunou, E., J.J. Fitzpatrick, and E.C. Synnott, *Characterisation of food powder flowability.* Journal of Food Engineering, 1999. **39**(1): p. 31-37.
32. Fitzpatrick, J.J., S.A. Barringer, and T. Iqbal, *Flow property measurement of food powders and sensitivity of Jenike's hopper design methodology to the measured values.* Journal of Food Engineering, 2004. **61**(3): p. 399-405.
33. Fitzpatrick, J.J., et al., *Effect of composition and storage conditions on the flowability of dairy powders.* International Dairy Journal, 2007. **17**(4): p. 383-392.
34. Podczeck, F. and Y. Miah, *The Influence of Particle Size and Shape on the Angle of Internal Friction and the Flow Factor of Unlubricated and Lubricated Powders.* International Journal of Pharmaceutics, 1996. **144**(2): p. 187-194.
35. Guerin, E., et al., *Rheological Characterization of Pharmaceutical Powders Using Tap Testing, Shear Cell and Mercury Porosimeter.* International Journal of Pharmaceutics, 1999. **189**(1): p. 91-103.
36. Lavoie, F., L. Cartilier, and R. Tibert, *New Methods Characterizing Avalanche Behavior to Determine Powder Flow.* Pharmaceutical Research, 2002. **19**(6): p. 7.
37. Taylor, M.K., et al., *Composite Method to Quantify Powder Flow as a Screening Method in Early Tablet or Capsule Formulation Development.* AAPS PharmSciTech, 2000. **1**(3): p. 11.
38. Lindberg, N.-O., et al., *Flowability Measurements of Pharmaceutical Powder Mixtures with Poor Flow Using Five Different Techniques.* Drug Development and Industrial Pharmacy, 2004. **30**(7): p. 785-791.
39. Hancock, B.C., et al., *Development of a Robust Procedure for Assesing Powder Flow Using a Commercial Avalanche Testing Instrument.* Journal of Pharmaceutical and Biomedical Analysis, 2004. **35**: p. 12.
40. Schwedes, J., *Consolidation and flow of cohesive bulk solids.* Chemical Engineering Science, 2002. **57**(2): p. 287-294.
41. Leturia, M., et al., *Characterization of flow properties of cohesive powders: A comparative study of traditional and new testing methods.* Powder Technology, 2014. **253**(0): p. 406-423.
42. Vasilenko, A., B.J. Glasser, and F.J. Muzzio, *Shear and flow behavior of pharmaceutical blends -- Method comparison study.* Powder Technology, 2011. **208**(3): p. 628-636.
43. Pingali, K.C., et al., *Practical methods for improving flow properties of active pharmaceutical ingredients.* Drug Dev Ind Pharm, 2009. **35**(12): p. 1460-1469.
44. Faqih, A.M.N., et al., *Effect of moisture and magnesium stearate concentration on flow properties of cohesive granular materials.* International Journal of Pharmaceutics, 2007. **336**(2): p. 338-345.

45. Zhou, Q., et al., *Effect of mechanical dry particle coating on the improvement of powder flowability for lactose monohydrate: A model cohesive pharmaceutical powder.* Powder Technology, 2011. **207**(1–3): p. 414-421.
46. Orband, J.L.R. and D. Geldart, *The Use of an Antistatic Agent to Improve Powder Flowability.* Particle & Particle Systems Characterization, 1995. **12**(4): p. 204-206.
47. Pingali, K.C., et al., *Use of a static eliminator to improve powder flow.* International Journal of Pharmaceutics, 2009. **369**(1–2): p. 2-4.
48. Mullarney, M.P., et al., *Applying dry powder coatings to pharmaceutical powders using a comil for improving powder flow and bulk density.* Powder Technology, 2011. **212**(3): p. 397-402.
49. Jallo, L.J., et al., *Improvement of flow and bulk density of pharmaceutical powders using surface modification.* International Journal of Pharmaceutics, 2012. **423**(2): p. 213-225.
50. Faqih, A.N., et al., *A method for predicting hopper flow characteristics of pharmaceutical powders.* Chemical Engineering Science, 2007. **62**(5): p. 1536-1542.
51. Vanarase, A.U., J.G. Osorio, and F.J. Muzzio, *Effects of powder flow properties and shear environment on the performance of continuous mixing of pharmaceutical powders.* Powder Technology, 2013. **246**(0): p. 63-72.
52. Bouffard, J., et al., *Experimental investigation of the effect of particle cohesion on the flow dynamics in a spheronizer.* Aiche Journal, 2013. **59**(5): p. 1491-1501.
53. He, X., et al., *Assessing powder segregation potential by near infrared (NIR) spectroscopy and correlating segregation tendency to tabletting performance.* Powder Technology, 2013. **236**(0): p. 85-99.
54. Podczeck, F., *Rheological studies of physical properties of powder used in capsule filling.* Pharmaceutical Technology Europe, 1999. **11**(9): p. 16-24.
55. Podczeck, F., *Rheological studies of physical properties of powder used in capsule filling.* Pharmaceutical Technology Europe, 1999. **11**(10): p. 34-42.
56. Nase, S.T., et al., *Discrete characterization tools for cohesive granular material.* Powder Technology, 2001. **116**(2–3): p. 214-223.
57. Alexander, A.W., et al., *Avalanching flow of cohesive powders.* Powder Technology, 2006. **164**(1): p. 13-21.
58. Faqih, A., et al., *An experimental/computational approach for examining unconfined cohesive powder flow.* International Journal of Pharmaceutics, 2006. **324**(2): p. 116-127.
59. Lee, Y.S.L., et al., *Development of a Dual Approach to Assess Powder Flow from Avalanching Behavior.* AAPS PharmSciTech, 2000. **1**(3).
60. Krantz, M., H. Zhang, and J. Zhu, *Characterization of powder flow: Static and dynamic testing.* Powder Technology, 2009. **194**: p. 239-245.
61. Davies, C.E., et al., *A New Approach to Monitoring the Movement of Particulate Material in Rotating Drums.* Developments in Chemical Engineering and Mineral Processing, 2004. **12**(3-4): p. 263-275.
62. Carson, J.W. and H. Wilms, *Development of an international standard for shear testing.* Powder Technology, 2006. **167**(1): p. 1-9.
63. Berry, R.J. and M.S.A. Bradley, *Investigation of the effect of test procedure factors on the failure loci and derived failure functions obtained from annular shear cells.* Powder Technology, 2007. **174**(1–2): p. 60-63.
64. Pillai, J.R., M.S.A. Bradley, and R.J. Berry, *Comparison between the angles of wall friction measured on an on-line wall friction tester and the Jenike wall friction tester.* Powder Technology, 2007. **174**(1–2): p. 64-70.
65. Abdullah, E.C. and D. Geldart, *The use of bulk density measurements as flowability indicators.* Powder Technology, 1999. **102**(2): p. 151-165.
66. Grey, R.O. and J.K. Beddow, *On the Hausner Ratio and its relationship to some properties of metal powders.* Powder Technology, 1969. **2**(6): p. 323-326.

67. Rhodes, M., *Intoroduction to Particle Technology*. 2 ed. 2008, West Sussex, England: John Wiley and Sons, Ltd. 450.
68. Carr, R.L., *Evaluating flow properties of solids.* Chemical Engineering, 1965. **72**: p. 163-168.
69. Hausner, H., *Friction conditions in a massive metal powder.* International Journal of Powder Metallurgy, 1967. **7**.
70. Freeman, R., *Measuring the flow properties of consolidated, conditioned and aerated powders — A comparative study using a powder rheometer and a rotational shear cell.* Powder Technology, 2007. **174**(1–2): p. 25-33.
71. Faqih, A., et al., *Flow - induced dilation of cohesive granular materials.* AIChE Journal, 2006. **52**(12): p. 4124-4132.
72. Trivedi, M.R. and R.H. Dave, *To study physical compatibility between dibasic calcium phosphate and cohesive actives using powder rheometer and thermal methods.* Drug Dev Ind Pharm. **0**(0): p. 1-12.
73. Bemrose, C.R. and J. Bridgwater, *A review of attrition and attrition test methods.* Powder Technology, 1987. **49**(2): p. 97-126.
74. Remon, J.P. and J.B. Schwartz, *Effect of Raw Materlals and Processing on the Quality of Granules Prepared from Microcrystalline Cellulose-Lactose Mixtures.* Drug Dev Ind Pharm, 1987. **13**(1): p. 1-14.
75. Gohel, M.C. and P.D. Jogani, *Exploration of Melt Granulation Technique for the Development of Coprocessed Directly Compressible Adjuvant Containing Lactose and Microcrystalline Cellulose.* Pharmaceutical Development and Technology, 2003. **8**(2): p. 175-185.
76. Chevalier, E., et al., *Comparison of low-shear and high-shear granulation processes: effect on implantable calcium phosphate granule properties.* Drug Dev Ind Pharm, 2009. **35**(10): p. 1255-1263.
77. Freeman, R.E., J.R. Cooke, and L.C.R. Schneider, *Measuring shear properties and normal stresses generated within a rotational shear cell for consolidated and non-consolidated powders.* Powder Technology, 2009. **190**(1-2): p. 65-69.
78. Mendez, R., C. Velazquez, and F.J. Muzzio, *Effect of feed frame design and operating parameters on powder attrition, particle breakage, and powder properties.* Powder Technology, 2012. **229**(0): p. 253-260.
79. Prestidge, C.A. and G. Tsatouhas, *Wettability studies of morphine sulfate powders.* International Journal of Pharmaceutics, 2000. **198**(2): p. 201-212.
80. Llusa, M., et al., *Measuring the hydrophobicity of lubricated blends of pharmaceutical excipients.* Powder Technology, 2010. **198**(1): p. 101-107.
81. Washburn, E.W., *The Dynamics of Capillary Flow.* Physical Review, 1921. **17**(3): p. 273-283.
82. Siebold, A., et al., *Capillary Rise for Thermodynamic Characterization of Solid Particle Surface.* Journal of Colloid and Interface Science, 1997. **186**(1): p. 60-70.
83. Pingali, K., et al., *Evaluation of strain-induced hydrophobicity of pharmaceutical blends and its effect on drug release rate under multiple compression conditions.* Drug Dev Ind Pharm, 2011. **37**(4): p. 428-35.
84. Eilbeck, J., et al., *Effect of contamination of pharmaceutical equipment on powder triboelectrification.* International Journal of Pharmaceutics, 2000. **195**(1–2): p. 7-11.
85. Harper, W.R., *The Volta Effect as a Cause of Static Electrification.* Proceedings of the Royal Society of London. Series A. Mathematical and Physical Sciences, 1951. **205**(1080): p. 83-103.
86. Lowell, J. and A.C. Rose-Innes, *Contact electrification.* Advances in Physics, 1980. **29**(6): p. 947-1023.
87. Jones, T.B., *Electromechanics of Particles*. 1995: Cambridge University Press.

88. Matsusaka, S. and H. Masuda, *Electrostatics of particles.* Advanced Powder Technology, 2003. **14**(2): p. 143-166.
89. Rowley, G., *Quantifying electrostatic interactions in pharmaceutical solid systems.* International Journal of Pharmaceutics, 2001. **227**(1–2): p. 47-55.
90. Thomas B. Jones, J.L.K., Jack F. Yablonsky, *Powder Handling and Electrostatics: Understanding and Preventing Hazards*. 1991: CRC Press.
91. Pingali, K.C., et al., *An Observed Correlation Between Flow and Electrical Properties of Pharmaceutical Blends.* Powder Technology, 2009. **192**: p. 157-165.
92. Liss, E.D. and B.J. Glasser, *The influence of clusters on the stress in a sheared granular material*. Powder Technology, 2001. **116**(2–3): p. 116-132.
93. A, A., et al., *A method to quantitatively describe powder segregation during discharge from vessels.* Pharmaceutical Technology Yearbook, 2000.
94. Wold, S., K. Esbensen, and P. Geladi, *Principal Component Analysis.* Chemometrics and Intelligent Laboratory Systems, 1987. **2**(1-3): p. 37-52.
95. Boukouvala, F., F.J. Muzzio, and M.G. Ierapetritou, *Predictive modeling of pharmaceutical processes with missing and noisy data.* AIChE Journal, 2010. **56**(11): p. 2860-2872.
96. Walczak, B. and D.L. Massart, *Dealing with missing data Part I.* Chemometrics and Intelligent Laboratory Systems, 2001. **58**(1): p. 15-27.
97. Walczak, B. and D.L. Massart, *Dealing with missing data: Part II.* Chemometrics and Intelligent Laboratory Systems, 2001. **58**(1): p. 29-42.
98. de la Fuente, R.L.N., S. Garcia-Munoz, and L.T. Biegler, *An efficient nonlinear programming strategy for PCA models with incomplete data sets.* Journal of Chemometrics, 2010. **24**(5-6): p. 301-311.
99. Vandeginste, B.G.M., C. Sielhorst, and M. Gerritsen, *The Nipals Algorithm for the Calculation of the Principal Components of a Matrix.* Trac-Trends in Analytical Chemistry, 1988. **7**(8): p. 286-287.
100. ASTM, *Standard shear test method for bulk solids using the Schulze ring shear tester*. 2002, ASTM International.
101. Freeman, R., *Measuring the flow properties of consolidated, conditioned and aerated powders — A comparative study using a powder rheometer and a rotational shear cell.* Powder Technology, 2007. **174**: p. 25-33.
102. Schulze, D., *Round robin test on ring shear testers.* Advanced Powder Technology, 2011. **22**(2): p. 197-202.
103. Bruni, G., et al., *A rheological model for the flowability of aerated fine powders.* Chemical Engineering Science, 2007. **62**(1–2): p. 397-407.
104. Janssen, R.J.M., et al., *Visualization of the shear region in a cohesive powder by scanning with a polarized neutron beam.* Powder Technology, 2005. **159**(2): p. 87-94.
105. Hughes, H., et al., *Development of a Material Sparing Bulk Density Test Comparable to a Standard USP Method for Use in Early Development of API's.* AAPS PharmSciTech, 2014: p. 1-6.
106. Chi-Ying Wong, A., *Characterisation of the flowability of glass beads by bulk densities ratio.* Chemical Engineering Science, 2000. **55**(18): p. 3855-3859.
107. Kojima, T. and J.A. Elliott, *Incipient flow properties of two-component fine powder systems and their relationships with bulk density and particle contacts.* Powder Technology, 2012. **228**(0): p. 359-370.
108. Saw, H.Y., et al., *Shear testing of lactose powders: The influence of consolidation stress and particle size on bulk density and estimated cohesion.* Advanced Powder Technology, 2014. **25**(4): p. 1164-1170.

109. Stanley-Wood, N., et al., *The relationships between powder flowability, particle re-arrangement, bulk density and Jenike failure function.* Advanced Powder Technology, 1993. **4**(1): p. 33-40.
110. Tallon, S. and C.E. Davies, *In-situ monitoring of axial particle mixing in a rotating drum using bulk density measurements.* Powder Technology, 2008. **186**(1): p. 22-30.
111. Zuurman, K., G.K. Bolhuis, and H. Vromans, *Effect of binder on the relationship between bulk density and compactibility of lactose granulations.* International Journal of Pharmaceutics, 1995. **119**(1): p. 65-69.
112. Zuurman, K., et al., *The relationship between bulk density and compactibility of lactose granulations.* International Journal of Pharmaceutics, 1994. **102**(1–3): p. 1-9.
113. Faulhammer, E., et al., *The effects of material attributes on capsule fill weight and weight variability in dosator nozzle machines.* International Journal of Pharmaceutics, 2014. **471**(1–2): p. 332-338.
114. Wong, A.C.-Y., *Use of angle of repose and bulk densities for powder characterization and the prediction of minimum fluidization and minimum bubbling velocities.* Chemical Engineering Science, 2002. **57**(14): p. 2635-2640.
115. Shenoy, P., et al., *Effect of powder densities, particle size and shape on mixture quality of binary food powder mixtures.* Powder Technology, 2015. **272**(0): p. 165-172.
116. Ziegelmeier, S., et al., *An experimental study into the effects of bulk and flow behaviour of laser sintering polymer powders on resulting part properties.* Journal of Materials Processing Technology, 2015. **215**(0): p. 239-250.
117. Sonnergaard, J.M., *A critical evaluation of the Heckel equation.* International Journal of Pharmaceutics, 1999. **193**(1): p. 63-71.
118. Gioia, G., et al., *Two-Phase Densification of Cohesive Granular Aggregates.* Physical Review Letters, 2002. **88**(20): p. 204302.
119. Gao, Y., et al., *Measurement of residence time distribution in a rotary calciner.* Aiche Journal, 2013. **59**(11): p. 4068-4076.
120. Lacey, P.M.C., *Developments in the theory of particle mixing.* Journal of Applied Chemistry, 1954. **4**(5): p. 257-268.
121. Harris, A., J. Davidson, and R. Thorpe, *The influence of the riser exit on the particle residence time distribution in a circulating fluidised bed riser.* Chemical Engineering Science, 2003. **58**(16): p. 3669-3680.
122. Harris, A., J. Davidson, and R. Thorpe, *Particle residence time distributions in circulating fluidised beds.* Chemical Engineering Science, 2003. **58**(11): p. 2181-2202.
123. Gao, Y., et al., *Characterizing continuous powder mixing using residence time distribution.* Chemical Engineering Science, 2011. **66**(3): p. 417-425.
124. Njeng, A.B., et al., *Effect of lifter shape and operating parameters on the flow of materials in a pilot rotary kiln: Part II. Experimental hold-up and mean residence time modeling.* Powder Technology, 2014.
125. Debacq, M., et al., *Transverse motion of cohesive powders in flighted rotary kilns: experimental study of unloading at ambient and high temperatures.* Powder Technology, 2013. **245**: p. 56-63.
126. Arntz, M., et al., *Granular Mixing and Segregation in a Horizontal Rotating Drum: A Simulation Study on the Impact of Rotational Speed and Fill Level.* Aiche Journal, 2008. **54**(12): p. 3133-3146.
127. Bridgewater, J., *Mixing of powders and granular materials by mechanical means—A perspective.* Particuology, 2012. **10**(4): p. 397-427.
128. Portillo, P.M., et al., *Investigation of the effect of impeller rotation rate, powder flow rate, and cohesion on powder flow behavior in a continuous blender using PEPT.* Chemical Engineering Science, 2010. **65**(21): p. 5658-5668.

129. Alexander, A., T. Shinbrot, and F.J. Muzzio, *Scaling surface velocities in rotating cylinders as a function of vessel radius, rotation rate, and particle size*. Powder Technology, 2002. **126**(2): p. 174-190.
130. Sherritt, R.G., et al., *Axial dispersion in the three-dimensional mixing of particles in a rotating drum reactor.* Chemical Engineering Science, 2003. **58**(2): p. 401-415.
131. Parker, D.J., et al., *Positron emission particle tracking studies of spherical particle motion in rotating drums.* Chemical Engineering Science, 1997. **52**(13): p. 2011-2022.
132. Hogg, R., et al., *Diffusional mixing in an ideal system.* Chemical Engineering Science, 1966. **21**(11): p. 1025-1038.
133. Rao, S.J., S.K. Bhatia, and D.V. Khakhar, *Axial transport of granular solids in rotating cylinders. Part 2: Experiments in a non-flow system.* Powder Technology, 1991. **67**(2): p. 153-162.
134. Cahn, D.S. and D.W. Fuerstenau, *Simulation of diffusional mixing of particulate solids by Monte Carlo techniques*. Powder Technology, 1967. **1**(3): p. 174-182.
135. Carley-Macauly, K.W. and M.B. Donald, *The mixing of solids in tumbling mixers—I.* Chemical Engineering Science, 1962. **17**(7): p. 493-506.
136. Wightman, C. and F.J. Muzzio, *Mixing of granular material in a drum mixer undergoing rotational and rocking motions I. Uniform particles.* Powder Technology, 1998. **98**(2): p. 113-124.
137. Hogg, R., G. Mempel, and D.W. Fuerstenau, *The mixing of trace quantities into particulate solids.* Powder Technology, 1969. **2**(4): p. 223-228.
138. Shoji, K., R. Hogg, and L.G. Austin, *Axial mixing of particles in batch ball mills.* Powder Technology, 1973. **7**(6): p. 331-336.
139. Singh, D.K., *A Fundamental Study of the Mixing of Solid Particles*. 1979: University of Rochester.
140. Rutgers, R., *Longitudinal mixing of granular material flowing through a rotating cylinder: Part II. Experimental.* Chemical Engineering Science, 1965. **20**(12): p. 1089-1100.
141. Abouzeid, A.Z.M.A., et al., *The influence of operating variables on the residence time distribution for material transport in a continuous rotary drum.* Powder Technology, 1974. **10**(6): p. 273-288.
142. Hehl, M., et al., *Longitudinal mixing in horizontal rotary drum reactors.* Powder Technology, 1978. **20**(1): p. 29-37.
143. Woodle, G.R. and J.M. Munro, *Particle motion and mixing in a rotary kiln.* Powder Technology, 1993. **76**(3): p. 241-245.
144. Orr, N. and E. Shotton, *Mixing of cohesive powders.* CHEMICAL ENGINEER-LONDON, 1973(269): p. 12-19.
145. Sai, P., et al., *Residence time distribution and material flow studies in a rotary kiln.* Metallurgical Transactions B, 1990. **21**(6): p. 1005-1011.
146. Moriyama, A. and T. Suga, *Axial dispersion and residence time distribution of spherical particles in rotary kiln.* Tetsu-to-Hague, 1974. **60**(9): p. 1283-1288.
147. Cussler, E.L., *Diffusion: Mass Transfer in Fluid Systems*. 1997: Cambridge University Press.
148. Mellmann, J., *The transverse motion of solids in rotating cylinders—forms of motion and transition behavior.* Powder Technology, 2001. **118**(3): p. 251-270.
149. Sherritt, R.G., *Three-dimensional particle diffusion in a rotating drum reactor*. 2001: University of Calgary.